

ABSTRACT

LIM, MINA. Understanding the Thermal, Structural, and Electrical Properties of the High Entropy Ceramics, High Entropy Oxides and Carbides, using Computational Modeling. (Under the direction of Dr. Donald W. Brenner).

Starting from the development of high entropy alloys (HEAs), the concept of high entropy has been extended with the exploration of high entropy ceramic compositions. Adding five or more atoms into the system creates high entropy characteristics which contains fewer phases in mostly solid solutions. This research field has great potentials growing to find new and exciting properties and future applications.

It is difficult to measure the fundamental physical interactions and explain the complexity of the high entropy ceramics through the experiments. Understanding the atomistic level of the detailed physical properties of high entropy ceramics has been explored using the computational simulations like the Molecular Dynamics (MD) simulations and the first principle study in this thesis. Chapter one introduces general concepts of high entropy materials and computational modeling method. The development of the high entropy materials and common modeling approaches are discussed.

Experimentally, the thermal conductivity reduction was measured with the addition of a sixth cation to the entropy stabilized oxide J14 ($\text{Mg}_{0.1}\text{Co}_{0.1}\text{Ni}_{0.1}\text{Cu}_{0.1}\text{Zn}_{0.1}\text{O}_{0.5}$). Chapter two contains original work published in Journal of Applied Physics. This chapter summarizes the reduction behavior of the phonon thermal conductivity of five entropy stabilized oxides using classical molecular dynamics simulations. The five systems are J14 and J14 plus Sc, Sn, Cr or Ge in equi molar cation proportions. It is found that the phonon scattering from disorder in atomic charges can explain prior experimental result that show a lowering of thermal

conductivity by adding a sixth cation to J14. Additional analysis using the Bridgeman equation is performed.

The properties of high entropy carbides (HECs) are examined and predicted in the chapter three and four using the Density Functional Theory (DFT). Nine HECs are examined which created by equi-molar combinations of five of the set of eight refractory metals Hf, Nb, Mo, Ta, Ti, V, W, and Zr.

Chapter three explores the relationship between high entropy carbides and their respective binaries. First, the predictability of the HECs properties from their respective binary compounds is described. Second, it was explored the practical relationship between the properties of the binary compounds corresponding to a give HEC composition and its entropy forming ability (EFA). It is found that lattice constant, binding energy, bulk modulus, average carbon vacancy formation energy (CVFE) and the energy difference between the Fermi Level and the pseudo-gap (ζ) in the electronic Density of States are well approximated by binary carbide averages. We have found correlations between EFA and the standard deviation of the distribution of bulk moduli, ζ of the constituent binaries and the standard deviation of the CVFEs for each HEC. This finding proves the EFA as a central quantity for estimating properties of HECs beyond phase stability.

Chapter four is focused on understanding the electronic structure of high entropy carbides by the Density Functional Theory (DFT) and BoltzTraP calculations. The number of electrons in HECs are well predicted from the averages of the binaries. But the electrical conductivity is not correlated with the number of the electrons. The electrical conductivities of all HECs resulted lower than the ones of all the respective binaries. This can be used as a prediction guideline of the electrical conductivity for HECs from known electrical conductivities of binary carbides. The

density of states study found that the electronic structure in HECs kept the same from the binaries regardless adding more metals in the structure. Furthermore, partial density of states (PDOS) reveals that HECs have the strong covalent bonds with metallic characterization.

Chapter five includes concluding remarks and some future works.

© Copyright 2020 by Mina Lim

All Rights Reserved

Understanding the Thermal, Structural, and Electrical Properties of the High Entropy Ceramics,
High Entropy Oxides and Carbides, using Computational Modeling

by
Mina Lim

A dissertation submitted to the Graduate Faculty of
North Carolina State University
in partial fulfillment of the
requirements for the degree of
Doctor of Philosophy

Materials Science & Engineering

Raleigh, North Carolina
2020

APPROVED BY:

Dr. Donald W. Brenner
Committee Chair

Dr. Jon-Paul Maria

Dr. Srikanth Patala

Dr. Melissa Pasquinelli

DEDICATION

To my parents,

To Sungkwan and Doyoon,

I love you all.

BIOGRAPHY

Mina Lim graduated with a Bachelor of Science in Chemical engineering degree from Texas A&M university in 2006. She continued her career as an engineer working at Samsung Electronics in Korea till 2012. She started pursuing her Ph.D. degree in Materials Science Engineering at North Carolina State University in 2013, under supervision of Prof. Donald W. Brenner.

ACKNOWLEDGMENTS

First of all, I would like to express my tremendous gratitude to my advisor, Prof. Donald W. Brenner. If it weren't for his endless support, encouragement, patience and immense scientific guidance, I would not be writing this dissertation. I deeply appreciate his dedication to works and students. I would also like to thank the rest of my thesis committee: Prof. Jon-Paul Maria, Prof. Srikanth Patala, and Prof. Melissa Pasquinelli, for their insightful comments and encouragement, to widen my research from various perspectives. I cannot forget the past and present group members: Dr. Zsolt Rak, Dr. Eric Bucholz, Dr. Dong Li, Dr. Liagliang Su, Dr. Farshad Saberi Movahed, Samuel Daigle and Leah Granger. I have had the pleasure working with such a great group of you. I also want to thank the staff in the Materials Science Department, who work so hard to support the students. Especially, I thank Edna Deas. I am touched by her kindness and uncountable supports. You always cheered and comforted me in every situation I have been through during my graduate study. Lastly, but the most, I wish to express my love and appreciation for my family. My mom and dad, and my sister, and my brother, who love and support me unconditionally. Sungkwan, my husband, whose kindness and patience trumps any person I have ever known. Doyoon, my son, you are my sunshine and motivation and love you forever.

TABLE OF CONTENTS

LIST OF TABLES	vii
LIST OF FIGURES	viii
Chapter 1. Introduction	1
1.1 High Entropy Materials.....	2
1.2 Molecular Dynamics Simulations	11
1.3 Density Functional Theory.....	14
References.....	18
Chapter 2. Influence of mass and charge disorder on the phonon thermal conductivity of entropy stabilized oxides determined by molecular dynamics simulations	27
2.1 Abstract.....	27
2.2 Introduction.....	28
2.3 Methodology	30
2.4 Simulation Results and Discussion	32
2.5 Bridgman Equation	39
2.6 Conclusion	41
References.....	43
Chapter 3. An exploration of relationships between high entropy carbides and their respective binaries..	46
3.1 Abstract.....	46
3.2 Introduction.....	47
3.3 Computational Method	50
3.4 HEC Properties	52
3.5 Correlating Binary Properties with the EFA.....	58
3.6 Carbon Vacancy Formation Energies	61
3.7 Discussion.....	68
3.8 Conclusions.....	76

References.....	78
Chapter 4. Understanding the electronic structure of high entropy carbides by first principle study	83
4.1 Introduction.....	83
4.2 Computational Method	84
4.3 Results.....	85
4.4 Conclusion	106
References.....	107
Chapter 5. Conclusion and Future work	111
Appendix.....	114

LIST OF TABLES

Table 2.1	Thermal conductivity from experiment, simulations, and the Bridgeman equation discussed below. ^a reference 25; ^b reference 18.	34
Table 2.2	Thermal conductivities using different combinations of homogeneous charge (HMC), heterogeneous charge (HTC), homogeneous mass (HMM) and heterogeneous mass (HTM).	35
Table 2.3	Properties from MD simulation used to estimate thermal conductivity via Eq. (2) ^c reference 36; ^d reference 37; ^e reference 38	40
Table 3.1	Composition abbreviations used in this paper and phase stability from reference [37].	48
Table 3.2	Properties of the binary carbides in a rocksalt structure calculated from DFT.	53
Table 3.3	Properties of the HECs calculated from DFT.	54
Table 3.4	Average carbon-metal bond lengths and the difference (Δ) between the shortest and largest bond lengths for each HEC composition broken down by component.....	60
Table 3.5	Properties of the two approaches used to calculate CVFEs. STDEV=standard deviation; MSE=mean squared error.....	65
Table 4.1	Composition the calculated σ/τ and the experimental electrical conductivity of the binaries.....	86
Table 4.2	The number of electrons at the Fermi level and the electrical conductivity over the relaxation time of the binary carbides and the HECs calculated from DFT and BoltzTraP.	88

LIST OF FIGURES

Figure 1.1	Ashby map showing fracture toughness as a function of yield strength for high entropy alloys in relation to a wide range of material systems. Adapted from ³⁴	5
Figure 1.2	Gibbs energy G, and enthalpy H, plot with temperature T, showing the temperature dependence of Gibbs free energy and enthalpy. Adapted from ⁴⁶	6
Figure 1.3	X-ray diffraction (XRD) patterns for high entropy oxide J14. Adapted from Rost ⁴⁷	8
Figure 1.4	Time dependence of the heat auto correlation function in J14, J14+Sc and MgO at 300K.	13
Figure 2.1	Thermal conductivities for the various compositions from experiment, from the MD simulations, and from the Bridgeman equation.....	33
Figure 2.2	Data from Table 2.2 plotted as histograms.	36
Figure 2.3	Dependence of thermal conductivity calculated from MD simulations on the averaged mass and average charge used in the J14 HMC/HMM system.....	38
Figure 3.1	Electronic properties of the HECs. (a) Example Density of States from the DFT calculations. The arrow to the left denoted the pseudo-gap between bonding and anti-bonding states. The right arrow indicates the Fermi level. The difference between the two is denoted as ζ , while the shaded region is the Valence Electron Concentration. (b) Graph illustrating the linear dependence for VEC and ζ for the binary carbides and the HECs.....	51
Figure 3.2	Plots of the properties of the nine HECS in Table 3.1 calculated as averages of the constituent binaries as a function of the same properties calculated from DFT.....	55
Figure 3.3	Properties in Figure 3.2 calculated from DFT as a function of ζ for each of the HEC compositions in Table 3.1. R^2 is the linear correlation coefficient for each plot.....	57
Figure 3.4	Average values (left column) and standard deviations (right column) plotted against EFA for the HEC compositions in Table 3.1. (a)-(e) refer to cohesive energy, lattice constant, bulk modulus, CVFE and ζ , respectively.....	61
Figure 3.5	Plot of the average CVFE's for the HECs and binaries calculated from DFT as function of the ζ values for each, also calculated from DFT.	63

Figure 3.6	CVFE's for each composition in Table 3.1 calculated as either a weighted sum of the CVFE for the binaries that correspond to the environment surrounding the vacancy (open circles) or a function of the weighted sum of the ζ values from the same binaries (solid circles) as a function of the DFT energies. The arrows indicate the highest and lowest values of the CVFE's of the constitutive binaries for each composition.....	66
Figure 3.7	CVFE properties from the constitutive binaries (open circles) and from the full distribution of all 15626 local compositions (solid circles) for all 56 compositions as a function of their EFA value. The full distribution values use the ζ model for calculating CVFEs. (a) Average CVFE values. (b) Standard deviation of the CVFE values.....	68
Figure 3.8	Partial density of states for the cations in the binaries and in HEC9. The ζ , which vary widely in the binaries, equilibrate to the same value of 1.28 eV in the HEC.....	71
Figure 3.9	Distributions of the 15,625 CVFEs for each of the 56 compositions, denoted by their EFA value. The black histogram bars are calculated from the function of constitutive ζ values. The grey histogram bars correspond to a Normal function with the same average and standard deviation as the black bars.....	72
Figure 4.1	The calculated electrical conductivity over the relaxation time for the binaries as function of the experimental electrical conductivity.....	87
Figure 4.2	The comparison of the number of the electrons at the Fermi level near +/- 0.1 eV and the calculated electrical conductivity over the relaxation time for the binaries and HECs.....	89
Figure 4.3	The Density of States (DOS) of HECs and the respective binaries are superimposed.....	90
Figure 4.4	The Partial Density of States (PDOS) of nine HECs.....	95
Figure 4.5	PDOS of eight respective binary carbides.....	101
Figure 4.6	Prediction of the number of the electrons of HECs from their respective binaries at the Fermi level near +/- 0.1 eV.....	104
Figure 4.7	Comparison of the number of electrons between HECs and the respective binaries average.....	105

Chapter1. Introduction

Computational materials science is a computational prediction of material properties from atomic to microstructure level. Numerical computational simulations are performed to calculate materials properties and investigate the physical mechanism. Many system parameters like potential approximation, system sizes, and boundary conditions are the uncertainties and the limitations for the simulations. However, computational studies of the materials have been continuously developed to characterize and predict properties and mechanisms. In addition, computational simulations help to bridge the gap between theories and experiments.

Computational simulations provide numerical solutions when theoretical models become too complex and difficult to solve analytically. The time scale of simulations and experiments has closely met due to the development of the high performance computation techniques and the continuous improvement in experimental characterization over the past two decades. Since modern materials have been become more complex and advanced, so the computation simulation methods have been highlighted to understand the detailed role of the materials' composition, microstructure, defects, properties, designing.

The interest of high entropy materials has been rapidly raised due to the combination of useful properties and promising applications. Starting from high entropy alloys, the study has been extended to high entropy ceramics such as oxides, borides, and carbides relatively recent. The high entropy materials are designed by the high configurational entropy associated with multi component, such as four or more elements, solid solution. To characterize and predict the high entropy ceramics' (high entropy stabilized oxides and carbides) thermal and mechanical properties, computational simulations, e.g., molecular dynamics simulation and density functional theory, are performed in this thesis. The computational simulations are used not only

to crosscheck the results from the experiments, but also to predict and suggest the properties of high entropy ceramics prior to examining by experiments.

1.1 High Entropy Materials

A new class of materials with multi principal elements is proposed. The new material type of alloy is formed by mixing equimolar of five or more elements. Cantor et al.¹ fabricated the five equimolar metal component alloy, FeCrMnNiCo, forming a fcc single solid solution phase. From their earlier work, the metallic systems with 16 and 20 metal elements containing equimolar amount were synthesized, but it formed multi phases rather than a single phase. Yeh et al.² has named the materials as “High Entropy Alloys” (HEA) indicating those composed of five or more principal elements in equimolar ratio. They synthesized the alloys CuCoNiCrAl_xFe and explored the fcc, bcc, or fcc+bcc depending on Al content. In 2008, Senkov et al.³ produced two single phase bcc structures with the refractory transition metals which are Nb₂₅Mo₂₅Ta₂₅W₂₅ and V₂₀Nb₂₀Mo₂₀Ta₂₀W₂₀. Also, several single phase hcp of HEAs⁴⁵ are introduced and Middleburg et al.⁶ extended the study in modelling on the atomic scale using DFT methods with Mo, Pd, Rh, Ru, Tc systems.

The large mixing entropy results the solid solution of many elements more stable. The configurational entropy change can be calculated during the formation of a solid solution from equimolar n elements as below.

$$\Delta S_{conf} = R \ln n \quad (1.1.1)$$

where R is gas constant, n is the number of elements.

Based on the effect of entropy mixing, Yeh⁷ suggested the three criteria of alloys. One is the low entropy alloys that are traditional alloys. Second is the medium entropy alloys containing 2-4 major elements. High entropy alloys are characterized that are containing five or more elements with the entropy mixing value of $1.6R$. High entropy effect enhances the formation of simple solid solution phases. The number of possible combinations is very large, which combined with the dearth of thermodynamic data for multiple components has made the prediction of stable high entropy materials challenging. The calculation of the enthalpy mixing is widely used in a regular phase selection model.⁸ Thermodynamically stable structures are involved with empirical relations of the distribution of atomic radii of a given chemical constitution that have been developed by Hume-Rothery rules.⁹⁻¹²

A high entropy mixing concept between alloying elements has been developed for both functional and structural applications.^{13,14,15,16,17} These alloys have brought a significant attention in materials science and engineering because they have potentially desirable properties. The properties of strength, ductility, tensile strength, oxidation resistance and thermal stability are examined.^{18,19,20,21,22,23,24,25,26} The electrical^{27,28,29} and magnetic^{30,29,31,32,33} properties are also studied. Yeh et al.² synthesized the multiple principal HE alloys and found their excellent properties such as hardness, resistance, stability, high-temperature strength, and ductility. Gludovatz³⁴ found that the alloy of FeCrMnNiCo has a yield strength and a tensile strength between 759 and 1280 MPa, respectively. The fracture toughness is over $217 \text{ MPa}\cdot\text{m}^{1/2}$ which exceeds than those in nickel-based super alloy, stainless alloy and tungsten alloy. Figure 1.1 shows that the high entropy alloys are in high regime for both of fracture toughness and yield strength. Other functional properties include to develop thin film nitride coatings as diffusion barriers^{35,36}, hydrogen storage^{37,38}, catalysts³⁹, thermoelectric properties⁴⁰ and radiation damage resistance.⁴¹ HEA

systems with the transition metal alloys have been emphasized because of the high temperature structure characteristics which are in high demand of aerospace and thermal specific applications.

These high entropy alloys are also thermodynamically stable because the Gibbs free energy G is reduced by increasing entropy S .

$$G = H - TS \quad (1.1.2)$$

where H is the enthalpy of formation and T is the temperature. Figure 1.2 shows that enthalpy increases with temperature, and entropy becomes negative at high temperature. Therefore, the high entropy materials are more thermodynamically stable at high temperatures since the phase stability occurs favor at high temperature with mainly the entropy contribution. Gorr et al.⁴² introduced a new refractory HEA system of MoWAlCr_x with a high melting temperature of about 1700°C and thermally stable at high temperatures between 1077°C and 1700°C. The high entropy TiVZrNbHf alloy is used for the nitride coating showing high hardness and thermal stability in the temperature range to 1100°C.⁴³

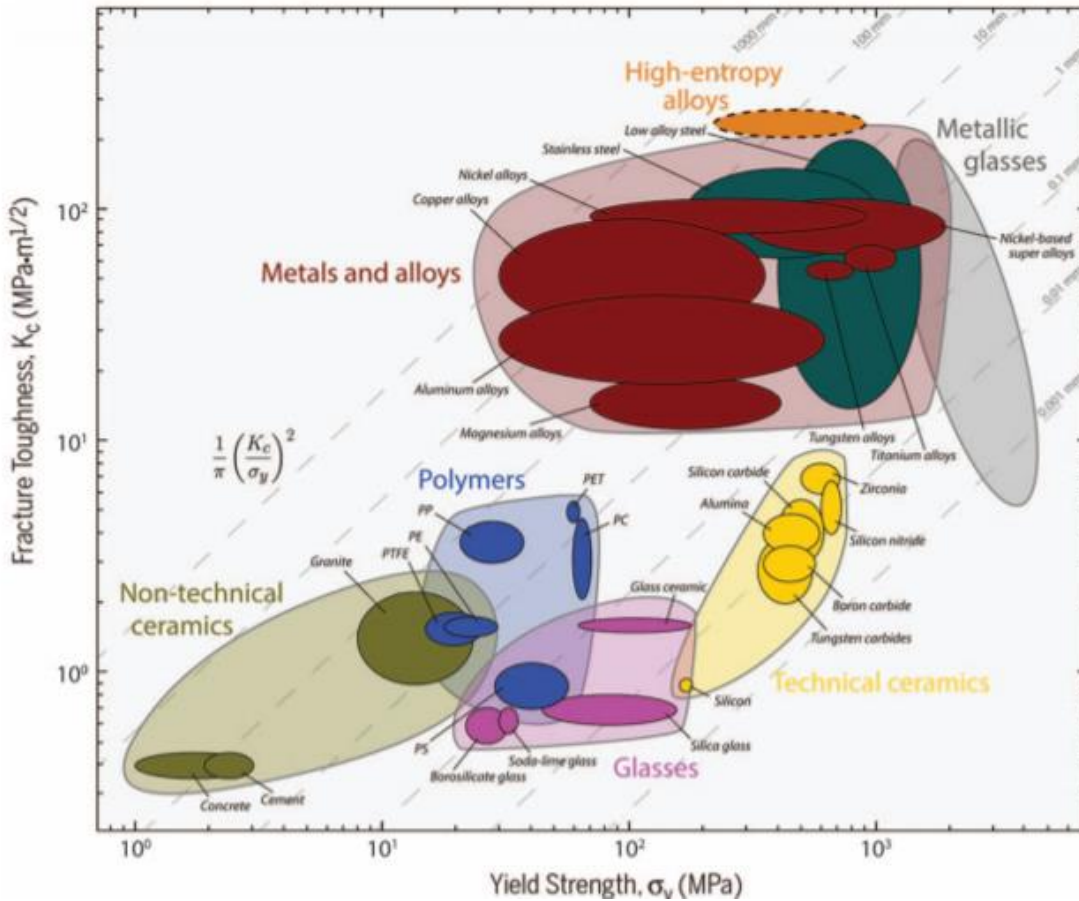


Figure 1.1 Ashby map showing fracture toughness as a function of yield strength for high entropy alloys in relation to a wide range of material systems. Adapted from ³⁴

$\text{Cr}_{18}\text{Mn}_{27}\text{Fe}_{27.5}\text{Ni}_{27.5}$ HEA performs a high corrosion resistant behavior and thermal stability at 700°C for 1000 hours.⁴⁴ Refractory high entropy $\text{Nb}_{25}\text{Mo}_{25}\text{Ta}_{25}\text{W}_{25}$ and $\text{V}_{20}\text{Nb}_{20}\text{Mo}_{20}\text{Ta}_{20}\text{W}_{20}$ are shown excellent compression yield strength and good ductility at temperature between 600°C and 1600°C .³ Pacheco et al.⁴⁵ investigate the thermal stability of phase composition of the HfNbTiVZr alloy that stays stable single bcc phase between 830°C and 1490°C .

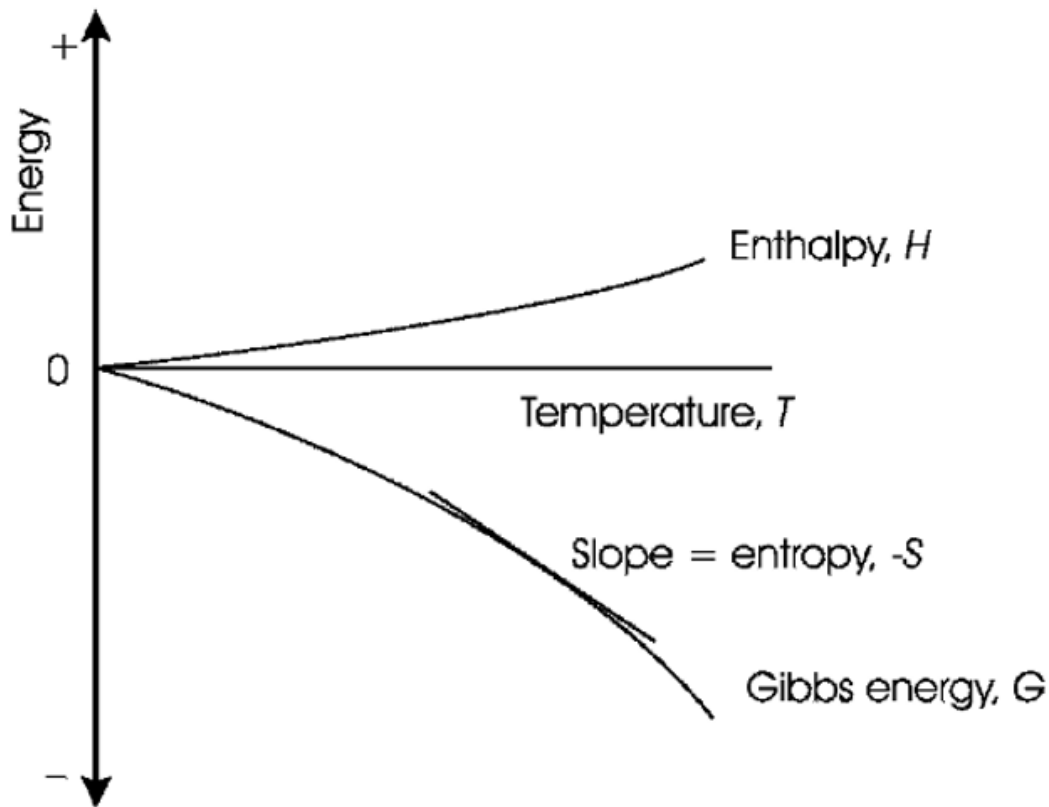


Figure 1.2 Gibbs energy G , and enthalpy H , plot with temperature T , showing the temperature dependence of Gibbs free energy and enthalpy. Adapted from ⁴⁶

Since the high entropy alloys approach and potentials had been introduced in 2004, research into those materials has been rigorously expanded for more alloy and material design. Inspired by the high entropy alloys discovery, in 2015, Rost et. al⁴⁷ extended the entropy concept to five-metal component oxides. The configurational disorder corresponds to randomness of cations in a single sublattice promote novel and entropy stabilized forms of crystalline matter. They demonstrated the existence of a new class of mixed oxides with an equimolar mixture of MgO, CoO, NiO, CuO and ZnO. The outcome material is

$(\text{Mg}_{0.2}\text{Co}_{0.2}\text{Ni}_{0.2}\text{Cu}_{0.2}\text{Zn}_{0.2})\text{O}$, which they named it as 'J14'. The entropic stabilization hypothesis was supported from all experimental results such as testing reversibility, entropy through composition variation, endothermicity, and homogeneity. They successfully fabricated a single rocksalt phase entropy stabilized oxide with randomly distributed of five equimolar metal cations in a single sublattice. Figure 3. shows X-ray diffraction (XRD) patterns for J14 and there are two prominent phases, rocksalt and tenorite (monoclinic structure) are observed after 700C. It clearly shows the tenorite phases are reducing by increasing the temperature and full conversion to the rocksalt phase occurs between 850°C and 900°C. Besides HEO in a rocksalt structure, a single fluorite phase high entropy oxide with the composition of $(\text{Ce}_{0.2}\text{Zr}_{0.2}\text{Hf}_{0.2}\text{Sn}_{0.2}\text{Ti}_{0.2})\text{O}_2$ is synthesized.⁴⁸ The results demonstrate a clear single fluorite phase about 1500°C which is much higher than the one of J14 reported by Rost.⁴⁷ Also, perovskite type of multicomponent oxides containing up to 10 different cations in equi-atomic are studied. The system of $(\text{Gd}_{0.2}\text{La}_{0.2}\text{Nd}_{0.2}\text{Sm}_{0.2}\text{Y}_{0.2})\text{MnO}_3$ ⁴⁹ shows a single perovskite phase at high temperature about 900°C. Phase stability occurs at high temperature and it indicates the typical entropy stabilization behavior which the entropic term dominates the free energy of the system.

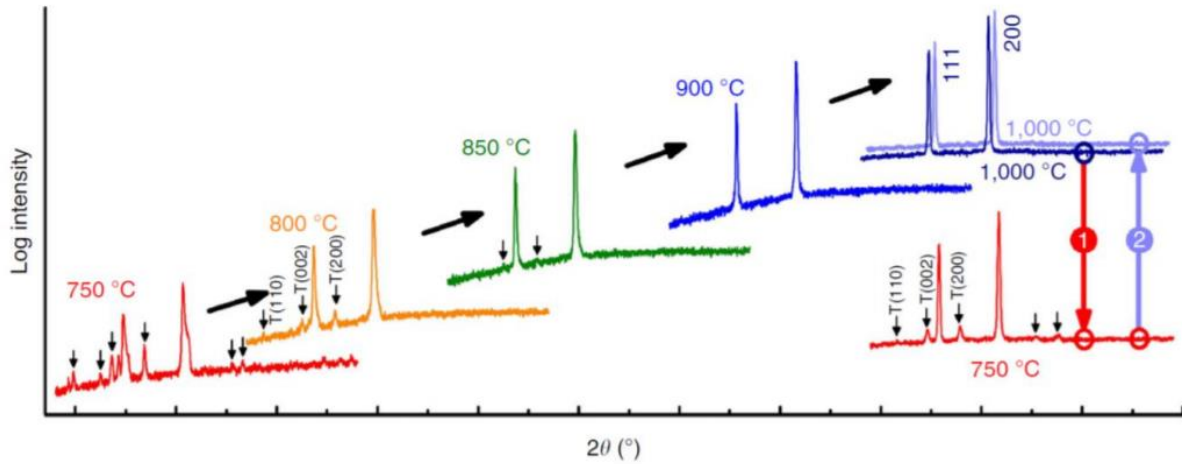


Figure 1.3 X-ray diffraction (XRD) patterns for high entropy oxide J14. Adapted from Rost ⁴⁷

This study extends the high entropy stabilization concept from the rocksalt oxides to multicomponent perovskite type oxides. The properties of HEOs can be utilized in many different applications⁵⁰⁵¹⁵²⁵³⁵⁴⁵⁵ with their mechanical⁵⁶⁵², magnetic⁵⁷ and optical⁵⁴ properties. Recently, the thermal properties are reported observing the correlation between the low thermal conductivity and the phonon scattering from the disorder in the system.⁵⁶⁵³

In 2016, Gild et al.⁵⁸ extended the state of the art of the crystalline high entropy ceramics to the high entropy metal borides (HEB). They successfully synthesized seven different high entropy metal boride compounds with six single hexagonal boride phase including $(\text{Hf}_{0.2}\text{Zr}_{0.2}\text{Ta}_{0.2}\text{Nb}_{0.2}\text{Ti}_{0.2})\text{B}_2$, $(\text{Hf}_{0.2}\text{Zr}_{0.2}\text{Ta}_{0.2}\text{Mo}_{0.2}\text{Ti}_{0.2})\text{B}_2$, $(\text{Hf}_{0.2}\text{Zr}_{0.2}\text{Mo}_{0.2}\text{Nb}_{0.2}\text{Ti}_{0.2})\text{B}_2$, $(\text{Hf}_{0.2}\text{Mo}_{0.2}\text{Ta}_{0.2}\text{Nb}_{0.2}\text{Ti}_{0.2})\text{B}_2$, $(\text{Mo}_{0.2}\text{Zr}_{0.2}\text{Ta}_{0.2}\text{Nb}_{0.2}\text{Ti}_{0.2})\text{B}_2$, and $(\text{Hf}_{0.2}\text{Zr}_{0.2}\text{Ta}_{0.2}\text{Cr}_{0.2}\text{Ti}_{0.2})\text{B}_2$ and one multi phase of $(\text{Hf}_{0.2}\text{Zr}_{0.2}\text{W}_{0.2}\text{Mo}_{0.2}\text{Ti}_{0.2})\text{B}_2$. This work is the first time crystalline high entropy non oxide ceramics have been synthesized with exhibiting a unique layered hexagonal crystal structure that consists of alternating rigid two dimensional boron nets and metal cations

on the other two layers. Metals are randomly distributed on the layers with mixed ionic and covalent bonds between metals and boron. Tallarita et al.⁵⁹ fabricated a bulk high entropy metal boride $(\text{Hf}_{0.2}\text{Mo}_{0.2}\text{Ta}_{0.2}\text{Nb}_{0.2}\text{Ti}_{0.2})\text{B}_2$ by Self propagating High temperature Synthesis (SHS) followed by processing the SHS powders at 1950°C through Spark Plasma Sintering (SPS). It gives a single hexagonal phase of borides which is similar to the one produced by Gild et al. but performs better hardness and improved oxidation resistances.⁵⁹ Zhang et al.⁶⁰ also synthesized high entropy boride powders $(\text{Hf}_{0.2}\text{Zr}_{0.2}\text{Ta}_{0.2}\text{Cr}_{0.2}\text{Ti}_{0.2})\text{B}_2$, $(\text{Hf}_{0.2}\text{Mo}_{0.2}\text{Zr}_{0.2}\text{Nb}_{0.2}\text{Ti}_{0.2})\text{B}_2$, and $(\text{Hf}_{0.2}\text{Mo}_{0.2}\text{Ta}_{0.2}\text{Nb}_{0.2}\text{Ti}_{0.2})\text{B}_2$ from metal oxides and amorphous boron powder by improved sintering. These sintered powders results high hardness values of 28.3, 26.3, and 25.9 Gpa, respectively.⁶⁰

The high entropy ceramic studies started with the oxides and borides and have been extended to the carbides. Castle et al.⁶¹ fabricated two bulk equiatomic Ultra High Temperature Ceramic (UHTC) carbide compositions, i.e., $(\text{Hf-Ta-Zr-Ti})\text{C}$ and $(\text{Hf-Ta-Zr-Nb})\text{C}$, from transition metal carbides HfC, TaC, ZrC, NbC, and TiC. A single phase rocksalt structures were formed. They used two steps which are ball milling and Spark Plasma Sintering (SPS) with a maximum sintering temperature of 2573K. The nanoindentation test result of the carbides showed a significantly enhanced hardness ($36.1\pm 1.6\text{GPa}$), in comparison to the hardest binary carbides (HfC, $31.5\pm 1.3\text{GPa}$) and the $(\text{Hf-Ta})\text{C}$ ($32.9\pm 1.8\text{GPa}$). Other properties like the microstructure, atomic structure, and localized chemical disorder of the $(\text{Hf-Ta-Zr-Nb})\text{C}$ composition was investigated by Dusza et al.⁶²

Sarker et al.⁶³ proposed the ab initio entropy descriptor which is called the Entropy Forming Ability (EFA) from first principles study. It provides a new systematic understanding for the formation of single phase high entropy carbides by evaluating the energy distribution

spectra of the structures that are generated by Automatic FLOW (AFLOW) partial occupation (AFLOWPOCC) method.⁶⁴ The standard deviation is used to characterize the energy distribution spectrum quantitatively. A total 56 five component systems can be generated from eight refractory metals (Hf, Nb, Mo, Ta, Ti, V, W, and Zr), and the ab-initio calculated EFA values are provided. Nine candidate systems were experimentally synthesized, and the experiments validated the prediction of the phase from the EFA.

In 2018, Harrington et al.²⁶ have selected the candidate compositions for synthesis of high entropy and stabilized carbides from the ab initio entropy descriptor, EFA⁶³ and synthesized twelve different high entropy transition metal carbides. They concentrated a systematic study on the phase stability and mechanical properties of HEC synthesized from group IV, V and VI metal carbides. The phase stability has been analyzed and found that it depends on a trade off between enthalpy and entropy. Mechanical properties are also examined in terms of hardness and elastic modulus. The high entropy transition metal carbides result significantly enhanced hardness over the weighted average binary constituent carbides. Nine of the twelve compositions are determined to be a single phase at a high temperature over 2400K. Their study explores that these materials great potentials of a new composition space in ceramics that may lead to improved Ultra High Temperature Ceramics (UHTCs).

1.2 Molecular Dynamics Simulations

Molecular dynamics (MD) simulation is a useful computer simulation method that calculates atoms and molecules physical movement. MD method is based on the classical mechanics by numerically solving Newton's equations of motion and determines the positions of the particles by discrete time integration. It generates the information at the atomistic level of the system. To calculate a trajectory, an initial state is needed sufficiently with the atom positions as coordinate and momenta. Forces acting on every atoms are obtained by deriving equations, the force field, where potential energy is deduced from the molecular structure.⁶⁵⁻⁷⁰ The system total energy is divided into a potential energy and a kinetic energy and it should be conserved. The kinetic energy is the sum of kinetic energies due to the all particles' motion. The potential energy is calculated based on the selected potentials. Potential functions are obtained from three different methods, i.e., empirical, semi-empirical, and ab-initio, that based on the degree of electron states approximation.

The interatomic potentials are divided into pair potentials and many-body potentials. Lennard-Jones and Columbic are the pair potentials which are non-directional and are used for the non-bonded system. If electrostatics between the atoms are significant, Columbic interactions need to include with atomic charges. A periodic boundary condition is applied in order to keep particles near the simulation box surface with an imaginary replica of the same simulation box. Significant computation time can be saved by neglecting pair interactions beyond a cut-off and long range interactions. Some of examples of many body potentials are the Stillinger-Weber potential⁷¹, EAM^{72,73}, Tersoff^{74,75}, ReaxFF⁷⁶, and COMB^{77,78}. Usually, many body potentials consider to be more accurate, but higher usage of computer time.

We have used an open source software modeling code from Sandia National Laboratories which is called Large-scale Atomic/Molecular Massively Parallel Simulator (LAMMPS) for our simulations.⁷⁹ In this dissertation, the phonon thermal conductivity of J14 systems is calculated using equilibrium molecular dynamics (EMD) with Green-Kubo method.⁸⁰⁻⁸² There are two molecular dynamics, equilibrium (EMD) and non-equilibrium (NEMD) are widely used to predict the thermal conductivity in a solid structure.⁸³⁻⁸⁵ NEMD is required the temperature gradient to calculate the thermal conductivity, and it might contain nonlinear effects.⁸² Even though both EMD and NEMD have finite size effects, it occurs much more severe in NEMD because of the presence of interfaces at the heat source and sink.⁸⁶ Moreover, EMD is more useful for the systems with periodic boundary conditions since EMD predicts the thermal conductivity in all directions at one simulation, whereas NEMD is needed the thermal gradients for every direction.⁸⁶

The Green-Kubo is an useful formula to study the transport phenomena and the thermal conductivity is determined from integrating the autocorrelation function of the heat current of a system in thermodynamic equilibrium simulations of atomic systems.⁸⁷ The thermal conductivity is calculated in EMD as a result of the fluctuation dissipation and linear response theorem.⁸⁶ Local fluctuation dissipates are considered as perturbations to the local thermal equilibrium since there is no external disturbance. The local fluctuation heats the atom and in the equilibrium states, the heat flow in a system of particles fluctuates around zero. All atoms are having the same energy level and converges which means to have no energy exchange between atoms. The heat flux vectors and their correlations, the Heat Auto-Correlation Functions (HACF), decays to zero with the time and used through the Green-Kubo relations. Green-Kubo theorem relies on relating the integral of the autocorrelation function of the heat current $J(t)$ in equilibrium.

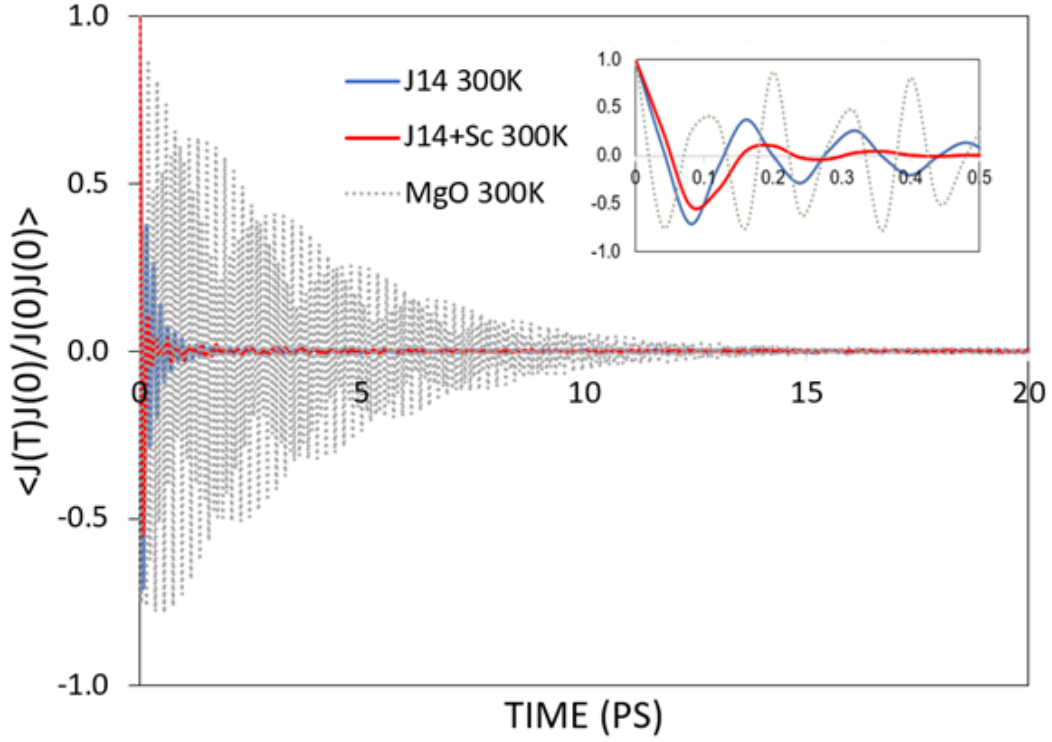


Figure 1.4 Time dependence of the heat auto correlation function in J14, J14+Sc and MgO at 300K.

For the case of heat transport, the thermal conductivity from Green-Kubo formula is expressed by,

$$k_{ij} = \frac{1}{VK_B T^2} \int_0^\tau \langle J_i(0)J_j(t) \rangle dt \quad (1.2.1)$$

where k is the thermal conductivity, V is the system volume, K_B is the Boltzmann's constant, T is the temperature, τ is the time needed for HACF decay, i, j is $x, y,$ or z directions, $J_i(0)$ and $J_j(t)$ are the instantaneous heat flux in the j direction at time zero and in the i direction at time t . Total heat current in the system is

$$J(t) = \int j(x,t)dx \quad (1.2.2)$$

where $j(x,t)$ is the heat flux density.

The figure 1.4 shows the corresponding HACF decay to indicate the thermal conductivity convergence. In this dissertation, the heat flux is obtained with the Buckingham potential for the short range interaction and the Ewald summation method for the long range interaction. The details of the system potentials will be discussed later chapter.

1.3 Density Functional Theory

Density Functional Theory (DFT) is one of the standard computational tools in condensed matter, chemistry, and biochemistry in academia and industry. It provides descriptions of electronic structure and enables to perform the calculation of total energies and forces for the structure, thermodynamics and kinetics prediction.

Many body Schrodinger equation is the fundamental equation in a quantum mechanics. The linear partial differential equation describes the wave function of coordinates of all electrons and ions to predict structural, electronic, optical, vibrational, and thermodynamic properties of molecules, surfaces and bulk materials.

The many body wavefunction represents the coordinates in the configuration space of electrons, becomes a function of $3N$ variables that are nuclear, electronic and mixed. Practically, the many body Schrodinger equation is not tractable to solve the properties of many materials with even today's supercomputer powers.

The variational principle is a basic technique used to solve the Schrodinger equation. The Born-Oppenheimer approximation assumes that the nuclei moves limitedly in a fixed position

while the electrons are relaxed to their position, since the nuclei is a lot heavier than the electrons. So, it simplifies the Hamiltonian into three parts: the kinetic energy of electrons, the potential between electrons and the nucleus, and the potential between electrons. The electronic wave function is independent from the nuclear coordinate and needs to be solved. However, solving the electronic wave function using the existing several methods, such as the Hartree-Fock method requires massive computational effort and disregards the correlation energy between electrons.

Hohenberg and Kohn⁸⁸ developed the ground state of an interacting electrons gas in an external potential which there exists a universal functional of the electron density $F[n(r)]$. This means that it applies to all electronic systems in their ground state no matter what the external potential is. However, Hohenberg-Kohn demonstrated a theory of the electronic ground state in two limiting cases: 1. a nearly constant density, and 2. slowly varying density, which actual electron systems do not belong either of cases.

In the following year, Kohn and Sham⁸⁹ developed the approximation method for treating an inhomogeneous system of interacting electrons. Kohn-Sham equation generates the same electron densities of the many electron and single electron systems, since the approximation replaces the many electron Schrodinger equation with a single non interacting particle expression in the single electron orbitals and an effective potential. The Kohn-Sham kinetic energy of non interacting particles is expressed in terms of the Kohn-Sham orbitals by a Slater determinant. All unknowns in the Kohn-Sham approach is mapped in the exchange-correlation potential.

Even though the Kohn-Sham equation is grouped the all unknowns into the exchange-correlation functional, it is a challenge to solve the exchange-correlation functional as a function of electron density. The exchange-correlation functional is certain in the case of uniform electron

gas. The properties of the uniform electron gas purely depend on the constant electronic density at the ground state. So, there was an approach to assume that the unknown functional is the same to the uniform electron gas where the electron density is a uniform quantity. This approach is called Local Density Approximation (LDA). In addition to approximate the local electron density, how the electron density varies in space needs to be considered in an approximation for more sophisticated systems. This approach is known as the Generalized Gradient Approximation (GGA).

Once the exchange-correlation approximation has been properly selected, the Kohn-Sham equation can be solved. There can be an approximation applied for the systems having the large number of electrons because it causes huge computational power. This approximation considers only the valence electrons for electronic interactions with the fixed core electrons. The valence electrons can only relax in the calculations. This method is called pseudopotentials. The calculations in density functional theory became greatly faster giving fairly similar results as the those using full electron potentials.

The Kohn-Sham wave function is decomposed in the plane wave basis set. From Bloch's theorem^{90,91}, the periodic function at each k-point can be expanded in an infinite number of plane wave functions. The plane waves with small kinetic energies are more important than those with large kinetic energies because lower kinetic energies have much larger contribution to the overall energy. The cut off energy is used to truncate the plane wave expansion. The total energy convergence test is necessary in order to validate the cut off energy for the systems.

DFT calculations of the high entropy carbides in this study were performed using Vienna Ab initio Simulation Package (VASP).⁹²⁻⁹⁴ It is one of the computational software that uses DFT to solve the quantum problem for the materials. The pseudopotential and the exchange and

correlation functionals are implemented in VASP. All systems are computed in a periodic boundary condition and VASP uses a plane wave basis set is used to solve the Kohn-Sham wave function. In this thesis, the calculations were carried out using plane wave PAW pseudopotential method^{94,95} and the generalized gradient approximation as parameterized by Perdew et al.⁹⁶ was used for the exchange-correlation potential. The calculation details will be explained in the later chapters.

The metals of the high entropy oxides and carbides are randomly distributed. The disordered metal elements in these solid solutions are modelled with the Special Quasi-random Structure (SQS) method.⁹⁷ The Alloy Theoretic Automated Toolkit (ATAT)^{98,99} is used to generate SQS structures. Basic idea of creating SQS is to build a periodic structure of a small number of atoms per unit cell that meets the correlation function for the first few nearest neighbor shells are close to those of a target random alloy as possible. Generally, interactions between far located neighbors are contributing little to the system energy compare to between near neighbors. Therefore, a SQS can be considered as the best possible structure representing a given randomness.

References

1. Cantor, B., Chang, I. T. H., Knight, P. & Vincent, A. J. B. Microstructural development in equiatomic multicomponent alloys. *Mater. Sci. Eng. A* (2004). doi:10.1016/j.msea.2003.10.257
2. Yeh, J. W. *et al.* Nanostructured high-entropy alloys with multiple principal elements: Novel alloy design concepts and outcomes. *Adv. Eng. Mater.* (2004). doi:10.1002/adem.200300567
3. Senkov, O. N., Wilks, G. B., Scott, J. M. & Miracle, D. B. Mechanical properties of Nb₂₅Mo₂₅Ta₂₅W₂₅ and V₂₀Nb₂₀Mo₂₀Ta₂₀W₂₀ refractory high entropy alloys. *Intermetallics* (2011). doi:10.1016/j.intermet.2011.01.004
4. Feuerbacher, M., Heidelmann, M. & Thomas, C. Hexagonal High-entropy Alloys. *Mater. Res. Lett.* (2014). doi:10.1080/21663831.2014.951493
5. Takeuchi, A., Amiya, K., Wada, T., Yubuta, K. & Zhang, W. High-Entropy Alloys with a Hexagonal Close-Packed Structure Designed by Equi-Atomic Alloy Strategy and Binary Phase Diagrams. *JOM* (2014). doi:10.1007/s11837-014-1085-x
6. Middleburgh, S. C., King, D. M. & Lumpkin, G. R. Atomic scale modelling of hexagonal structured metallic fission product alloys. *R. Soc. Open Sci.* (2015). doi:10.1098/rsos.140292
7. Yeh, J. W., Chen, Y. L., Lin, S. J. & Chen, S. K. High-entropy alloys - A new era of exploitation. in *Materials Science Forum* (2007). doi:10.4028/www.scientific.net/msf.560.1
8. Guo, S., Hu, Q., Ng, C. & Liu, C. T. More than entropy in high-entropy alloys: Forming solid solutions or amorphous phase. *Intermetallics* (2013). doi:10.1016/j.intermet.2013.05.002
9. Hume-Rothery, W., Mabbott, G. W. & Evans, K. M. C. The Freezing Points, Melting Points, and Solid Solubility Limits of the Alloys of Silver, and Copper with the Elements of the B Sub-Groups. *Philos. Trans. R. Soc. A Math. Phys. Eng. Sci.* (1934). doi:10.1098/rsta.1934.0014
10. Hume-Rothery, W. Atomic diameters, atomic volumes and solid solubility relations in alloys. *Acta Metall.* (1966). doi:10.1016/0001-6160(66)90267-7

11. Wang, Z., Huang, Y., Liu, C. T., Li, J. & Wang, J. Atomic packing and size effect on the Hume-Rothery rule. *Intermetallics* (2019). doi:10.1016/j.intermet.2019.04.001
12. Hume-Rothery, W. & Coles, B. R. The transition metals and their alloys. *Adv. Phys.* (1954). doi:10.1080/00018735400101193
13. Tsai, M. H. Physical properties of high entropy alloys. *Entropy* (2013). doi:10.3390/e15125338
14. Tsai, M. H. & Yeh, J. W. High-entropy alloys: A critical review. *Mater. Res. Lett.* (2014). doi:10.1080/21663831.2014.912690
15. Zhang, Y. *et al.* Microstructures and properties of high-entropy alloys. *Progress in Materials Science* (2014). doi:10.1016/j.pmatsci.2013.10.001
16. Zhang, M. C. G.-W. Y. K. L. *High-entropy Alloys : Fundamentals and Applications.* (Springer Publishing Co., New York, NY, 2016).
17. B.S. Murty, J.-W. Yeh, S. R. *High-entropy Alloys.* (2019).
18. Yeh, J. W. Recent progress in high-entropy alloys. *Ann. Chim. Sci. des Mater.* (2006). doi:10.3166/acsm.31.633-648
19. Zhou, Y. J., Zhang, Y., Wang, Y. L. & Chen, G. L. Solid solution alloys of AlCoCrFeNi Tix with excellent room-temperature mechanical properties. *Appl. Phys. Lett.* (2007). doi:10.1063/1.2734517
20. Zhang, Y., Zhou, Y. J., Lin, J. P., Chen, G. L. & Liaw, P. K. Solid-solution phase formation rules for multi-component alloys. *Adv. Eng. Mater.* (2008). doi:10.1002/adem.200700240
21. Tong, C. J. *et al.* Microstructure characterization of Al_xCoCrCuFeNi high-entropy alloy system with multiprincipal elements. *Metall. Mater. Trans. A Phys. Metall. Mater. Sci.* (2005). doi:10.1007/s11661-005-0283-0
22. Tong, C. J. *et al.* Mechanical performance of the Al_xCoCrCuFeNi high-entropy alloy system with multiprincipal elements. in *Metallurgical and Materials Transactions A: Physical Metallurgy and Materials Science* (2005). doi:10.1007/s11661-005-0218-9
23. Li, Z., Zhao, S., Ritchie, R. O. & Meyers, M. A. Mechanical properties of high-entropy alloys with emphasis on face-centered cubic alloys. *Progress in Materials Science* (2019). doi:10.1016/j.pmatsci.2018.12.003
24. Wang, F., Zhang, Y., Chen, G. & Davies, H. A. Tensile and compressive mechanical

- behavior of a CoCrCuFeNiAl_{0.5} high entropy alloy. in *International Journal of Modern Physics B* (2009). doi:10.1142/s0217979209060774
25. Otto, F. *et al.* The influences of temperature and microstructure on the tensile properties of a CoCrFeMnNi high-entropy alloy. *Acta Mater.* (2013). doi:10.1016/j.actamat.2013.06.018
 26. Harrington, T. J. *et al.* Phase stability and mechanical properties of novel high entropy transition metal carbides. *Acta Mater.* (2019). doi:10.1016/j.actamat.2018.12.054
 27. Kao, Y. F. *et al.* Electrical, magnetic, and Hall properties of Al_xCoCrFeNi high-entropy alloys. *J. Alloys Compd.* (2011). doi:10.1016/j.jallcom.2010.10.210
 28. Chou, H. P., Chang, Y. S., Chen, S. K. & Yeh, J. W. Microstructure, thermophysical and electrical properties in Al_xCoCrFeNi (0 ≤ x ≤ 2) high-entropy alloys. *Mater. Sci. Eng. B Solid-State Mater. Adv. Technol.* (2009). doi:10.1016/j.mseb.2009.05.024
 29. Zhang, Y., Zuo, T., Cheng, Y. & Liaw, P. K. High-entropy alloys with high saturation magnetization, electrical resistivity, and malleability. *Sci. Rep.* (2013). doi:10.1038/srep01455
 30. Zuo, T. T., Li, R. B., Ren, X. J. & Zhang, Y. Effects of Al and Si addition on the structure and properties of CoFeNi equal atomic ratio alloy. *J. Magn. Magn. Mater.* (2014). doi:10.1016/j.jmmm.2014.07.023
 31. Singh, S., Wanderka, N., Kiefer, K., Siemensmeyer, K. & Banhart, J. Effect of decomposition of the Cr-Fe-Co rich phase of AlCoCrCuFeNi high entropy alloy on magnetic properties. *Ultramicroscopy* (2011). doi:10.1016/j.ultramic.2010.12.001
 32. Tariq, N. H., Naeem, M., Hasan, B. A., Akhter, J. I. & Siddique, M. Effect of W and Zr on structural, thermal and magnetic properties of AlCoCrCuFeNi high entropy alloy. *J. Alloys Compd.* (2013). doi:10.1016/j.jallcom.2012.12.095
 33. Wang, J., Zheng, Z., Xu, J. & Wang, Y. Microstructure and magnetic properties of mechanically alloyed FeSiBAlNi (Nb) high entropy alloys. *J. Magn. Magn. Mater.* (2014). doi:10.1016/j.jmmm.2013.11.049
 34. Gludovatz, B. *et al.* A fracture-resistant high-entropy alloy for cryogenic applications. *Science* (80-.). (2014). doi:10.1126/science.1254581
 35. Tsai, M. H., Wang, C. W., Lai, C. H., Yeh, J. W. & Gan, J. Y. Thermally stable amorphous (AlMoNbSiTaTiVZr)₅₀N₅₀ nitride film as diffusion barrier in copper

- metallization. *Appl. Phys. Lett.* (2008). doi:10.1063/1.2841810
36. Chang, S. Y., Chen, M. K. & Chen, D. S. Multiprincipal-element AlCrTaTiZr-nitride nanocomposite film of extremely high thermal stability as diffusion barrier for Cu metallization. *J. Electrochem. Soc.* (2009). doi:10.1149/1.3097186
 37. Kao, Y. F. *et al.* Hydrogen storage properties of multi-principal-component CoFeMnTi_xVyZr_z alloys. *Int. J. Hydrogen Energy* (2010). doi:10.1016/j.ijhydene.2010.06.012
 38. Kuncce, I., Polanski, M. & Bystrzycki, J. Structure and hydrogen storage properties of a high entropy ZrTiVCrFeNi alloy synthesized using Laser Engineered Net Shaping (LENS). *Int. J. Hydrogen Energy* (2013). doi:10.1016/j.ijhydene.2013.05.071
 39. Tsai, C. F., Wu, P. W., Lin, P., Chao, C. G. & Yeh, K. Y. Sputter deposition of multi-element nanoparticles as electrocatalysts for methanol oxidation. *Jpn. J. Appl. Phys.* (2008). doi:10.1143/JJAP.47.5755
 40. Çınar, E., Koçyiğit, S., Aytimur, A., Uslu, I. & Akdemir, A. Synthesis, characterization, and thermoelectric properties of electrospun boron-doped barium-stabilized bismuth-cobalt oxide nanoceramics. *Metall. Mater. Trans. A Phys. Metall. Mater. Sci.* (2014). doi:10.1007/s11661-014-2343-9
 41. Zinkle, S. J. & Snead, L. L. Designing Radiation Resistance in Materials for Fusion Energy. *Annu. Rev. Mater. Res.* (2014). doi:10.1146/annurev-matsci-070813-113627
 42. Gorr, B. *et al.* Phase equilibria, microstructure, and high temperature oxidation resistance of novel refractory high-entropy alloys. *J. Alloys Compd.* (2015). doi:10.1016/j.jallcom.2014.11.012
 43. Firstov, S. A. *et al.* Thermal Stability of Superhard Nitride Coatings from High-Entropy Multicomponent Ti–V–Zr–Nb–Hf Alloy. *Powder Metall. Met. Ceram.* (2014).
 44. Mohamed Elbakhshwan, William Doniger, Cody Falconer, Michael Moorehead, Calvin Parkin, Chuan Zhang, K. S. & A. C. Corrosion and Thermal Stability of CrMnFeNi High Entropy Alloy in Molten FLiBe Salt. *Sci. Rep.* **9**, (2019).
 45. Pacheco, V. *et al.* Thermal Stability of the HfNbTiVZr High-Entropy Alloy. *Inorg. Chem.* (2019). doi:10.1021/acs.inorgchem.8b02957
 46. Tilley, R. Understanding Solids; The Science of Materials. *Mater. Technol.* (2004). doi:10.1080/10667857.2004.11753095
 47. Rost, C. M. *et al.* Entropy-stabilized oxides. *Nat. Commun.* **6**, 8485 (2015).

48. Chen, K. *et al.* A five-component entropy-stabilized fluorite oxide. *J. Eur. Ceram. Soc.* (2018). doi:10.1016/j.jeurceramsoc.2018.04.063
49. Sarkar, A. *et al.* Rare earth and transition metal based entropy stabilised perovskite type oxides. *J. Eur. Ceram. Soc.* (2018). doi:10.1016/j.jeurceramsoc.2017.12.058
50. Bérardan, D., Franger, S., Dragoe, D., Meena, A. K. & Dragoe, N. Colossal dielectric constant in high entropy oxides. *Phys. Status Solidi - Rapid Res. Lett.* (2016). doi:10.1002/pssr.201600043
51. Chen, H. *et al.* Entropy-stabilized metal oxide solid solutions as CO oxidation catalysts with high-temperature stability. *J. Mater. Chem. A* (2018). doi:10.1039/c8ta01772g
52. Hong, W. *et al.* Microstructural evolution and mechanical properties of (Mg,Co,Ni,Cu,Zn)O high-entropy ceramics. *J. Am. Ceram. Soc.* (2019). doi:10.1111/jace.16075
53. Braun, J. L. *et al.* Charge-induced disorder controls the thermal conductivity of entropy-stabilized oxides. *Adv. Mater.* (2018). doi:10.1002/adma.201805004
54. Sarkar, A. *et al.* Multicomponent equiatomic rare earth oxides with a narrow band gap and associated praseodymium multivalency. *Dalt. Trans.* (2017). doi:10.1039/c7dt02077e
55. Sarkar, A. *et al.* High-Entropy Oxides: Fundamental Aspects and Electrochemical Properties. *Adv. Mater.* (2019). doi:10.1002/adma.201806236
56. Gild, J. *et al.* High-entropy fluorite oxides. *J. Eur. Ceram. Soc.* (2018). doi:10.1016/j.jeurceramsoc.2018.04.010
57. Meisenheimer, P. B., Kratochil, T. J. & Heron, J. T. Giant enhancement of exchange coupling in entropy-stabilized oxide heterostructures. *Sci. Rep.* (2017). doi:10.1038/s41598-017-13810-5
58. Gild, J. *et al.* High-Entropy Metal Diborides: A New Class of High-Entropy Materials and a New Type of Ultrahigh Temperature Ceramics. *Sci. Rep.* (2016). doi:10.1038/srep37946
59. Tallarita, G., Licheri, R., Garroni, S., Orrù, R. & Cao, G. Novel processing route for the fabrication of bulk high-entropy metal diborides. *Scr. Mater.* (2019). doi:10.1016/j.scriptamat.2018.08.039
60. Zhang, Y. *et al.* Dense high-entropy boride ceramics with ultra-high hardness. *Scr. Mater.* (2019). doi:10.1016/j.scriptamat.2019.01.021
61. Castle, E., Csanádi, T., Grasso, S., Dusza, J. & Reece, M. Processing and Properties of

- High-Entropy Ultra-High Temperature Carbides. *Sci. Rep.* (2018). doi:10.1038/s41598-018-26827-1
62. Dusza, J. *et al.* Microstructure of (Hf-Ta-Zr-Nb)C high-entropy carbide at micro and nano/atomic level. *J. Eur. Ceram. Soc.* (2018). doi:10.1016/j.jeurceramsoc.2018.05.006
 63. Sarker, P. *et al.* High-entropy high-hardness metal carbides discovered by entropy descriptors. *Nat. Commun.* (2018). doi:10.1038/s41467-018-07160-7
 64. Yang, K., Oses, C. & Curtarolo, S. Modeling off-stoichiometry materials with a high-throughput ab-initio approach. *Chem. Mater.* (2016). doi:10.1021/acs.chemmater.6b01449
 65. Hermans, J., Berendsen, H. J. C., Van Gunsteren, W. F. & Postma, J. P. M. A consistent empirical potential for water–protein interactions. *Biopolymers* (1984). doi:10.1002/bip.360230807
 66. MacKerell, A. D., Wiórkiewicz-Kuczera, J., Karplus, M. & MacKerell, A. D. An All-Atom Empirical Energy Function for the Simulation of Nucleic Acids. *J. Am. Chem. Soc.* (1995). doi:10.1021/ja00153a017
 67. Ott, K. H. & Meyer, B. Parametrization of GROMOS force field for oligosaccharides and assessment of efficiency of molecular dynamics simulations. *J. Comput. Chem.* (1996). doi:10.1002/(SICI)1096-987X(199606)17:8<1068::AID-JCC14>3.0.CO;2-A
 68. Kaminski, G. A., Friesner, R. A., Tirado-Rives, J. & Jorgensen, W. L. Evaluation and reparametrization of the OPLS-AA force field for proteins via comparison with accurate quantum chemical calculations on peptides. *J. Phys. Chem. B* (2001). doi:10.1021/jp003919d
 69. MacKerell, A. D. *et al.* All-atom empirical potential for molecular modeling and dynamics studies of proteins. *J. Phys. Chem. B* (1998). doi:10.1021/jp973084f
 70. Cornell, W. D. *et al.* A 2nd Generation Force-Field for the Simulation of Proteins, Nucleic-Acids, and Organic-Molecules. *J. Am. Chem. Soc.* (1995).
 71. Dodson, B. W. Evaluation of the Stillinger-Weber classical interaction potential for tetragonal semiconductors in nonideal atomic configurations. *Phys. Rev. B* (1986). doi:10.1103/PhysRevB.33.7361
 72. Daw, M. S. & Baskes, M. I. Embedded-atom method: Derivation and application to impurities, surfaces, and other defects in metals. *Phys. Rev. B* (1984). doi:10.1103/PhysRevB.29.6443

73. Daw, M. S., Foiles, S. M. & Baskes, M. I. The embedded-atom method: a review of theory and applications. *Materials Science Reports* (1993). doi:10.1016/0920-2307(93)90001-U
74. Tersoff, J. New empirical approach for the structure and energy of covalent systems. *Phys. Rev. B* (1988). doi:10.1103/PhysRevB.37.6991
75. Tersoff, J. Modeling solid-state chemistry: Interatomic potentials for multicomponent systems. *Phys. Rev. B* (1989). doi:10.1103/PhysRevB.39.5566
76. Van Duin, A. C. T., Dasgupta, S., Lorant, F. & Goddard, W. A. ReaxFF: A reactive force field for hydrocarbons. *J. Phys. Chem. A* (2001). doi:10.1021/jp004368u
77. Shan, T. R., Devine, B. D., Kemper, T. W., Sinnott, S. B. & Phillpot, S. R. Charge-optimized many-body potential for the hafnium/hafnium oxide system. *Phys. Rev. B - Condens. Matter Mater. Phys.* (2010). doi:10.1103/PhysRevB.81.125328
78. Liang, T. *et al.* Classical atomistic simulations of surfaces and heterogeneous interfaces with the charge-optimized many body (COMB) potentials. *Materials Science and Engineering R: Reports* (2013). doi:10.1016/j.mser.2013.07.001
79. Plimpton, S. Fast parallel algorithms for short-range molecular dynamics. *J. Comput. Phys.* (1995). doi:10.1006/jcph.1995.1039
80. Green, M. S. Markoff random processes and the statistical mechanics of time-dependent phenomena. II. Irreversible processes in fluids. *J. Chem. Phys.* (1954). doi:10.1063/1.1740082
81. Kubo, R. Statistical' Mechanical Theory of Irreversible Processes. I. General Theory and Simple Applications to Magnetic and Conduction Problems. *J. Phys. Soc. Japan* (1957). doi:10.1143/JPSJ.12.570
82. Schelling, P. K., Phillpot, S. R. & Keblinski, P. Comparison of atomic-level simulation methods for computing thermal conductivity. *Phys. Rev. B - Condens. Matter Mater. Phys.* (2002). doi:10.1103/PhysRevB.65.144306
83. Jund, P. & Jullien, R. Molecular-dynamics calculation of the thermal conductivity of vitreous silica. *Phys. Rev. B - Condens. Matter Mater. Phys.* (1999). doi:10.1103/PhysRevB.59.13707
84. Che, J., Çağın, T., Deng, W. & Goddard, W. A. Thermal conductivity of diamond and related materials from molecular dynamics simulations. *J. Chem. Phys.* (2000).

doi:10.1063/1.1310223

85. Tretiakov, K. V. & Scandolo, S. Thermal conductivity of solid argon from molecular dynamics simulations. *J. Chem. Phys.* (2004). doi:10.1063/1.1642611
86. Khadem, M. H. & Wemhoff, A. P. Comparison of Green-Kubo and NEMD heat flux formulations for thermal conductivity prediction using the Tersoff potential. *Comput. Mater. Sci.* (2013). doi:10.1016/j.commatsci.2012.12.016
87. Kundu, A., Dhar, A. & Narayan, O. The Green-Kubo formula for heat conduction in open systems. *J. Stat. Mech. Theory Exp.* (2009). doi:10.1088/1742-5468/2009/03/L03001
88. Hohenberg, P. & Kohn, W. Inhomogeneous electron gas. *Phys. Rev.* (1964). doi:10.1103/PhysRev.136.B864
89. Kohn, W. & Sham, L. J. Self-consistent equations including exchange and correlation effects. *Phys. Rev.* (1965). doi:10.1103/PhysRev.140.A1133
90. Bochner, S. Bloch's theorem for real variables. *Bulletin of the American Mathematical Society* (1946). doi:10.1090/S0002-9904-1946-08640-1
91. Landau, E. Über die Blochsche Konstante und zwei verwandte Weltkonstanten. *Math. Zeitschrift* (1929). doi:10.1007/BF01187791
92. Kresse, G. & Furthmüller, J. Efficient iterative schemes for ab initio total-energy calculations using a plane-wave basis set. *Phys. Rev. B - Condens. Matter Mater. Phys.* (1996). doi:10.1103/PhysRevB.54.11169
93. Kresse, G. & Hafner, J. Ab initio molecular dynamics for liquid metals. *Phys. Rev. B* (1993). doi:10.1103/PhysRevB.47.558
94. Kresse, G. & Furthmüller, J. Efficiency of ab-initio total energy calculations for metals and semiconductors using a plane-wave basis set. *Comput. Mater. Sci.* (1996). doi:10.1016/0927-0256(96)00008-0
95. Nosé, S. A unified formulation of the constant temperature molecular dynamics methods. *J. Chem. Phys.* (1984). doi:10.1063/1.447334
96. Perdew, J. P., Burke, K. & Ernzerhof, M. Generalized gradient approximation made simple. *Phys. Rev. Lett.* (1996). doi:10.1103/PhysRevLett.77.3865
97. Zunger, A., Wei, S. H., Ferreira, L. G. & Bernard, J. E. Special quasirandom structures. *Phys. Rev. Lett.* (1990). doi:10.1103/PhysRevLett.65.353
98. van de Walle, A. Multicomponent multisublattice alloys, nonconfigurational entropy and

other additions to the Alloy Theoretic Automated Toolkit. *Calphad Comput. Coupling Phase Diagrams Thermochem.* (2009). doi:10.1016/j.calphad.2008.12.005

99. Van de Walle, A., Asta, M. & Ceder, G. The alloy theoretic automated toolkit: A user guide. *Calphad Comput. Coupling Phase Diagrams Thermochem.* (2002). doi:10.1016/S0364-5916(02)80006-2

Chapter 2. Influence of mass and charge disorder on the phonon thermal conductivity of entropy stabilized oxides determined by molecular dynamics simulations

Published in Journal of Applied Physics, 01 February (2019) DOI: 10.1063/1.5080419

M. Lim,¹ Zs. Rak,¹ J. L. Braun,² C. M. Rost,² G. N. Kotsonis,⁵ P. E. Hopkins,^{2,3,4} J-P. Maria,⁵ and D. W. Brenner¹

¹*Department of Materials Science and Engineering, North Carolina State University, Raleigh, North Carolina 27695-7907, USA*

²*Department of Mechanical and Aerospace Engineering, University of Virginia, Charlottesville, Virginia 22904, USA*

³*Department of Materials Science and Engineering, University of Virginia, Charlottesville, Virginia 22904, USA*

⁴*Department of Physics, University of Virginia, Charlottesville, Virginia 22904, USA*

⁵*Department of Materials Science and Engineering, Pennsylvania State University, State College, Pennsylvania, 16802.*

2.1 Abstract

It is shown using classical molecular dynamics simulations that phonon scattering from disorder in the interatomic forces introduced by charge transfer and not from mass disorder is needed to explain the thermal conductivity reduction measured experimentally that accompanies the addition of a sixth cation to the entropy stabilized oxide J14 ($\text{Mg}_{0.1}\text{Co}_{0.1}\text{Ni}_{0.1}\text{Cu}_{0.1}\text{Zn}_{0.1}\text{O}_{0.5}$). The simulations were performed on five entropy-stabilized oxides, J14, and J14 plus Sc, Sn, Cr or Ge in equi-molar cation proportions. Comparing the simulation results to predictions from the Bridgeman equation using properties from the simulations suggest that despite phonon scattering from disorder in both atomic forces and mass, the thermal conductivity for these systems is still above an analytical limit for an amorphous structure.

2.2 Introduction

High entropy alloys can be defined as having a composition of five or more approximately equimolar principle elements that are randomly arranged on a crystalline lattice.¹⁻³ These materials were developed primarily within the metal alloy community, where it was recognized that they could be designed such that mixing entropy is a major contributor to stability. Inspired by that work, Rost *et al.* demonstrated the solid state and vapor synthesis of a new class of high entropy material, entropy stabilized oxides, in which the cation sublattice in a rocksalt structure is randomly populated by five elements.⁴ Following this seminal paper, several other high-entropy ceramics have been reported that have mixed single component/multicomponent sublattices.⁵⁻¹³

The original rocksalt composition studied by Rost *et al.*⁴, termed J14, was $(\text{Mg}_{0.1}\text{Co}_{0.1}\text{Ni}_{0.1}\text{Cu}_{0.1}\text{Zn}_{0.1})\text{O}_{0.5}$. This choice of composition satisfied several criteria thought to be important for both promoting and proving entropy stabilization. These criteria included similar formal charges and ionic radii, limited immiscibility for some of the binary pairs and some of the lowest energy binary oxide structures not being rocksalt. For example, the wurtzite rather than the rocksalt structure is most stable for ZnO. Subsequent studies demonstrated that other elements can be introduced into the J14 cation sublattice at equimolar concentrations that do not necessarily have radii and formal charges similar to the ions in J14. These elements include Sc, Cr, Sb, Ge, Sn, Li, Ga and Ca.^{5,6,14}

Bader charges from Density Functional Theory (DFT) calculations have been used to probe how charge is compensated with the addition of Sc (+3 oxidation state) or Li (+1 oxidation state) into the J14 cation sublattice.¹⁵ It was found that adding Sc reduces a majority of Cu

cations and a few Co and Ni cations, while adding Li oxidizes some of the Co cations as well as some Ni and Cu cations. DFT has also been used to validate conclusions based on EXAFS data that a majority of the lattice distortion in J14 is taken up by the oxygen sublattice,¹⁶ and that the Cu may show Jahn-Teller distortions involving axial expansion or contraction depending on the relative positions of the Cu cations in the lattice.¹⁷

Being an electrical insulator with relatively large mass disorder, J14 should have a relatively small thermal conductivity that is dominated by phonon heat transport. Recent experimental measurements by Braun *et al.* have confirmed this expectation,¹⁸ but also revealed an unanticipated trend. Traditional heat transport theory suggests that mass scattering should saturate by the addition of the five distinct cations at equimolar concentrations within a high-entropy oxide,¹⁹ yet experimental measurements showed that the thermal conductivity of J14 is further (and substantially) reduced by the addition of a sixth cation – Sc, Sn, Cr or Ge – in an equi-molar proportion. Molecular dynamics simulations using Lennard-Jones potentials suggested that disorder in the inter-atomic forces can potentially explain the further drop in thermal conductivity in these systems,^{19–21} a result that is supported by scattering theory and further analysis of the experimental data.¹⁸ Lennard-Jones potentials, however, are not in general a good approximation to forces in oxides, which are dominated by long-range Coulombic forces, and therefore the physical origin of any inter-atomic force disorder is unclear from these studies.

In this paper we report the results from a series of molecular dynamics simulations of J14, and J14+Sc, Sn, Cr or Ge using the Green-Kubo method^{22–24} for calculating phonon-mediated thermal conductivity. The simulations use a Buckingham potential energy function plus Coulombic electrostatic forces from atom-centered fixed partial charges. To model the randomness introduced by the charge transfer predicted by DFT within the disordered system,

the partial charges were assigned to DFT Bader charges.¹⁵ The remaining parameters in the Buckingham potential were taken unmodified from a literature potential for MgO.²⁵ The simulations show a decrease in thermal conductivity with the introduction of a sixth cation in J14, in agreement with experiment. Furthermore, by manipulating the masses and charges in the simulations, it is shown that while both mass and charge disorder can lower the thermal conductivity with addition of a sixth cation, the thermal conductivity lowering can be largely reproduced with disorder in interatomic forces from the charges without an accompanying mass disorder. We also show that when parameterized to the simulations, thermal conductivities from the Bridgman equation, which has been used for ionic liquids where scattering lengths are of the order of inter-atomic distances,²⁶ are significantly lower than those from the MD simulations. This result suggests that the thermal conductivities of these entropy stabilized oxides are still above an amorphous limit for these systems.

2.3 Methodology

Molecular dynamics simulations were carried out using the LAMMPS modeling code²⁷ with thermal conductivity calculated using the Green-Kubo method.²²⁻²⁴ The interatomic potential was modeled using a pair sum of an exponential-6 function plus long-range Coulomb interactions of the form

$$U = \sum_{i=1}^{N-1} \sum_{j=i+1}^N \left[A_{ij} \exp\left(-\frac{r_{ij}}{\rho}\right) - \frac{C_{ij}}{r_{ij}^6} + \frac{q_i q_j}{4\pi\epsilon_0 r_{ij}} \right] \quad (2.3.1)$$

where N is the total number of atoms, ρ is a parameter, r_{ij} is the distance between atoms i and j , and A_{ij} , and C_{ij} are parameters that depend on atoms i and j , and q_i is the charge centered on atom i . The charges were set equal to the Bader charges from DFT calculations on supercells as described below. The other parameters A_{ij} , ρ and C_{ij} , for the short ranged repulsive interactions were taken unmodified from a literature potential that was parameterized to model MgO structure and thermal-mechanical properties, including the experimental room temperature lattice constant, thermal expansion coefficient and bulk modulus.²⁵ The Bader charge from the DFT calculations on MgO was +/- 1.7q, which is the same charge reported in reference²⁵ from their fitting procedure. This interatomic potential model allows us to capture not only the randomness of the atomic masses, but also the randomness of the oxygen and cation charges (including charge transfer) as given by DFT.

The DFT calculations were carried out on supercells that were sufficiently large to allow a random population of cations on the face-centered cubic sublattice within the rocksalt structure. For the MD simulations, these supercells were replicated with corresponding periodic boundaries to create larger systems. The DFT supercells contained 240 oxygen anions and 240 cations. There are 8 atoms in the rocksalt unit cell, which was replicated 3X4X5 to make a 480 atom supercell with equimolar metal contents. The arrangement of the latter was generated using the special quasi-random structure algorithm.²⁸ J14 has five different cations so that each DFT unit cell had 48 of each cation type. The other compositions contained six different cation types and therefore 40 of each type in the DFT unit cell. The DFT calculations were carried out using plane wave PAW pseudopotential methods as implemented in VASP²⁹⁻³³. The computational parameters are described in detail in reference¹⁵. The atom positions were held fixed on a

rocksalt lattice while the total energy was minimized with respect to lattice constant. The final atom positions and calculated Bader charges for each DFT supercell are given in the appendix.

The MD simulations used 4x4x4 replicates of the DFT unit cells for a total of 30720 atoms. For the MD simulations the potential energy was first minimized with respect to atom positions and lattice constant, followed by equilibration at zero pressure and 300 K for 32 picoseconds using the Nose-Hoover method with a 4 fs time step.^{34,35} After equilibration, the equations of motion were integrated at constant energy for 20 ns, over which heat current autocorrelation functions were generated for calculating thermal conductivity. Based on the decay of the autocorrelation functions and the change in calculated thermal conductivity with simulation time, it was determined that this procedure produces converged values of both properties.

2.4 Simulation Results and Discussion

Given in Table 2.1 and plotted in Figure 2.1 are thermal conductivities measured experimentally¹⁸, calculated from the MD simulations, and given by the Bridgeman equation discussed below. Both the experiment and MD simulations show a roughly order of magnitude drop in thermal conductivity for J14 compared to MgO, with a further but less dramatic drop with the addition of a sixth cation to J14. For the experiment, the latter is reduced from 3 W/m-K to an average of about 1.6 W/m-K, a drop of about 50%. The corresponding reduction from the MD simulations is from 4.9 W/m-K to an average of 3.2 W/m-K, or a drop of about 35% from the simulated thermal conductivity of J14.

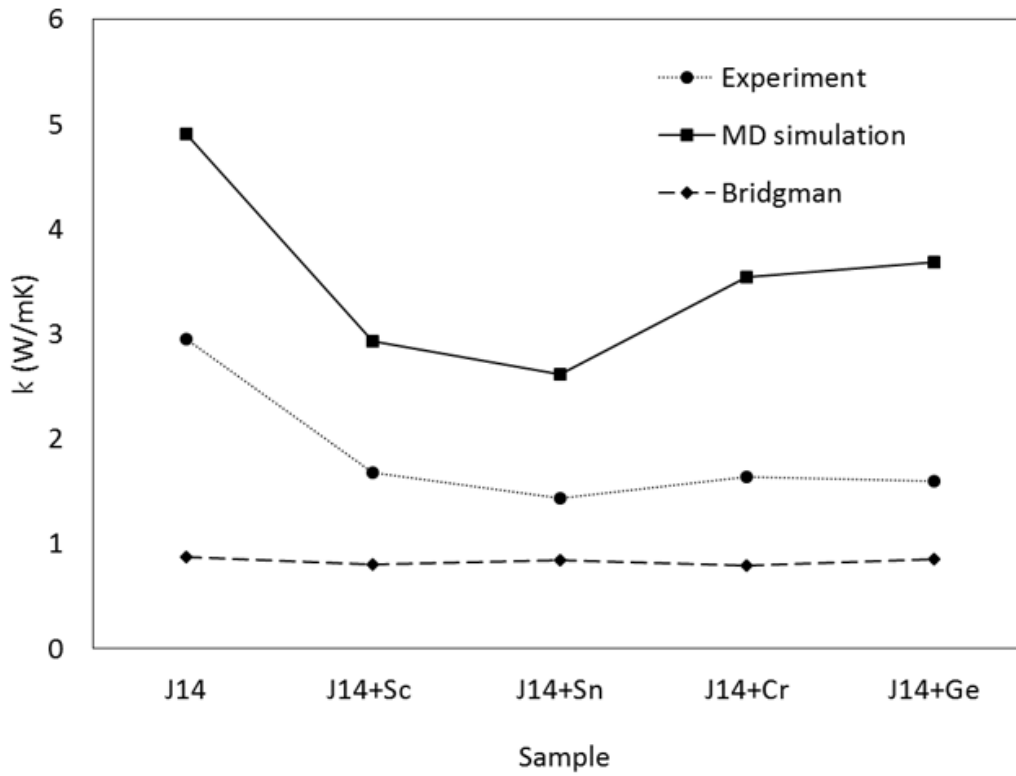


Figure 2.1 Thermal conductivities for the various compositions from experiment, from the MD simulations, and from the Bridgeman equation.

Table 2.1 Thermal conductivity from experiment, simulations, and the Bridgeman equation discussed below. ^a reference 25; ^b reference 18.

Sample	Thermal conductivity (W/m·K)		
	Experiment	MD simulation	Bridgman
MgO	45-60 ^a	56	4.33
J14	3.0 ^b	4.9	0.87
J14+Sc	1.7 ^b	2.9	0.81
J14+Sn	1.4 ^b	2.6	0.85
J14+Cr	1.6 ^b	3.5	0.79
J14+Ge	1.6 ^b	3.7	0.86

To better understand the origin of the thermal conductivity drop with the addition of a sixth cation, additional MD simulations were carried out in which atomic mass and charge were manipulated so that their effects on thermal conductivity could be delineated and compared. Three additional cases were studied for each composition, one in which the masses were kept the same but the charges on the oxygen and on the cations were replaced with their respective average charges, one in which the charges from the DFT calculations were kept constant but the atomic masses were replaced with a single mass that gives a reduced mass that matches the reduced mass of the original system, and one in which both the charge and mass are replaced with their average charge and a single mass that produces the reduced mass of the original system, respectively. These cases are referred to as homogeneous charge/heterogeneous mass (HMC/HTM), heterogeneous charge/homogeneous mass (HTC/HMM), and homogeneous charge/homogeneous mass (HMC/HMM), respectively. The thermal conductivities from MD simulations for each of these systems, plus the original system, heterogeneous charge/heterogeneous mass (HTC/HTM), are given in Table 2.2 and plotted as histograms in

Figure 2.2. Values of the homogeneous charge and mass used in the simulations are also given in Table 2.2. From Table 2.2 and Figure 2.2 it is clear that heterogeneity in either mass or in charge alone lowers the thermal conductivity from the HMC/HMM systems for all compositions, and of the two, charge heterogeneity has the largest influence on reducing thermal conductivity. Furthermore, for each composition, charge heterogeneity without mass heterogeneity reduces thermal conductivity to a value equal (or very close) to that for heterogeneity in both mass and charge. In other words, the effects of phonon scattering from heterogeneity in the mass and in the charge are not additive, and the latter makes a larger contribution to the reduction in thermal conductivity that occurs with the addition of a sixth cation to J14.

Table 2.2 Thermal conductivities using different combinations of homogeneous charge (HMC), heterogeneous charge (HTC), homogeneous mass (HMM) and heterogeneous mass (HTM).

Sample	Thermal conductivity (W/m·K)				Average Charge	Average Mass
	HTC/HMM	HTC/HTM	HMC/HTM	HMC/HMM		
J14	4.9	4.9	5.7	11.5	1.285	47.09
J14+Sc	2.9	2.9	7.6	15.0	1.333	46.72
J14+Sn	3.0	2.6	4.3	9.8	1.299	52.35
J14+Cr	3.9	3.5	5.7	11.4	1.283	47.84
J14+Ge	4.3	3.7	4.9	9.9	1.284	50.02

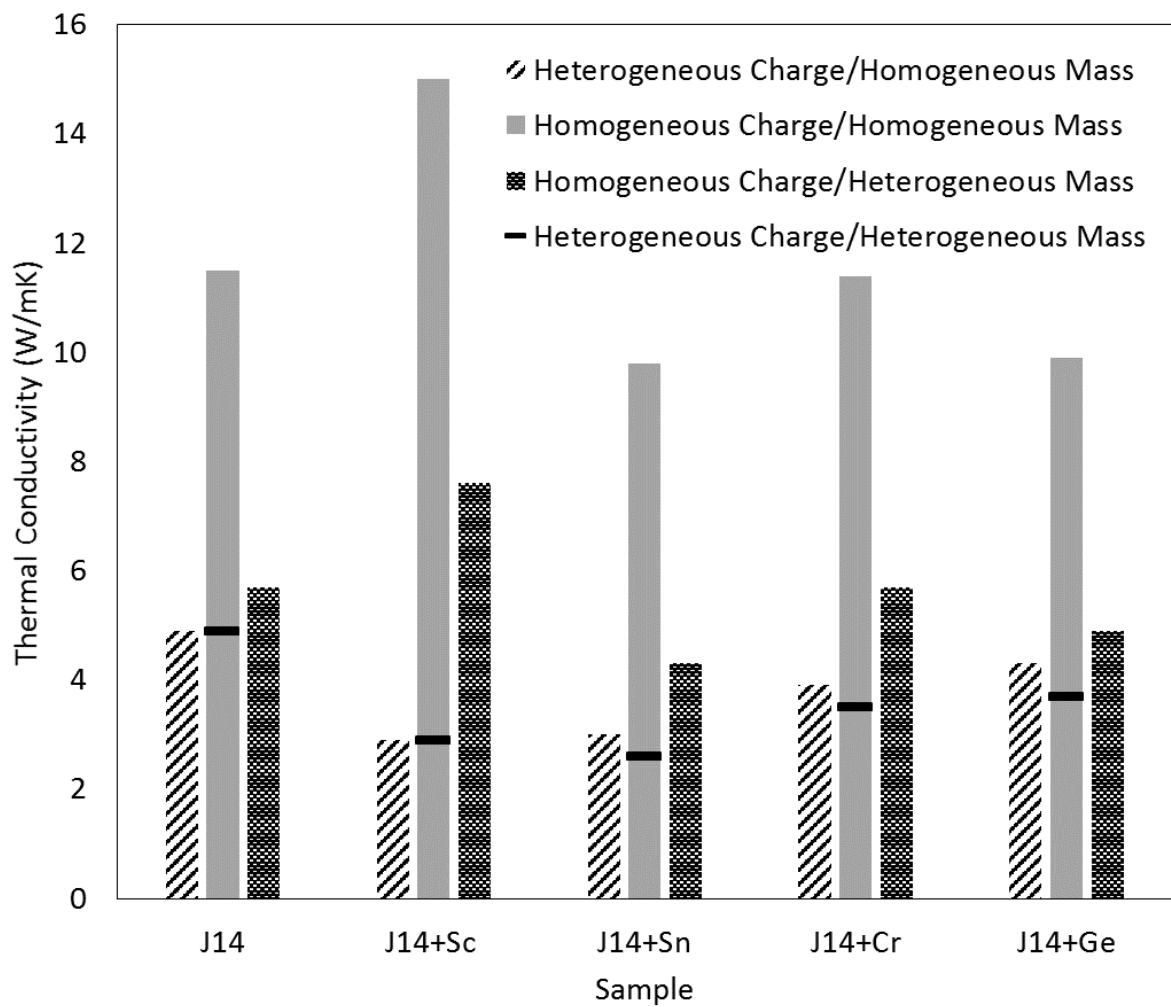


Figure 2.2 Data from Table 2.2 plotted as histograms.

Additional insight can be obtained from further analysis of the data in Figure 2.2. Adding Sc to J14 and considering mass scattering only (i.e. comparing the HMC/HTM samples for J14 and J14+Sc) the lighter mass of Sc causes the thermal conductivity to increase with Sc addition to J14. This is despite any enhanced phonon scattering from the added mass disorder. In contrast, considering only scattering from charge disorder (i.e. comparing the HTC/HMM samples for J14 and J14+Sc), the extra charge scattering from adding Sc with a +3 oxidation state¹⁵ (together with the associated reduction of the other ions) overwhelms the mass effect, and the thermal conductivity of J14 decreases with Sc addition.

Adding Cr to J14 does not significantly change the average mass or charge of J14. Consequently, in Figure 2.2, the thermal conductivities of the HMC/HMM systems for J14 and J14+Cr are very close to one another. In addition, the thermal conductivities of the HMC/HTM systems for the two compositions are the same, implying that any additional phonon scattering from the added mass disorder with the addition of Cr is negligible. In contrast, adding Cr to J14 results in a HTC/HMM and a HTC/HTM model that has a lower thermal conductivity than the corresponding systems for J14. In other words, despite having close to the same average charge, the enhanced phonon scattering from additional charge disorder results in the reduction of thermal conductivity with addition of Cr to J14.

Adding Sn to J14 slightly increases the average charge and increases the average mass of J14; the latter should act to decrease the thermal conductivity while the former should increase the thermal conductivity (c.f. Fig. 2.3). Adding Ge to J14 makes a much smaller change in average charge, relative to the other additions, and a somewhat smaller increase in mass. Figure 2.2 indicates that the thermal conductivity of the HMC/HMM systems for addition of Sn or Ge are very similar, and both are lower than the equivalent systems for addition of Sc or Cr. Like the

other systems, disorder in charge is more effective for scattering phonons than mass disorder based on the thermal conductivities of the HTC versus HTM systems.

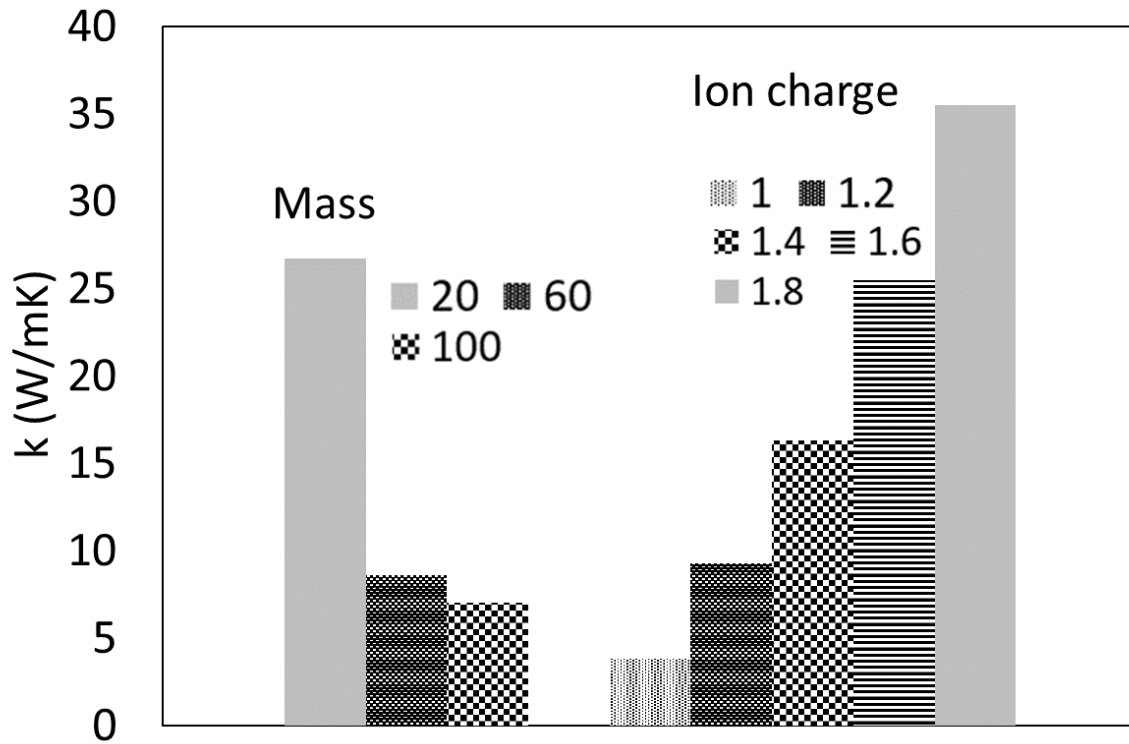


Figure 2.3 Dependence of thermal conductivity calculated from MD simulations on the averaged mass and average charge used in the J14 HMC/HMM system.

The results and analysis presented here for adding a sixth cation to J14 provides new insight into a prior experimental study that measured the thermal conductivity of entropy-stabilized oxides, and confirm the conclusion from a prior simulations that used Lennard-Jones pair potentials that phonon scattering from variations in interatomic forces are needed to explain the drop in thermal conductivity measured experimentally for the addition of a sixth cation to J14.²⁰ At the same time, the present work has provided some new insights; for example, without phonon scattering from the interatomic forces, addition of Sc to J14 would likely have increased thermal conductivity because of its lighter mass.

2.5 Bridgman Equation

To gain additional insight into the results of the MD simulations reported here, the thermal conductivity for each composition was also calculated using the Bridgman equation. This equation has been used for ionic liquids where scattering lengths are of the order of interatomic distances;²⁶ hence it represents an analytic limit of an amorphous structure for ionic materials. This equation gives the thermal conductivity k as a product of the density ρ , heat capacity c_v , unidirectional mean molecular speed v_y and lattice spacing a

$$k = \rho c_v V_y a. \quad (2.5.1)$$

For our calculations v_y is taken as the sound speed, which is approximated as the longitudinal sound speed given by the square root of the bulk modulus divided by the density, and the interatomic spacing is taken as $(V/N)^{1/3}$. The bulk moduli were calculated using the second derivative of a polynomial fit to the potential energy as a function of volume for each system after relaxation of the atom positions and periodic boundaries with respect to potential

energy. The heat capacities were calculated from the variance in the potential energy during the MD simulations as described above. Like the MD simulations, because the interatomic potentials have not been specifically fit to the J14 and related compositions, the calculations are not intended to be quantitative. Instead, by parameterizing the Bridgeman equations to the MD systems, these calculations are used to quantify how close our model approximates an amorphous limit.

Table 2.3 Properties from MD simulation used to estimate thermal conductivity via Eq. (2) ^c reference 36; ^d reference 37; ^e reference 38

	Bulk Modulus (GPa)	Cv (J/mol.K)	Sound Speed (km/s)
MgO	268 ^c (215)	26.8 ^d (36.8)	8.66 ^e (9.1)
J14	235	24.5	6.24
J14+Sc	331	24.5	7.71
J14+Sn	183	24.3	5.49
J14+Cr	239	24.9	6.35
J14+Ge	282	24.0	7.18

Given in Table 2.3 are the calculated properties for each model system that are used in the Bridgeman equation, the experiment values.^{36,37,38} The calculated thermal conductivities are given in Table 2.1 and Figure 2.1. The thermal conductivities from the Bridgeman equation are similar for all compositions, and significantly lower than those given by the MD simulations. Hence, we conclude that while the addition of a sixth cation to J14 lowers the thermal conductivity largely due to enhanced scattering from charge disorder, the systems are still above this amorphous scattering limit.

2.6 Conclusion

Classical molecular dynamics simulations have been used to characterize the influence of mass and charge disorder on the phonon-mediated thermal conductivity of five entropy stabilized oxides, J14 with composition $(\text{Mg}_{0.1}\text{Co}_{0.1}\text{Ni}_{0.1}\text{Cu}_{0.1}\text{Zn}_{0.1})\text{O}_{0.5}$, and J14 plus Sc, Sn, Cr or Ge in equi-molar cation proportions. By manipulating the mass and the atom-centered charges used in the Coulombic contribution to the potential energy, it was shown that the phonon scattering from disorder in atomic charges that enter the interatomic potential can explain prior experimental results that show a lowering of thermal conductivity with addition of a sixth cation to J14. A comparison of thermal conductivities from the MD simulations to predictions from the Bridgeman equation using properties from the simulations suggest that despite the added phonon scattering from disorder in mass and atomic forces, the thermal conductivity is still above an analytic limit for an amorphous system.

Supplementary Material

See Appendix A for the final atom positions and calculated Bader charges for each DFT supercell.

ACKNOWLEDGEMENTS

This work is supported by the U.S. Office of Naval Research MURI program (grant No. N00014-15-1-2863) and by NSF Ceramics through award 1610844.

References

1. Tsai, M.-H. & Yeh, J.-W. High-Entropy Alloys: A Critical Review. *Mater. Res. Lett.* **2**, 107–123 (2014).
2. Miracle, D. B. Critical Assessment 14:High entropy alloys and their development as structural materials. *Mater. Sci. Technol.* **31**, 1142–1147 (2015).
3. Gorse, S., Miracle, D. B. & Senkov, O. N. Mapping the world of complex concentrated alloys. *Acta Mater.* **135**, 177–187 (2017).
4. Rost, C. M. *et al.* Entropy-stabilized oxides. *Nat. Commun.* **6**, 8485 (2015).
5. Berardan, D., Franger, S., Dragoe, D., Meena, A. K. & Dragoe, N. Colossal dielectric constant in high entropy oxides. *Phys. Status Solidi - Rapid Res. Lett.* **10**, 328–333 (2016).
6. Berardan, D., Franger, S., Meena, A. K. & Dragoe, N. Room temperature lithium superionic conductivity in high entropy oxides. *J. Mater. Chem. A* 9536–9541 (2016). doi:10.1039/C6TA03249D
7. Biesuz, M., Spiridigliozzi, L., Dell’Agli, G., Bortolotti, M. & Sglavo, V. M. Synthesis and sintering of (Mg, Co, Ni, Cu, Zn)O entropy-stabilized oxides obtained by wet chemical methods. *J. Mater. Sci.* **53**, 8074–8085 (2018).
8. Sarkar, A. *et al.* Rare earth and transition metal based entropy stabilised perovskite type oxides. *J. Eur. Ceram. Soc.* **38**, 2318–2327 (2018).
9. Dąbrowa, J. *et al.* Synthesis and microstructure of the (Co,Cr,Fe,Mn,Ni)₃O₄ high entropy oxide characterized by spinel structure. *Mater. Lett.* **216**, 32–36 (2018).
10. Gild, J. *et al.* High-Entropy Metal Diborides: A New Class of High-Entropy Materials and a New Type of Ultrahigh Temperature Ceramics. *Sci. Rep.* **6**, 2–11 (2016).
11. Jiang, S. *et al.* A new class of high-entropy perovskite oxides. *Scr. Mater.* **142**, 116–120 (2018).
12. Chen, K. *et al.* A five-component entropy-stabilized fluorite oxide. *J. Eur. Ceram. Soc.* **38**, 4161–4164 (2018).
13. Mayrhofer, P. H., Kirnbauer, A., Ertelthaler, P. & Koller, C. M. High-entropy ceramic thin films; A case study on transition metal diborides. *Scr. Mater.* **149**, 93–97 (2018).
14. Rost, C. M. Entropically-Stabilized Oxides: Explorations of a Novel Class of Multicomponent Materials. (North Carolina State University, 2016).

15. Rak, Z. *et al.* Charge compensation and electrostatic transferability in three entropy-stabilized oxides: Results from density functional theory calculations. *J. Appl. Phys.* **120**, (2016).
16. Rost, C. M., Rak, Z., Brenner, D. W. & Maria, J.-P. Local structure of the $\text{Mg}_x\text{Ni}_x\text{Co}_x\text{Cu}_x\text{Zn}_x\text{O}(x=0.2)$ entropy-stabilized oxide: An EXAFS study. *J. Am. Ceram. Soc.* (2017). doi:10.1111/jace.14756
17. Rák, Z., Maria, J. P. & Brenner, D. W. Evidence for Jahn-Teller compression in the (Mg Co Ni Cu Zn)O entropy-stabilized oxide: A DFT study. *Mater. Lett.* **217**, 300–303 (2018).
18. Braun, J. L. *et al.* Charge Induced Disorder Controls the Thermal Conductivity of Entropy Stabilized Oxides. *Adv. Mater.* **1805004**, 1–8 (2018).
19. Giri, A., Braun, J. L., Rost, C. M. & Hopkins, P. E. On the minimum limit to thermal conductivity of multi-atom component crystalline solid solutions based on impurity mass scattering. *Scr. Mater.* **138**, 134–138 (2017).
20. Giri, A., Braun, J. L. & Hopkins, P. E. Reduced dependence of thermal conductivity on temperature and pressure of multi-atom component crystalline solid solutions. *J. Appl. Phys.* **123**, (2018).
21. Caro, M., Béland, L. K., Samolyuk, G. D., Stoller, R. E. & Caro, A. Lattice thermal conductivity of multi-component alloys. *J. Alloys Compd.* **648**, 408–413 (2015).
22. Green, M. S. Markoff random processes and the statistical mechanics of time-dependent phenomena. II. Irreversible processes in fluids. *J. Chem. Phys.* **22**, 398–413 (1954).
23. Kubo, R. Statistical Mechanical Theory of Irreversible Processes. I. General Theory and Simple Applications to Magnetic and Conduction Problems. *J. Phys. Soc. Japan* **12**, 570–586 (1957).
24. Schelling, P. K., Phillpot, S. R. & Keblinski, P. Comparison of atomic-level simulation methods for computing thermal conductivity. *Phys. Rev. B - Condens. Matter Mater. Phys.* **65**, 1–12 (2002).
25. Shukla, P., Watanabe, T., Nino, J. C., Tulenko, J. S. & Phillpot, S. R. Thermal transport properties of MgO and $\text{Nd}_2\text{Zr}_2\text{O}_7$ pyrochlore by molecular dynamics simulation. *J. Nucl. Mater.* **380**, 1–7 (2008).
26. Wu, K.-J., Chen, Q.-L. & He, C.-H. Speed of Sound of Ionic Liquids: Database, Estimation, and its Application for Thermal Conductivity Prediction. *AIChE J.* **60**, 1120–

- 1131 (2014).
27. Plimpton, S. Fast Parallel Algorithms for Short-Range Molecular Dynamics. *Journal of Computational Physics* **117**, 1–19 (1995).
 28. Zunger, A., Wei, S., Ferreira, L. & Bernard, J. Special Quasirandom Structures. *Phys. Rev. Lett.* **65**, 353–356 (1990).
 29. Blöchl, P. E. Projector augmented-wave method. *Phys. Rev. B* **50**, 17953–17979 (1994).
 30. Kresse, G. & Furthmüller, J. Efficiency of ab-initio total energy calculations for metals and semiconductors using a plane-wave basis set. *Comput. Mater. Sci.* **6**, 15–50 (1996).
 31. Kresse, G. & Furthmüller, J. Efficient iterative schemes for ab initio total-energy calculations using a plane-wave basis set. *Phys. Rev. B. Condens. Matter* **54**, 11169–11186 (1996).
 32. Kresse, G. & Hafner, J. Ab initio molecular dynamics for liquid metals. *Phys. Rev. B* **47**, 558–561 (1993).
 33. Perdew, J., Burke, K. & Ernzerhof, M. Generalized Gradient Approximation Made Simple. *Phys. Rev. Lett.* **77**, 3865–3868 (1996).
 34. Nosé, S. A molecular dynamics method for simulations in the canonical ensemble. *Mol. Phys.* **52**, 255–268 (1984).
 35. Nosé, S. & Nosé, S. A unified formulation of the constant temperature molecular dynamics methods. *J. Chem. Phys.* **81**, 511 (1984).
 36. Sun, X. W. *et al.* Shell and breathing shell model calculations for isothermal bulk modulus in MgO at high pressures and temperatures. *Mater. Chem. Phys.* (2009). doi:10.1016/j.matchemphys.2009.02.021
 37. Zhang, Y. H. & Huang, S. P. Molecular dynamics simulation study of MgO crystal. *Chinese Phys. Lett.* (1999). doi:10.1088/0256-307X/16/4/001
 38. ANDERSON, O. L. & ANDREATCH, P. Pressure Derivatives of Elastic Constants of Single-Crystal MgO at 23°C and 195.8°C. *J. Am. Ceram. Soc.* (1966). doi:10.1111/j.1151-2916.1966.tb15405.x

Chapter 3. An exploration of relationships between high entropy carbides and their respective binaries

M. Lim¹, Z. Rak¹, C. Toher², T. Harrington³, K.S. Vecchio³, J.-P. Maria⁴, S. Curtarolo⁵, D.W. Brenner¹

¹Department of Materials Science and Engineering
North Carolina State University, Raleigh, NC 27587

²Department of Mechanical Engineering and Materials Science
Duke University, Durham, NC 27708

³Department of NanoEngineering, Materials Science and Engineering Program,
University of California, San Diego, La Jolla, CA, 92093

⁴Department of Materials Science and Engineering

The Pennsylvania State University, University Park, PA 16802

⁵Materials Science, Electrical Engineering, Physics and Chemistry, Duke University, Durham,
NC, 27708, USA

3.1 Abstract

Using Density Functional Theory calculations, this paper addresses two questions: (1) to what degree can the properties of high entropy carbides created by equi-molar combinations of five of the eight refractory metals Hf, Nb, Mo, Ta, Ti, V, W, and Zr be predicted from their respective binary compounds, and (2) are there relationships between the properties of the binary compounds corresponding to a given HEC composition and the value of that composition's entropy forming ability (EFA). For the former question, it is shown that lattice constant, binding energy, bulk modulus, average carbon vacancy formation energy (CVFE) and the energy difference between the Fermi Level and the pseudo-gap (ζ) in the electronic Density of States are well approximated by binary carbide averages. To address the second question, correlations are explored between binary properties and the EFA of all 56 5-metal combinations. Correlations are found between EFA and the standard deviation of the distribution of bulk moduli and ζ of the

constituent binaries. Two models are explored for predicting CVFEs; both use the weighted averages of binary properties that correspond to the near-neighbor environment of the missing carbon atom. The first uses binary CVFEs, while the second uses a linear relation between CVFE and ζ that is derived from the binary compounds. Using the latter expression to calculate the CVFEs for all possible environments in each of the 56 compositions, it is shown that there is a correlation between the standard deviation of the CVFEs for each HEC and the EFA of that composition. This result supports the EFA as a central quantity for estimating properties of HECs beyond phase stability.

3.2 Introduction

High entropy ceramics, including oxides¹⁻¹⁰ diborides¹¹⁻¹⁴ and carbides,¹⁵⁻²⁰ have recently emerged as a new material class with potentially important structural and functional applications. Like their more-established cousins the high entropy metal alloys,^{21,22,31,23-30} these materials are typically defined by five or more components in roughly equi-molar proportions, homogeneously distributed on a single crystal lattice. To be thermodynamically stable, the free energy of the entropic phase must be lower than those of the intermediate phases formed from different constituent combinations. The number of possible combinations is very large, which combined with the dearth of thermodynamic data for multiple components has made the prediction of stable high entropy materials challenging. Alternatively, empirical relations involving e.g. the distribution of atomic radii have been developed that are similar to the Hume-Rothery rules traditionally used for alloys.^{11,32-35} In the case of ceramics, where charge transfer and electro-static bonding may play a large role in chemical bonding, such approaches quickly become complicated.³⁶

Curtarolo and co-workers recently introduced a first-principles based method for predicting the entropy forming ability (EFA) of a composition and lattice, and used this method to predict the synthesizability of 56 rocksalt high-entropy carbides (HECs) formed by equi-molar combinations of five of the set of eight refractory metals Hf, Nb, Mo, Ta, Ti, V, W, and Zr.³⁷ The predictions for the HECs involved calculating energies for a collection of possible geometrical configurations of each individual equi-molar composition containing five metals. The EFA was then taken as the inverse of the standard deviation of the energy spectrum of the configurations relative to the lowest energy subsystem. Nine of these structures were synthesized, and the presence of single or multiple phases, as determined from x-ray and related analysis, was compared against the first principles predictions. These nine compositions and their experimental phase stability are given in Table 3.1. In each case, the EFA correctly predicts the presence or absence of multiple phases.

Table 3.1 Composition abbreviations used in this paper and phase stability from reference [37].

Abbreviation	Composition	Phase Stability
HEC3	Hf, Nb, Ta, Ti, Zr	Single Phase
HEC4	Hf, Nb, Ta, Ti, V	Single Phase
HEC5	Nb, Ta, Ti, V, W	Single Phase
HEC6	Hf, Mo, Ta, W, Zr	Multiple
HEC7	Hf, Ta, Ti, W, Zr	Single Phase
HEC8	Hf, Mo, Ti, W, Zr	Multiple
HEC9	Hf, Nb, Ta, Ti, W	Single Phase
HEC10	Hf, Mo, V, W, Zr	Multiple
HEC16	Mo, Nb, Ta, V, W	Single Phase

In this paper, we further analyze the properties of these nine compositions using Density Functional Theory (DFT) calculations. This paper focuses on two questions: (1) to what degree can the properties of these HECs be predicted from their respective binaries, and (2) are there relationships between the properties of the binary compounds that correspond to a given HEC composition and the value of that composition's EFA. For the former question, we find that lattice constant, binding energy, bulk modulus, average carbon vacancy formation energy (CVFE) and the energy difference between the Fermi Level and the pseudo-gap (ζ) in the electronic density of states are all well approximated by averages of the constitutive binary carbides. To address the second question, we use the binary averaging to calculate properties of all 56 possible compositions and look for correlations between these properties and the EFA of the corresponding HECs. Significant correlations are not found between the averages or the standard deviations of the cohesive energies or lattice constants of the binaries that correspond to the constituents of each composition. The lack of a correlation between EFA and lattice constants is surprising given that relative atomic radius has been used as a relatively simple prediction of phase stability in other high entropy structures. Correlations were found, however, between the EFA and the standard deviation of the distribution of bulk moduli and the standard deviation of the distribution of ζ values for the constituent binaries (correlations were also found between ζ and bulk modulus).

Building on these results, we explore two models for predicting CVFEs. This first uses the weighted average of the binary CVFEs that correspond to the near-neighbor environment of the missing carbon atom. The second uses a linear relation between the weighted average of the binary ζ values that corresponds to the near-neighbor carbon atom environment and CVFE that is derived from the binary compounds. Finally, using this expression to calculate the CVFEs for all

possible environments in each of the 56 compositions, it is shown that there is a correlation between the standard deviation of the CVFEs for each HEC and the EFA of that composition. This result supports the EFA as a central quantity for estimating properties of HECs beyond phase stability. The paper ends with comments regarding the shapes of the calculated CVFE distributions, as well as some implications for bonding that come from the correlation strengths.

3.3 Computational Method

The DFT supercells used for the high entropy compositions and binary carbides contained 40 carbon atoms and 40 metal atoms on the two face-centered cubic sublattices of the rocksalt structure, respectively, with the latter containing equal numbers of five different atom types arranged on their sublattice using the special quasi-random structure (SQS) algorithm.³⁸ The calculations were carried out using plane wave PAW pseudopotential methods^{39,40} as implemented in the Vienna Ab initio Simulation Package.⁴⁰⁻⁴² The generalized gradient approximation as parameterized by Perdew *et al.*⁴³ was used for the exchange-correlation potential. The energy of the system was minimized with respect to atom positions and lattice constant. A cut-off energy for the plane wave basis was set to 520 eV, and convergence was assumed when the energy difference between two consecutive self-consistent cycles was less than 2 meV with the Γ -centered 3 X 3 X 3 points. For graphite, the hexagonal structure was used with 80 carbons in the unit cell. The Brillouin-zone was sampled by Γ -centered 8 X 8 X 1 k points.

Illustrated in Fig. 3.1(a) is an example density of states from the DFT calculations. The pseudo-gap, taken as the energy corresponding to the left arrow, separates bonding from anti-bonding states in the carbides. The energy difference between this and the Fermi energy (the

arrow to the right), an energy difference denoted here as ζ , along with the electron density between these two energies, the Valence Electron Concentration (VEC), are well-established as important quantities for determining properties of these materials.^{44–51} Plotted in Fig. 3.1(b) is the VEC versus ζ for each of the binaries and HECs studied here. Because there is a linear relationship between these two quantities, rather than use both the VEC and ζ for the analyses below, we use only the latter, because it is a more straight-forward quantity to obtain from the density of states.

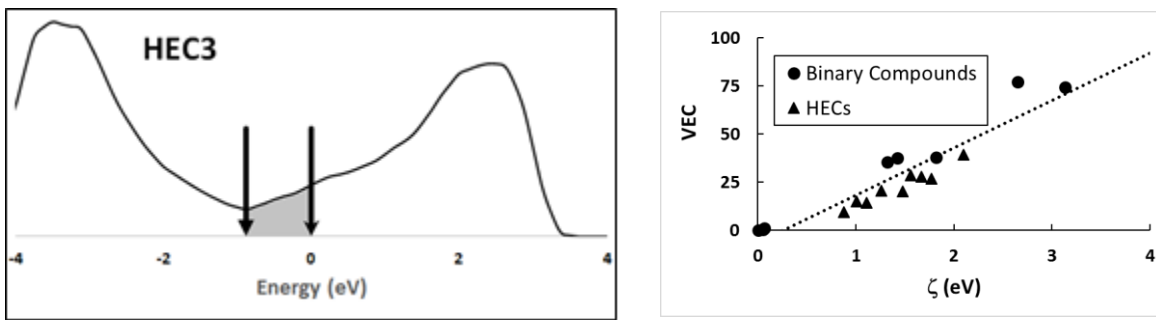


Figure 3.1 Electronic properties of the HECs. (a) Example Density of States from the DFT calculations. The arrow to the left denoted the pseudo-gap between bonding and anti-bonding states. The right arrow indicates the Fermi level. The different between the two is denoted as ζ , while the shaped region is the Valence Electron Concentration. (b) Graph illustrating the linear dependence for VEC and ζ for the binary carbides and the HECs.

The CVFE is taken as the difference between the energy of the DFT unit cell and the DFT unit cell missing a carbon atom, minus the energy of a carbon atom in graphite, taken as 7.97 eV/atom based on the DFT calculations. The latter uniformly shifts the CVFEs and does not change the range in energies. For each SQS cell a CVFE is calculated for each of the 40 carbon atoms by removing a single carbon atom one at a time. Hence the calculations correspond to a

composition of (cation)₁C_{0.975}. Furthermore, the calculations on the HECs are intended to be a sampling of random sites, and do not correspond to the most probable or lowest energy sites for missing C atoms in these structures.

3.4 HEC Properties

Summarized in Table 3.2 are the properties of the binary carbides in a rocksalt structure as given by the DFT calculations. For WC and MoC (indicated by a star) this structure is not the experimentally observed phase at room temperature but is used here for the sake of comparison. The cohesive energy is defined as the energy needed to separate the crystals into individual atoms at infinite separation; it is taken as the difference between the DFT energy for the relaxed unit cells and the sum of the energies for the isolated atoms. Experimental values for the bulk modulus and lattice constant are given in the parenthesis for the structures that are observed experimentally at ambient conditions.

Table 3.2 Properties of the binary carbides in a rocksalt structure calculated from DFT.

Composition (rocksalt)	Cohesive Energy (eV/atom)	CVFE (eV)	Bulk Modulus (GPa)	Lattice Constant (Å)	ζ (eV)
HfC	8.07	2.34	241 (242) ^a	4.65 (4.64) ^b	0.00338
MoC*	6.94	0.13	348	4.37	2.65
TaC	8.71	1.34	317 (344) ^a	4.48 (4.45) ^c	1.42
TiC	7.44	1.41	245 (233) ^d	4.33 (4.33) ^d	0.0508
ZrC	7.78	2.08	222 (265) ^b	4.67 (4.70) ^b	0.07
WC*	7.83	0.87	350	4.39	3.13
NbC	8.07	0.97	288 (300) ^a	4.48 (4.47) ^b	1.82
VC	6.75	1.52	300 (303) ^b	4.16 (4.16) ^b	1.32

*Experimental structure at ambient conditions is not rocksalt

^aReference ⁵², ^breference ⁵³, ^creference⁵⁴, ^dreference⁵⁵

Table 3.3 Properties of the HECs calculated from DFT.

Composition (rocksalt)	Cohesive Energy (eV/atom)		Lattice Constant (nm)		Bulk Modulus (GPa)		Average CVFE (eV/atom)		ζ (eV)	
	DFT	Binary	DFT	Binary	DFT	Binary	DFT	Binary	DFT	Binary
HEC3	8.1	8.01	4.53	4.49	266	263	1.76	1.63	0.88	0.67
HEC4	7.9	7.81	4.43	4.42	280	279	1.37	1.52	1.01	0.92
HEC5	7.89	7.76	4.38	4.37	323	300	1.05	1.22	1.77	1.55
HEC6	7.97	7.86	4.52	4.52	286	296	1.31	1.35	1.64	1.45
HEC7	8.09	7.97	4.51	4.48	280	275	1.48	1.61	1.11	0.93
HEC8	7.74	7.61	4.48	4.49	275	282	1.19	1.37	1.26	1.18
HEC9	8.12	8.02	4.47	4.43	284	289	1.38	1.39	1.48	1.28
HEC10	7.6	7.48	4.47	4.44	278	292	1.02	1.39	1.56	1.43
HEC16	7.75	7.66	4.38	4.37	325	320	0.81	0.97	2.1	2.07

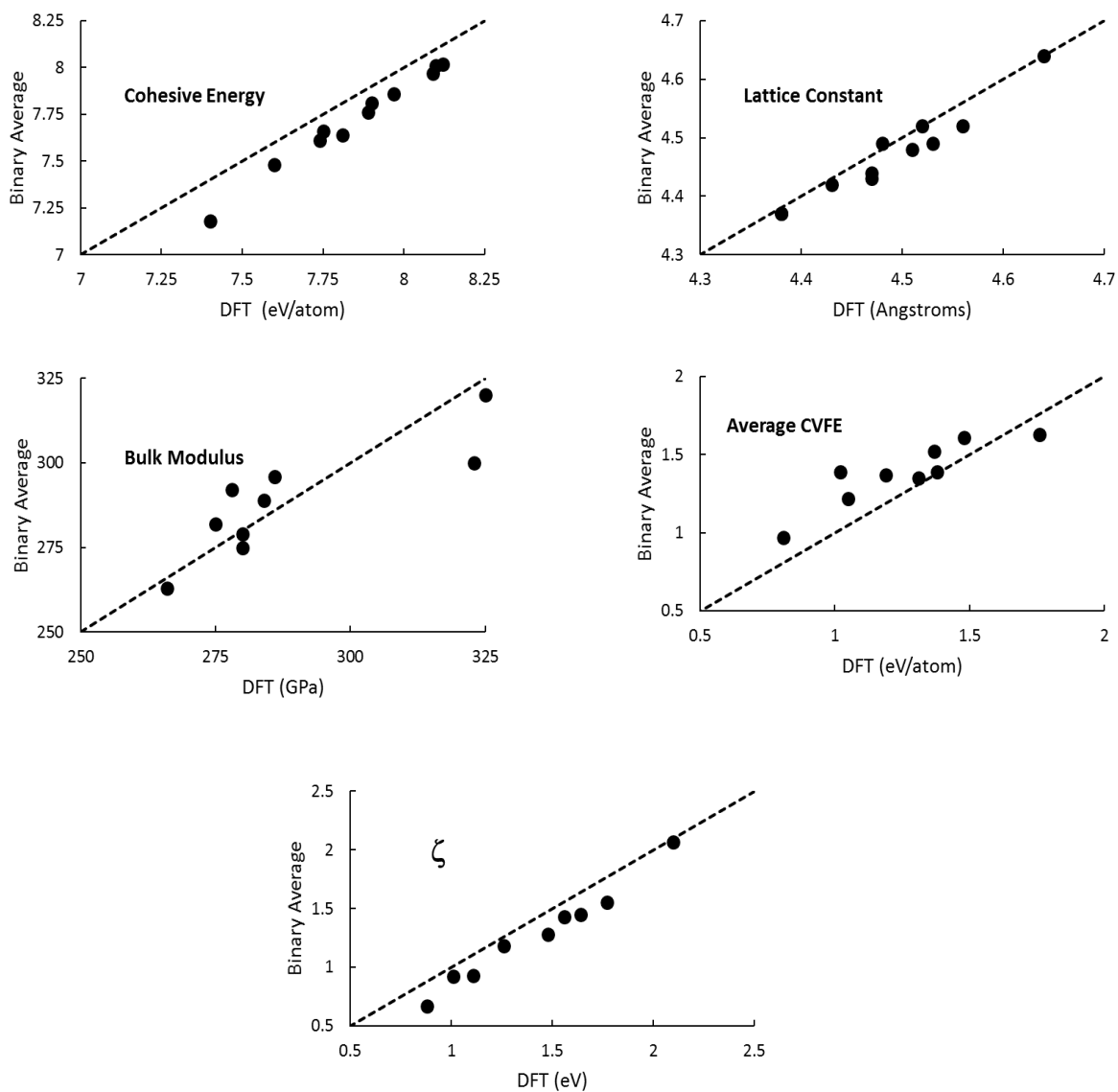


Figure 3.2 Plots of the properties of the nine HECS in Table 3.1 calculated as averages of the constituent binaries as a function of the same properties calculated from DFT.

Summarized in Table 3.3 and plotted in Fig. 3.2 are the cohesive energies, lattice constants, bulk moduli, average CVFEs and ζ for the 9 HEC compositions in Table 3.1. Values are given from the DFT calculations on the 80-atom supercell as described above, and by averaging the data from the binaries in Table 3.2. In each case averaging the binary properties is a reasonable approximation to the results of the full DFT calculations. For the lattice constant, the largest difference is 0.04Å or 0.88% for HEC3, while for the bulk modulus the largest difference between the values is 23 GPa, or 7.1%, for HEC5. The compositions with the largest deviation between the DFT values and the binary averages are different for each of these properties, so that there are no obvious compositions for which this averaging is particularly inaccurate. For the bulk moduli, the binary averages both over- and underestimate the DFT results, while for the lattice constants the binary averages either match or slightly underestimate the DFT results, with the exception of HEC8, where the DFT result is slightly below the binary average. In contrast, the binary approximation underestimates the DFT cohesive energy, i.e. the enthalpy of the HECs relative to the isolated atom limit is greater than what would be expected based on the respective binaries. For the CVFEs, the DFT calculations generally yield values that are smaller than those expected based on the binaries, meaning for most compositions there should be slightly more vacancies in the HEC compared to what would be expected from the binaries. The exception is HEC3, where the DFT average is slightly larger than the value from the average the CVFE's of the binaries. Distributions of CVFEs are discussed more in Sections 3.6 and 3.7. For ζ , the averages of the binaries are consistently lower than the direct DFT results, but with a clear correlation.

Plotted in Fig. 3.3 are the values of the first four quantities in Table 3.3 given by the DFT calculations as a function of ζ (also from the DFT calculations) for each of the HECs. The lines

correspond to least squares linear fits. Based on the correlation coefficients given in the plots, the strongest correlations with ζ are for the average CVFE and the bulk modulus. The latter has been discussed previously in the literature.^{56–59} The next strongest correlation with ζ is the lattice constant, followed by cohesive energy.

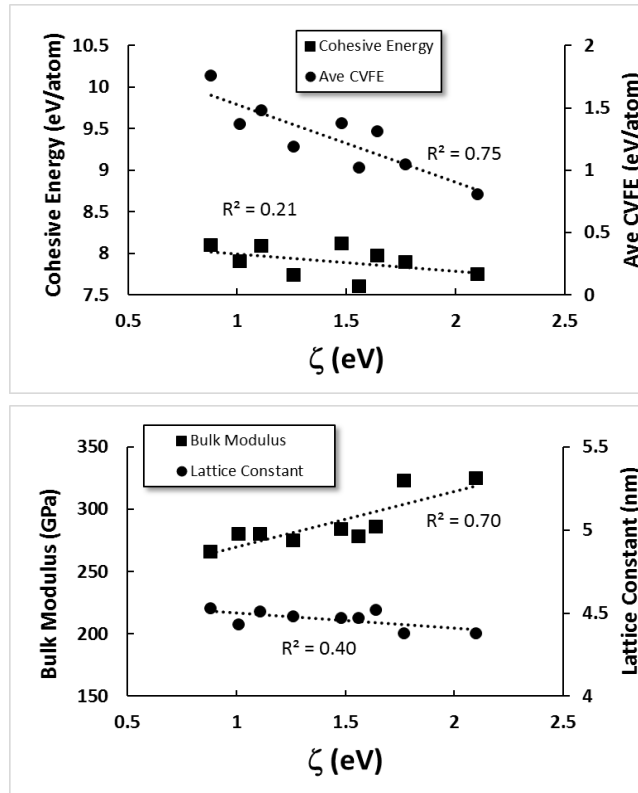


Figure 3.3 Properties in Figure 3.2 calculated from DFT as a function of ζ for each of the HEC compositions in Table 3.1. R^2 is the linear correlation coefficient for each plot.

Given in Table 3.4 are the average carbon-metal bond lengths as well as the difference between the shortest and largest bond lengths for each HEC composition broken down by component. Also given are the bond lengths for the binaries calculated from the data in Table 3.1. The average bond length across the HECs is 2.23Å, which is close to the average of 2.22Å for the binaries. However, the bond lengths for the binaries range from 2.08Å for V-C to 2.36Å in Zr-C for a range of 0.28Å. When incorporated into the HECs, these bonds still define the range in the average bond lengths (the second row of data in Table 3.4), but for the configurations studied here the range in average bond lengths shrinks to 0.22Å. The compositions that could not be produced in bulk as single phases, HEC6, HEC8 and HEC10, all have bond lengths for a given component that differ by 0.28Å or greater (these are bolded and underlined in Table 3.4). Each of these compositions contain a common four components, Hf, Mo, W and Zr. For HEC6 and HEC8, the largest variation in bond length is for the W-C bond, followed by the Mo-C bond. For HEC10, the largest bond length variation occurs for the V-C bond, followed by the Mo-C and then the W-C bond. Hence it appears from this data that the range in bond length for a given element may be an indicator of phase stability in the HECs, with a threshold somewhere between 0.37Å and 0.46Å.

3.5 Correlating Binary Properties with the EFA

As shown in the previous section, a number of bulk HEC properties can be calculated with reasonable accuracy as averages of the binary compounds whose constituents compose the HECs. These averages can in turn be used to estimate these properties for all 56 HEC combinations studied previously by Curtarolo³⁷ and co-workers. As mentioned above, one of the

goals of this study is to identify relationships between the properties of the binary compounds that correspond to a given HEC composition and the value of that composition's EFA.

Plotted in the left side of Figures 3.4 (a)-(e) are lattice constants, cohesive energies, bulk moduli, average CVFEs, and ζ values for each of the 56 HEC compositions taken as the averages of the binary compounds as a function of the EFA for that composition as reported by Curtarolo³⁷ and co-workers. Plotted to the right side of each figure is the standard deviation of each of these quantities for the binaries that correspond to the composition of each HEC as a function of the EFA. For each plot, the red and green circles correspond to the multi- and single-phase compositions listed in Table 3.1, respectively, while the solid lines are a least squares fit to the data with the R^2 value for each line also given in the plot. Based on this data, there is little correlation between the averaged HEC properties and the EFA. Furthermore, for most of these properties there is little correlation between the standard deviations in binary properties and the EFA. The exceptions are the bulk modulus and ζ , where smaller standard deviations generally reflect a higher EFA. This correlation is somewhat surprising given prior studies have used differences in bond lengths¹¹ or enthalpies³⁷ to predict phase stability. This is discussed more in Section 3.6.

While a strong correlation between binary CVFEs and EFA is not apparent from the data plotted in Figure 3.4(d), we note that, in general, for the compositions that have been studied experimentally, those that form single phase structures have standard deviation values for the CVFE from their constituent binaries that are at or below about 0.6 eV. All three of the HEC compositions that formed multi-phases include Mo and Hf (see Table 3.1), which corresponds to the binaries with the smallest and largest CVFEs, respectively. Of the 56 total five-element compositions, there are nine more that contain Mo and Hf. Of these, four have EFAs of 71³⁷,

which is well within the range of EFA values for which single phases are predicted. Additional experiments measuring the phase stability of these compositions are warranted to further validate the EFA as a strong indicator of phase stability.

Table 3.4 Average carbon-metal bond lengths and the difference (Δ) between the shortest and largest bond lengths for each HEC composition broken down by component

Composition (rocksalt)	Hf-C Ave (Δ)	Ta-C Ave (Δ)	Ti-C Ave (Δ)	Zr-C Ave (Δ)	W-C Ave (Δ)	Nb-C Ave (Δ)	Mo-C Ave (Δ)	V-C Ave (Δ)
Binary	2.32	2.24	2.17	2.36	2.19	2.24	2.18	2.08
Average	2.27 (0.04)	2.22 (0.05)	2.21 (0.05)	2.30 (0.03)	2.21 (0.04)	2.23 (0.05)	2.23 (0.05)	2.18 (0.04)
HEC3	2.29 (0.08)	2.25 (0.11)	2.23 (0.11)	2.31 (0.07)	-	2.26 (0.11)	-	-
HEC4	2.25 (0.11)	2.21 (0.11)	2.21 (0.18)	-	-	2.23 (0.15)	-	2.18 (0.21)
HEC5	-	2.21 (0.10)	2.18 (0.10)	-	2.19 (0.25)	2.21 (0.15)	-	2.16 (0.34)
HEC6	2.28 (0.15)	2.24 (0.20)	-	2.30 (0.14)	2.22 (0.46)	-	2.25 (0.23)	-
HEC7	2.28 (0.10)	2.24 (0.12)	2.22 (0.15)	2.30 (0.13)	2.23 (0.23)	-	-	-
HEC8	2.27 (0.13)	-	2.21 (0.18)	2.30 (0.13)	2.21 (0.48)	-	2.24 (0.42)	-
HEC9	2.26 (0.09)	2.22 (0.11)	2.21 (0.14)	-	2.22 (0.17)	2.24 (0.13)	-	-
HEC10	2.27 (0.23)	-	-	2.28 (0.16)	2.20 (0.37)	-	2.23 (0.42)	2.20 (0.62)
HEC16	-	2.20 (0.11)	-	-	2.20 (0.37)	2.22 (0.13)	2.20 (0.33)	2.16 (0.37)

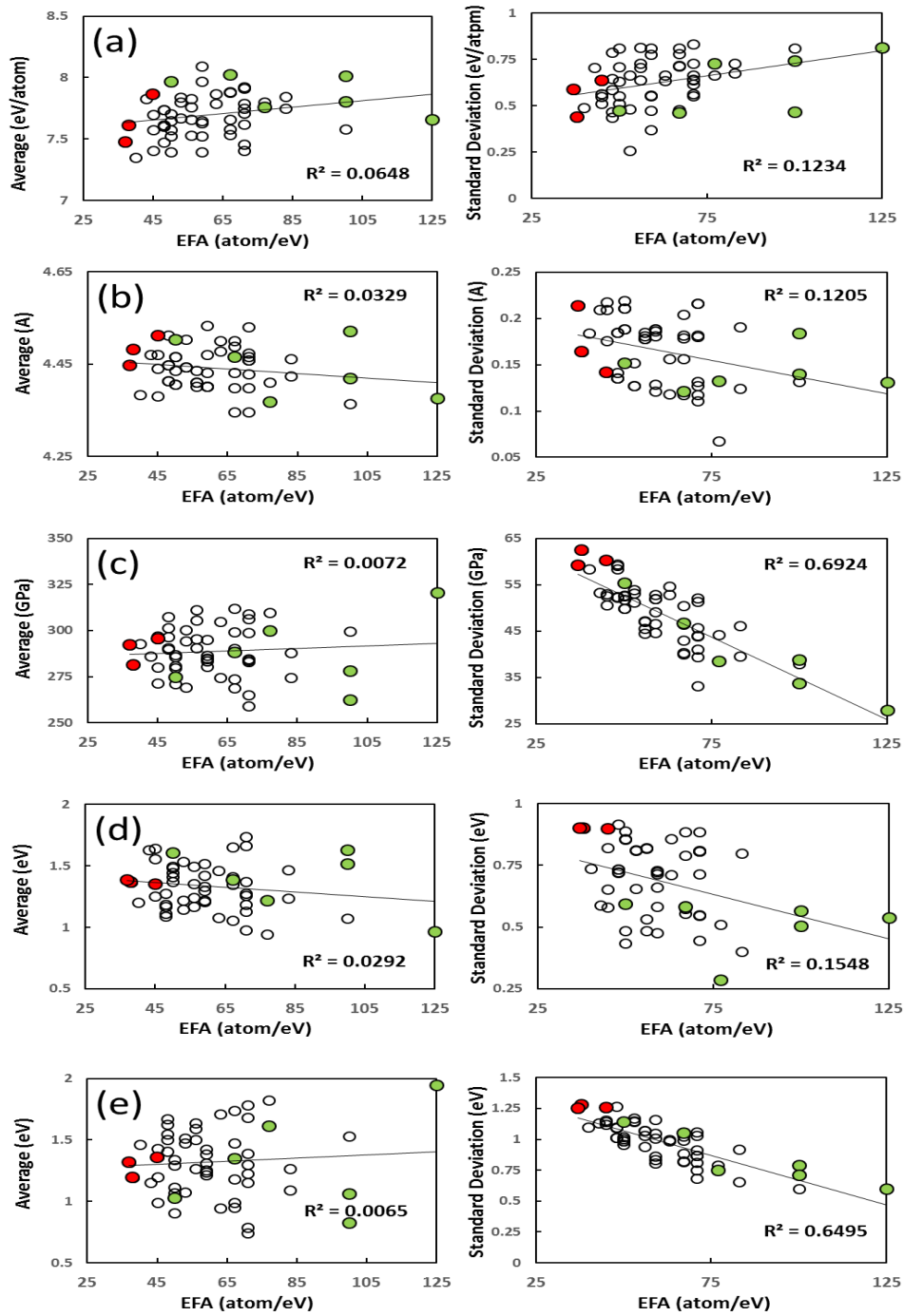


Figure 3.4 Average values (left column) and standard deviations (right column) plotted against EFA for the HEC compositions in Table 3.1. (a)-(e) refer to cohesive energy, lattice constant, bulk modulus, CVFE and ζ , respectively.

The relationships discussed above have focused on the average of the 40 CVFE values that were calculated from the SQS structures for each HEC. These calculations are intended to be a representative sampling of vacancies with a random atom arrangement and constant stoichiometry, and do not necessarily represent the most probable carbon vacancies or stoichiometry. Five cation types arranged over six sites (the number of neighbors for each carbon atom) leads to 210 possible local compositions. Taking into account degeneracies of each of these compositions leads to 15,625 possible vacancy sites in a five cation HEC. Explored in this section is the degree to which the energies of individual CVFEs within a HEC can be estimated from properties of the binaries, and what these estimates imply regarding relationships between CVFEs and EFA for each of the 56 HEC compositions.

Two methods were explored for estimating CVFEs from properties of the binaries; both assume that a CVFE depends only on the number and identity of different cation types within the first shell of neighbors. The first method assumes that a CVFE is just the weighted average of the binary CVFE's that correspond to the composition of the first neighbor shell. The second method is based on the ζ values for the same binaries. Plotted in Fig. 3.5 is the CVFE for the binaries as function of their ζ value, along with the average CVFE for the HECs in Table 3.1 as a function of the DFT ζ for these same compositions. A linear fit is made to the binary data that has a correlation coefficient of 0.71. Apparent from the plot is that this fit is also a reasonably good description of the HEC values. To obtain a CVFE energy, the ζ values for the binaries that correspond to the cations in the first neighbor shell are averaged, and the CVFE is obtained from the linear expression in Figure 3.5.

Plotted in Figure 3.6 are the CVFEs for the 40 carbon vacancies within each HEC SQS structure. The x axis corresponds to values from the DFT calculations on the 80-atom unit cells,

while the y axis corresponds to values obtained by the two methods. The open symbols are for the first method (averaging binary CVFE) while the closed symbols are for the second method (using averaged z values). The dashed line corresponds to exact agreement between the binary averages and the DFT results. The horizontal and vertical arrows denote the range of values between the lowest and highest binary CVFE from the components in each HEC. Given in Table 3.5 is a summary of the accuracy and limitations of both methods.

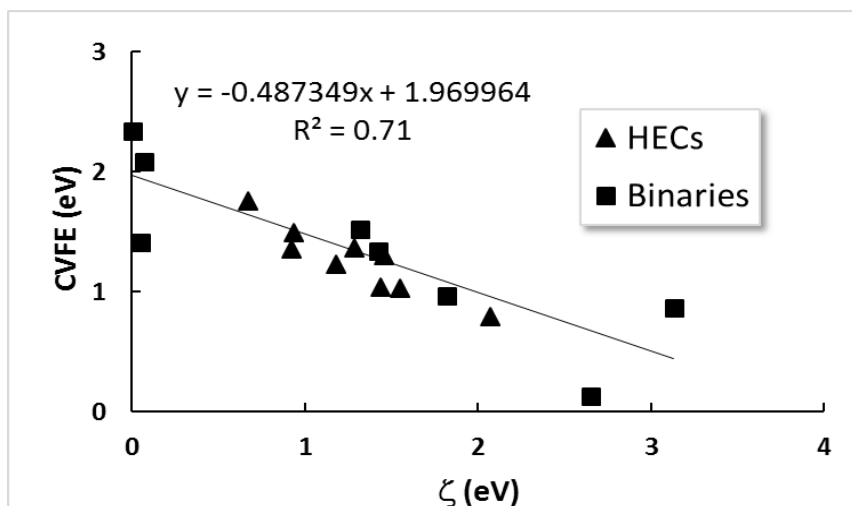


Figure 3.5 Plot of the average CVFE's for the HECs and binaries calculated from DFT as function of the ζ values for each, also calculated from DFT.

Several trends are apparent from the data in Figure 3.6 and Table 3.5. First, in general the overall fit between the two methods is similar. For six of the nine compositions the second method has a smaller mean-squared error and is closer to the average for five of compositions (in two cases the two methods yield the same average values). However, the second method yields a standard deviation that is closer to that derived from the 40 CVFEs values for six of the nine

compositions. Second, not all of the CVFEs from the DFT calculations fall within the bounds defined by the binary CVFE values. For example, HEC4, HEC5, HEC7, HEC8, HEC9 and HEC16 all have values that are less than what would be expected based on the binaries (these are values to the left of the end of the horizontal arrows). Similarly, HEC5 has CVFEs that are larger than what would be expected. It is impossible for the first method to reproduce HEC CVFEs that do not fall within the range of binary values, while the second method can. In HEC5, for example, all of the open circles fall within the range of values defined by the vertical arrow, while the second method yields values outside of the range, similar to the DFT results. The net result is that the cluster of open circles for the HEC distribution is more horizontal than the cluster of closed symbols, and hence with less correspondence to the DFT values. Finally, from the data in Figure 3.4, the HECs that have been reported as not forming bulk single phases (HEC6, HEC8 and HEC10) have a larger range of CVFEs than those that readily form single phases.

Table 3.5 Properties of the two approaches used to calculate CVFEs.
 STDEV=standard deviation; MSE=mean squared error.

DFT (eV)		Binary CVFE Average			z function		
Ave (eV)	STDEV (eV)	Ave (eV)	STDEV (eV)	MSE (eV ²)	Ave (eV)	STDEV (eV)	MSE (eV ²)
1.76	0.13	1.63	0.21	1.28	1.64	0.17	1.26
1.36	0.31	1.52	0.2	4.39	1.52	0.16	4.54
1.03	0.28	1.22	0.1	4.18	1.22	0.2	2.78
1.3	0.37	1.35	0.32	1.08	1.26	0.23	1.37
1.49	0.28	1.61	0.22	1.48	1.51	0.24	0.89
1.23	0.48	1.37	0.36	3.3	1.34	0.3	3.58
1.37	0.31	1.39	0.24	1.37	1.4	0.23	1.23
1.04	0.43	1.39	0.31	7.52	1.27	0.23	5.91
0.79	0.29	0.97	0.2	3.07	0.96	0.13	2.81

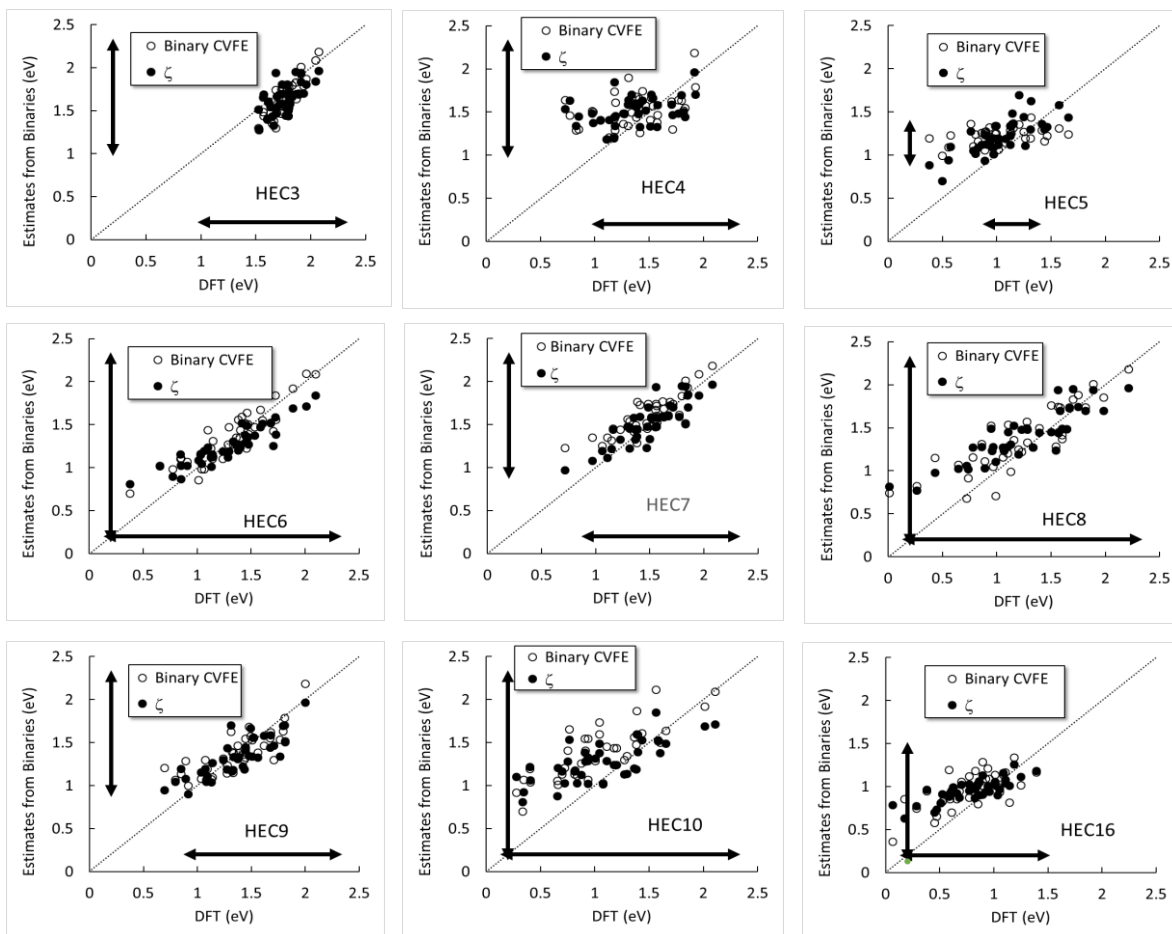


Figure 3.6 CVFE's for each composition in Table 3.1 calculated as either a weighted sum of the CVFE for the binaries that correspond to the environment surrounding the vacancy (open circles) or a function of the weighted sum of the ζ values from the same binaries (solid circles) as a function of the DFT energies. The arrows indicate the highest and lowest values of the CVFE's of the constitutive binaries for each composition.

With these methods, the CVFEs for all possible local configurations can be estimated for all 56 compositions, and the statistical properties of these values can be explored for correlations with the EFA. Plotted in Figures 3.7(a) and 3.7(b) are the average and the standard deviation of CVFEs, respectively, based on the CVFEs of the binaries that correspond to that compositions (open symbols) or based on calculations for all possible CVFE sites including degeneracies (closed symbols) for each of the 56 compositions as a function of their EFA value. The second model, based on ζ , was used for the calculations of all possible sites. There is clearly little to no correlation between the average CVFEs and EFA. However, there is a correlation between the distribution of CVFEs as measured by the standard deviation. This correlation is stronger (higher correlation coefficient) when using all of the CVFE values than when averaging strictly those for the corresponding binaries. The correlation between the range of CVFEs and the EFA suggests that the EFA may be useful for designing HECs beyond synthesizability, for example to control defects such as carbon vacancies.

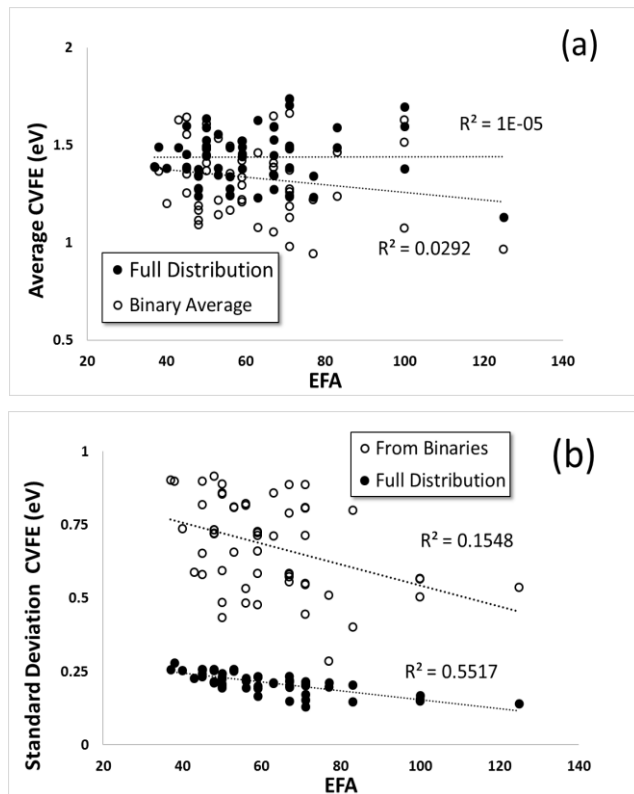


Figure 3.7 CVFE properties from the constitutive binaries (open circles) and from the full distribution of all 15626 local compositions (solid circles) for all 56 compositions as a function of their EFA value. The full distribution values use the ζ model for calculating CVFEs. (a) Average CVFE values. (b) Standard deviation of the CVFE values.

3.7 Discussion

One of the chief purposes of this study was to explore and quantify the degree to which the properties of HECs can be related to the properties of their constitutive binaries. This is important because it helps to clarify what properties of the class of HECs studied here are unique, and which are similar to what would be expected from a rule of mixtures based on binary properties. In addition, there are several new insights that can be gleaned from these results.

From Fig. 3.3, there appears to be a stronger correlation between average CVFE and ζ than there is between cohesive energy and ζ . At a first approximation this seems counterintuitive

because both involve breaking bonds. However, in the case of forming a vacancy, there are other effects. Chief among these is the strengthening of bonds between those surrounding the vacancy and their remaining neighbors due to the presence of valence electrons that otherwise would have participated in bonding to the missing atom. The higher the VEC of the atoms surrounding a vacancy, the more opportunity for strengthening the remaining bonds. Hence the stronger correlation between CVFEs and ζ (as a surrogate for VEC). This same effect is also apparent in Fig. 3.5 for the binaries, where higher ζ values correspond to smaller CVFEs.

Another interesting question arises from the additivity of ζ and the local electronic structure of each cation. Do cations in HECs retain a ζ that reflects that of the constitutive binary, or do the cations in a HEC all equilibrate to the same ζ , as might be expected given that they are electrical conductors? To illustrate this issue, plotted in Figure 3.8 is the local density of states for the cations in their binaries (left column) and the local density of states for the same cations in HEC9 (right column). In the binaries, the ζ values for Hf and Ti are 0.00338 eV and 0.0508 eV, respectively, while ζ for W, Ta and Nb are 3.13 eV, 1.42eV and 1.82eV, for an average value of 1.28eV. For all of the cations in this HEC, the same ζ value of 1.48 eV occurs as taken from the local density of states.

Finally, the analysis above established a correlation between the standard deviation of the distribution of all CVFEs (as given by the model that used ζ values) and the EFA for a given composition. However, no other information regarding the distributions was discussed. Plotted in Fig. 3.9 are histograms of the CVFE energy distributions given by the ζ model for all 56 compositions (black lines). Also plotted are Normal distributions with the same average and standard deviation of the CVFE's (gray lines). For some distributions, like that shown for the composition with an EFA of 125 (HEC16), the CVFE and corresponding Normal distribution are

similar. For other compositions, however, the CVFE distribution has well-separated peaks that do not resemble the corresponding Normal distribution. The distribution for the composition with an EFA of 38 (HEC8), for example, has a CVFE distribution with seven separated clusters of values (including the short cluster at about 0.5 eV). In addition, the number of sites associated with each of two lowest energy clusters, centered at about 0.5 eV and 0.7 eV, are larger than what would be expected for a Normal distribution. Hence there are additional features of the CVFE distributions beyond the average and spread of values that are important when considering carbon vacancies.

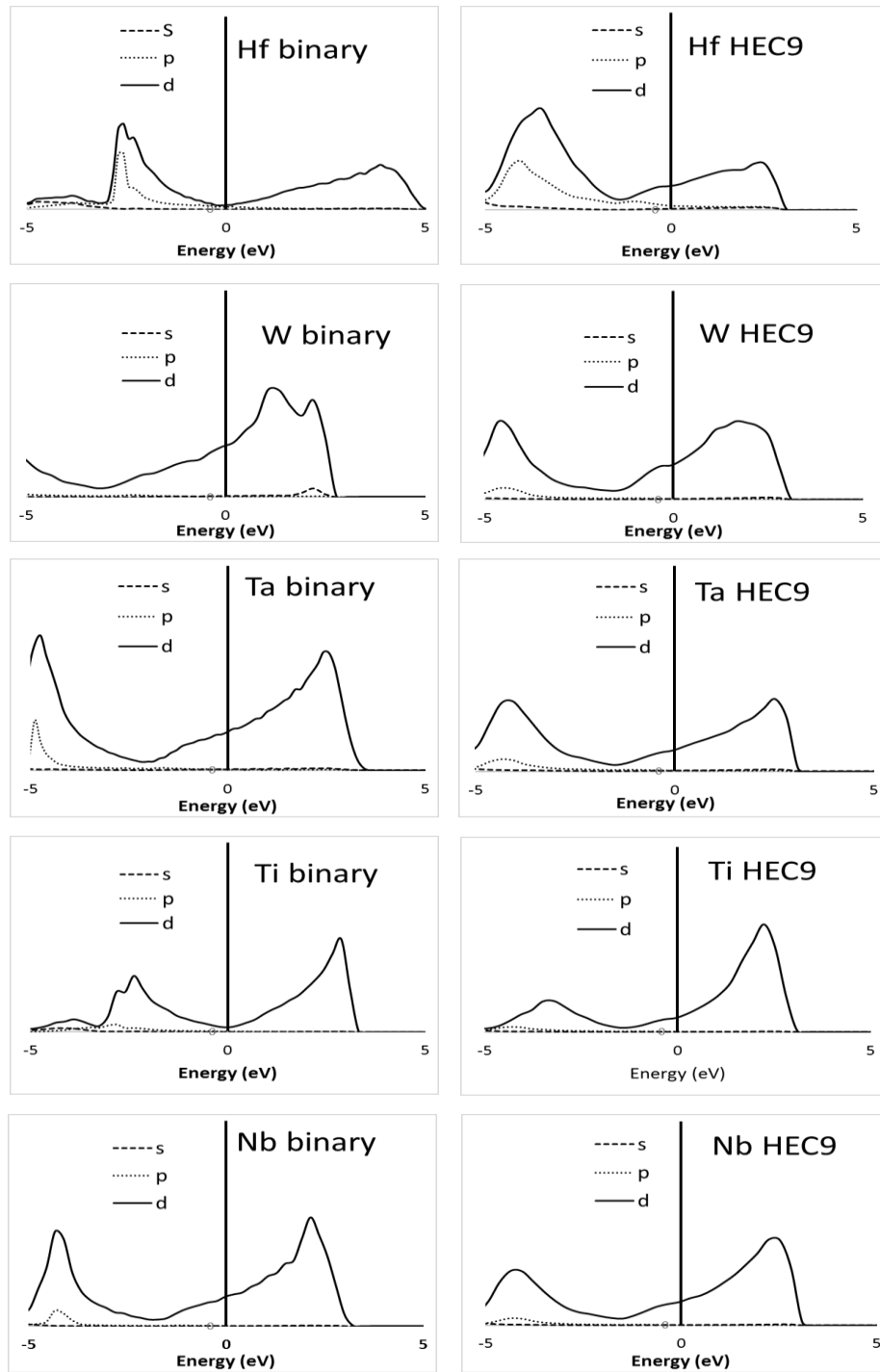
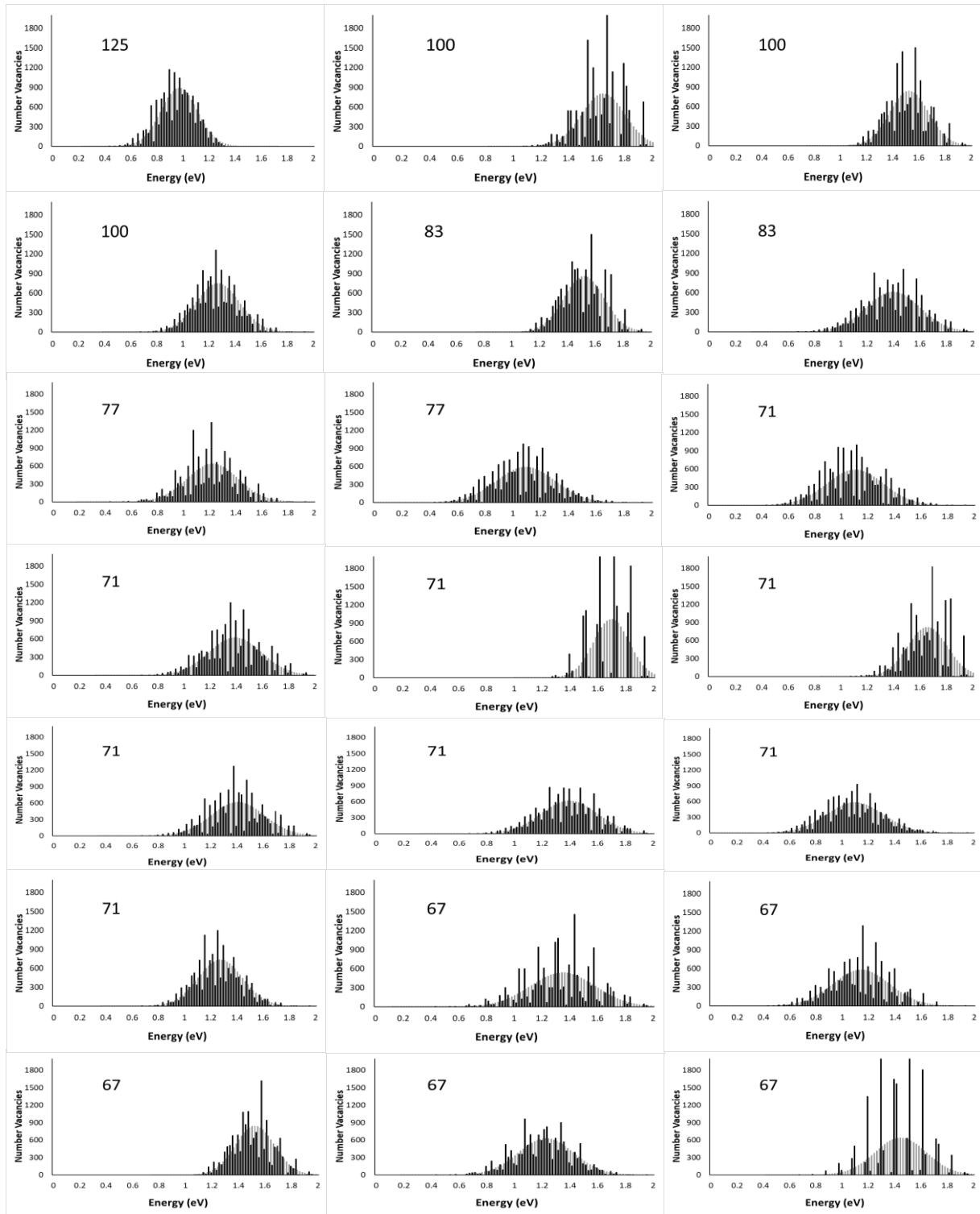
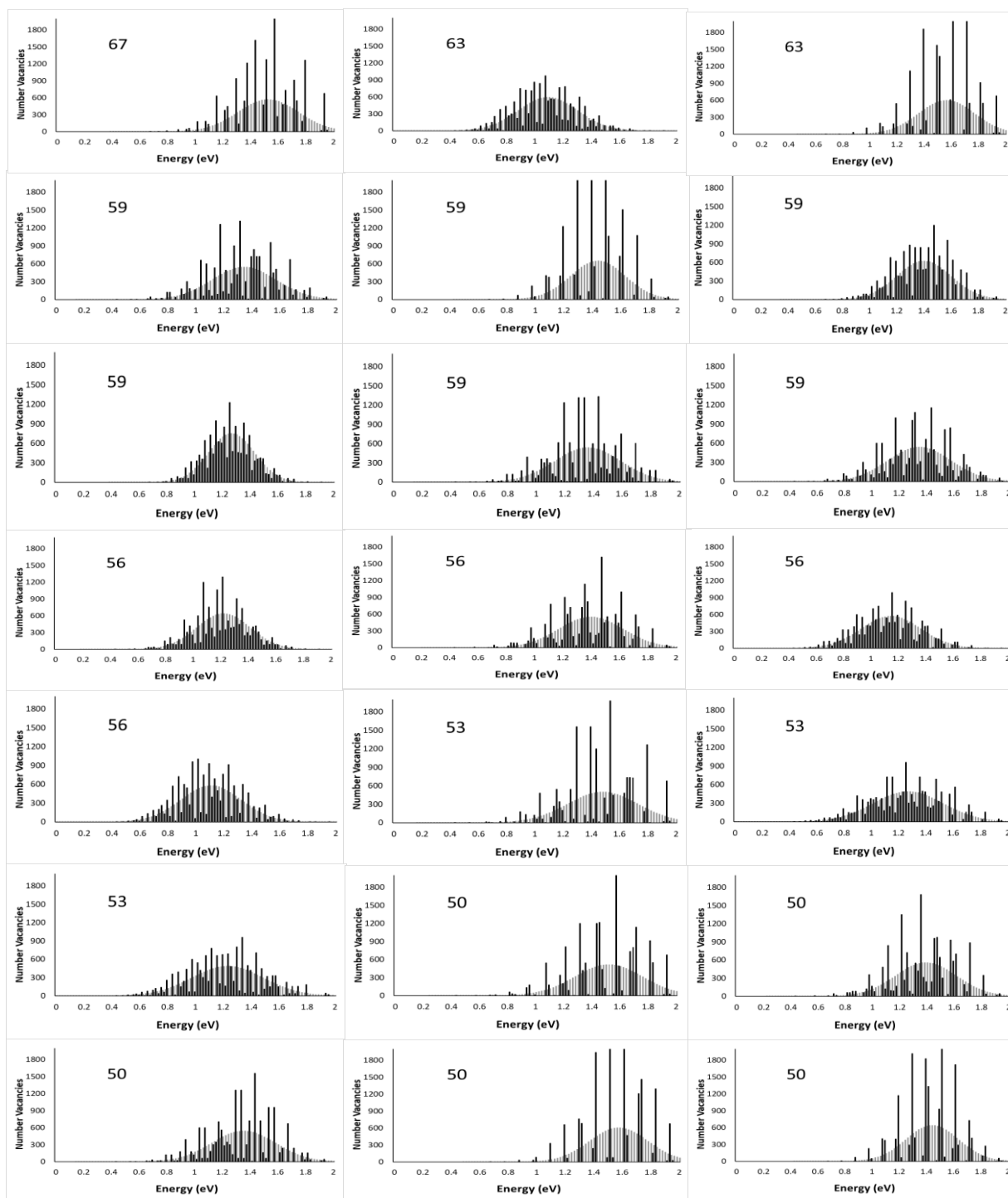
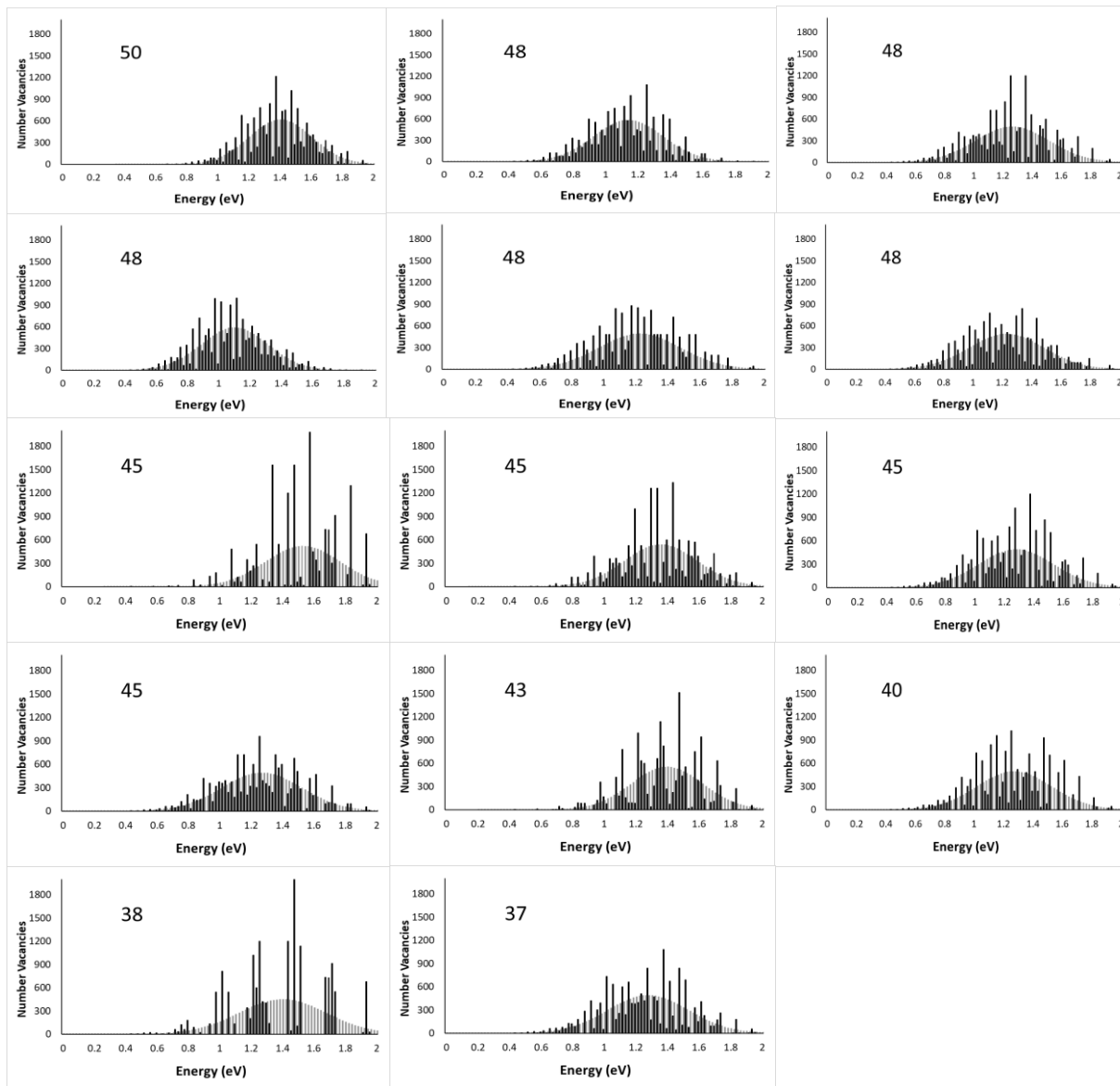


Figure 3.8 Partial density of states for the cations in the binaries and in HEC9. The ζ , which vary widely in the binaries, equilibrate to the same value of 1.28 eV in the HEC.

Figure 3.9 Distributions of the 15,625 CVFEs for each of the 56 compositions, denoted by their EFA value. The black histogram bars are calculated from the function of constitutive ζ values. The grey histogram bars correspond to a Normal function with the same average and standard deviation as the black bars.







3.8 Conclusions

This paper focused on two questions: (1) to what degree can the properties of HECs be predicted from their respective binaries, and (2) are there relationships between the properties of the binary compounds that correspond to a given HEC composition and the value of that composition's EFA. It was found that lattice constant, binding energy, bulk modulus, average CVFE and average ζ are all well approximated by averages of the constitutive binary carbides. Binary averaging was then used to calculate properties of all 56 possible compositions, and using these properties, correlations were discovered between the EFA of a given composition and the standard deviation of the distribution of bulk moduli and ζ of the constituent binaries. Two simple expressions were also developed from which individual CVFEs can be estimated from the local environment of the missing carbon atom. One method uses the weighted averaging of the binary CVFEs that correspond to near-neighbor vacancy composition, while the second uses a linear relation between the weighted average of the ζ of the binaries in the local environment of the missing carbon atom and the CVFE. Using this expression to calculate the CVFEs for all possible environments in each of the 56 compositions, it was shown that there is a correlation between the standard deviation of the CVFEs for each HEC and the EFA of that composition. This result supports the EFA as a central quantity for estimating properties of HECs beyond phase stability.

It was also shown that the distributions of CVFEs in these HECS may not be Normal depending on the composition, and that there may be additional analysis of these distributions that could lead to better correlations with EFA and additional insight into the point defect properties of these materials.

ACKNOWLEDGEMENTS

The authors acknowledge support through the Office of Naval Research ONR-MURI (grant No. N00014-15-1-2863).

References

1. Rost, C. M. *et al.* Entropy-stabilized oxides. *Nat. Commun.* **6**, 8485 (2015).
2. Sarkar, A. *et al.* High-Entropy Oxides: Fundamental Aspects and Electrochemical Properties. *Adv. Mater.* (2019). doi:10.1002/adma.201806236
3. Rost, C. M., Rak, Z., Brenner, D. W. & Maria, J.-P. Local structure of the $\text{Mg}_x\text{Ni}_x\text{Co}_x\text{Cu}_x\text{Zn}_x\text{O}(x=0.2)$ entropy-stabilized oxide: An EXAFS study. *J. Am. Ceram. Soc.* (2017). doi:10.1111/jace.14756
4. Berardan, D., Franger, S., Meena, A. K. & Dragoë, N. Room temperature lithium superionic conductivity in high entropy oxides. *J. Mater. Chem. A* 9536–9541 (2016). doi:10.1039/C6TA03249D
5. Sarkar, A. *et al.* Nanocrystalline multicomponent entropy stabilised transition metal oxides. *J. Eur. Ceram. Soc.* (2017). doi:10.1016/j.jeurceramsoc.2016.09.018
6. Sarkar, A. *et al.* Multicomponent equiatomic rare earth oxides with a narrow band gap and associated praseodymium multivalency. *Dalt. Trans.* (2017). doi:10.1039/c7dt02077e
7. Sarkar, A. *et al.* High entropy oxides for reversible energy storage. *Nat. Commun.* (2018). doi:10.1038/s41467-018-05774-5
8. Wang, Q. *et al.* High entropy oxides as anode material for Li-ion battery applications: A practical approach. *Electrochem. commun.* (2019). doi:10.1016/j.elecom.2019.02.001
9. Witte, R. *et al.* High-entropy oxides: An emerging prospect for magnetic rare-earth transition metal perovskites. *Phys. Rev. Mater.* (2019). doi:10.1103/PhysRevMaterials.3.034406
10. Oses, C., Toher, C. & Curtarolo, S. High-entropy ceramics. *Nature Reviews Materials* (2020). doi:10.1038/s41578-019-0170-8
11. Gild, J. *et al.* High-Entropy Metal Diborides: A New Class of High-Entropy Materials and a New Type of Ultrahigh Temperature Ceramics. *Sci. Rep.* **6**, 2–11 (2016).
12. Tallarita, G., Licheri, R., Garroni, S., Orrù, R. & Cao, G. Novel processing route for the fabrication of bulk high-entropy metal diborides. *Scr. Mater.* (2019). doi:10.1016/j.scriptamat.2018.08.039
13. Liu, D., Wen, T., Ye, B. & Chu, Y. Synthesis of superfine high-entropy metal diboride powders. *Scr. Mater.* (2019). doi:10.1016/j.scriptamat.2019.03.038

14. Mayrhofer, P. H., Kirnbauer, A., Ertelthaler, P. & Koller, C. M. High-entropy ceramic thin films; A case study on transition metal diborides. *Scr. Mater.* **149**, 93–97 (2018).
15. Harrington, T. J. *et al.* Phase stability and mechanical properties of novel high entropy transition metal carbides. *Acta Mater.* (2019). doi:10.1016/j.actamat.2018.12.054
16. Castle, E., Csanádi, T., Grasso, S., Dusza, J. & Reece, M. Processing and Properties of High-Entropy Ultra-High Temperature Carbides. *Sci. Rep.* (2018). doi:10.1038/s41598-018-26827-1
17. Yan, X. *et al.* (Hf_{0.2}Zr_{0.2}Ta_{0.2}Nb_{0.2}Ti_{0.2})C high-entropy ceramics with low thermal conductivity. *J. Am. Ceram. Soc.* (2018). doi:10.1111/jace.15779
18. Zhou, J. *et al.* High-entropy carbide: A novel class of multicomponent ceramics. *Ceram. Int.* (2018). doi:10.1016/j.ceramint.2018.08.100
19. Yang, Y., Wang, W., Gan, G. Y., Shi, X. F. & Tang, B. Y. Structural, mechanical and electronic properties of (TaNbHfTiZr)C high entropy carbide under pressure: Ab initio investigation. *Phys. B Condens. Matter* (2018). doi:10.1016/j.physb.2018.09.014
20. Dusza, J. *et al.* Microstructure of (Hf-Ta-Zr-Nb)C high-entropy carbide at micro and nano/atomic level. *J. Eur. Ceram. Soc.* (2018). doi:10.1016/j.jeurceramsoc.2018.05.006
21. Gao, M. C, Yeh, J. W, Liaw, P. K. & Zhang, Y. *High-Entropy Alloys: Fundamentals and Applications*. (Springer, 2016).
22. Tsai, M.-H. & Yeh, J.-W. High-Entropy Alloys: A Critical Review. *Mater. Res. Lett.* **2**, 107–123 (2014).
23. Miracle, D. B. Critical Assessment 14:High entropy alloys and their development as structural materials. *Mater. Sci. Technol.* **31**, 1142–1147 (2015).
24. Widom, M. Modeling the structure and thermodynamics of high-entropy alloys. *Journal of Materials Research* (2018). doi:10.1557/jmr.2018.222
25. Ye, Y. F., Wang, Q., Lu, J., Liu, C. T. & Yang, Y. High-entropy alloy: challenges and prospects. *Materials Today* (2016). doi:10.1016/j.mattod.2015.11.026
26. Lim, X. Mixed-up metals make for stronger, tougher, stretchier alloys. *Nature* (2016). doi:10.1038/533306a
27. Gludovatz, B. *et al.* A fracture-resistant high-entropy alloy for cryogenic applications. *Science* (80-.). (2014). doi:10.1126/science.1254581
28. Li, Z., Pradeep, K. G., Deng, Y., Raabe, D. & Tasan, C. C. Metastable high-entropy dual-

- phase alloys overcome the strength-ductility trade-off. *Nature* (2016).
doi:10.1038/nature17981
29. Tsao, T. K. *et al.* The High Temperature Tensile and Creep Behaviors of High Entropy Superalloy. *Sci. Rep.* (2017). doi:10.1038/s41598-017-13026-7
 30. Senkov, O. N., Wilks, G. B., Miracle, D. B., Chuang, C. P. & Liaw, P. K. Refractory high-entropy alloys. *Intermetallics* (2010). doi:10.1016/j.intermet.2010.05.014
 31. Li, Z., Tasan, C. C., Springer, H., Gault, B. & Raabe, D. Interstitial atoms enable joint twinning and transformation induced plasticity in strong and ductile high-entropy alloys. *Sci. Rep.* (2017). doi:10.1038/srep40704
 32. The Freezing Points, Melting Points, and Solid Solubility Limits of the Alloys of Silver, and Copper with the Elements of the B Sub-Groups. *Philos. Trans. R. Soc. A Math. Phys. Eng. Sci.* (1934). doi:10.1098/rsta.1934.0014
 33. Hume-Rothery, W. Atomic diameters, atomic volumes and solid solubility relations in alloys. *Acta Metall.* (1966). doi:10.1016/0001-6160(66)90267-7
 34. Hume-Rothery, W. & Coles, B. R. The transition metals and their alloys. *Adv. Phys.* (1954). doi:10.1080/00018735400101193
 35. Wang, Z., Huang, Y., Liu, C. T., Li, J. & Wang, J. Atomic packing and size effect on the Hume-Rothery rule. *Intermetallics* (2019). doi:10.1016/j.intermet.2019.04.001
 36. Rak, Z. *et al.* Charge compensation and electrostatic transferability in three entropy-stabilized oxides: Results from density functional theory calculations. *J. Appl. Phys.* **120**, (2016).
 37. Sarker, P. *et al.* High-entropy high-hardness metal carbides discovered by entropy descriptors. *Nat. Commun.* (2018). doi:10.1038/s41467-018-07160-7
 38. Zunger, A., Wei, S., Ferreira, L. & Bernard, J. Special Quasirandom Structures. *Phys. Rev. Lett.* **65**, 353–356 (1990).
 39. Nosé, S. & Nosé, S. A unified formulation of the constant temperature molecular dynamics methods. *J. Chem. Phys.* **81**, 511 (1984).
 40. Kresse, G. & Furthmüller, J. Efficiency of ab-initio total energy calculations for metals and semiconductors using a plane-wave basis set. *Comput. Mater. Sci.* **6**, 15–50 (1996).
 41. Kresse, G. & Furthmüller, J. Efficient iterative schemes for ab initio total-energy calculations using a plane-wave basis set. *Phys. Rev. B. Condens. Matter* **54**, 11169–

- 11186 (1996).
42. Kresse, G. & Hafner, J. Ab initio molecular dynamics for liquid metals. *Phys. Rev. B* **47**, 558–561 (1993).
 43. Perdew, J. P., Burke, K. & Ernzerhof, M. Generalized gradient approximation made simple. *Phys. Rev. Lett.* (1996). doi:10.1103/PhysRevLett.77.3865
 44. Kamal, M., El-Bediwi, A. B., El-Ashram, T. & Dorgham, M. E. The Role of Valence Electron Concentration on the Structure and Properties of Rapidly Solidified Sn-Ag Binary Alloys. *Mater. Sci. Appl.* (2012). doi:10.4236/msa.2012.33028
 45. Sangiovanni, D. G., Hultman, L. & Chirita, V. Supertoughening in B1 transition metal nitride alloys by increased valence electron concentration. *Acta Mater.* (2011). doi:10.1016/j.actamat.2010.12.013
 46. Guo, S., Ng, C., Lu, J. & Liu, C. T. Effect of valence electron concentration on stability of fcc or bcc phase in high entropy alloys. in *Journal of Applied Physics* (2011). doi:10.1063/1.3587228
 47. Guo, S. & Liu, C. T. Phase stability in high entropy alloys: Formation of solid-solution phase or amorphous phase. *Prog. Nat. Sci. Mater. Int.* (2011). doi:10.1016/S1002-0071(12)60080-X
 48. Keil, T., Bruder, E. & Durst, K. Exploring the compositional parameter space of high-entropy alloys using a diffusion couple approach. *Mater. Des.* (2019). doi:10.1016/j.matdes.2019.107816
 49. Tian, F., Varga, L. K. & Vitos, L. Predicting single phase CrMoWX high entropy alloys from empirical relations in combination with first-principles calculations. *Intermetallics* (2017). doi:10.1016/j.intermet.2016.12.007
 50. Balasubramanian, K., Khare, S. V. & Gall, D. Valence electron concentration as an indicator for mechanical properties in rocksalt structure nitrides, carbides and carbonitrides. *Acta Mater.* (2018). doi:10.1016/j.actamat.2018.04.033
 51. Tian, F., Varga, L. K., Chen, N., Shen, J. & Vitos, L. Empirical design of single phase high-entropy alloys with high hardness. *Intermetallics* (2015). doi:10.1016/j.intermet.2014.10.010
 52. Brown, H. L., Armstrong, P. E. & Kempter, C. P. Elastic Properties of Some Polycrystalline Transition-Metal Monocarbides. *J. Chem. Phys.* (1966).

doi:10.1063/1.1727602

53. Isaev, E. I. *et al.* Anomalously enhanced superconductivity and ab initio lattice dynamics in transition metal carbides and nitrides. *Phys. Rev. B - Condens. Matter Mater. Phys.* (2005). doi:10.1103/PhysRevB.72.064515
54. Bowman, A. L. THE VARIATION OF LATTICE PARAMETER WITH CARBON CONTENT OF TANTALUM CARBIDE 1 . *J. Phys. Chem.* (2007). doi:10.1021/j100905a028
55. Guemmaz, M., Mosser, A., Ahujab, R. & Johansson, B. Elastic properties of sub-stoichiometric titanium carbides. Comparison of FP-LMTO calculations and experimental results. *Solid State Commun.* (1999). doi:10.1016/S0038-1098(99)00091-5
56. Zhang, T. *et al.* First-principles study on the mechanical properties and electronic structure of V doped WCoB and W₂CoB₂ ternary borides. *Materials (Basel)*. (2019). doi:10.3390/ma12060967
57. Komsa, H. P. & Krashenninnikov, A. V. Native defects in bulk and monolayer MoS₂ from first principles. *Phys. Rev. B - Condens. Matter Mater. Phys.* (2015). doi:10.1103/PhysRevB.91.125304
58. De Oliveira, C., Salahub, D. R., De Abreu, H. A. & Duarte, H. A. Native defects in α -Mo₂C: Insights from first-principles calculations. *J. Phys. Chem. C* (2014). doi:10.1021/jp507947b
59. Zhu, M., Wu, P., Li, Q. & Xu, B. Vacancy-induced brittle to ductile transition of W-M co-doped Al₃Ti (M=Si, Ge, Sn and Pb). *Sci. Rep.* (2017). doi:10.1038/s41598-017-14398-6

Chapter 4. Understanding the electronic structure of high entropy carbides by first principle study

4.1 Introduction

High entropy materials are known as a single phase crystalline which stabilized by entropic contributions. Their superior properties like high strength^{1,2,3,4}, ductility^{3,5,6}, hardness^{1,7,8}, and superconductivity⁹ to conventional ceramics or metals are reported and highlighted. Started from the study of the high entropy alloys, entropy concept has been extended to entropy stabilized oxides^{10,11,12,13}, high entropy borides¹⁴, and high entropy carbides¹⁵⁻¹⁷. The latter ceramic classes also offer remarkable thermo mechanical properties and the higher oxidation resistance.¹⁸ Especially, the high entropy carbides have great potentials for thermal protection coatings with the resistance to extreme heat^{19,20} and oxidation¹⁵. Understanding their thermal and electronic transport behavior would be open new possibilities to improve the performance of thermoelectric materials.

Recently, Sarker et al²¹ introduced the ab initio entropy descriptor that is called the Entropy Forming Ability (EFA) of a composition and lattice using a first principle study for the high entropy carbides (HECs). The formation of single phase high entropy carbides is systematically evaluated by the energy distribution spectra of the structures that are generated by Automatic FLOW (AFLOW) partial occupation (AFLOWPOCC) method.²² They have used equi-molar combinations of five of the set of eight transition metals Hf, Nb, Mo, Ta, Ti, V, W and Zr and generate a total of 56 five-metal composition carbides. Nine candidate systems were experimentally synthesized, and the experiments validated the prediction of the phase from the EFA. Harrington et al.²³ synthesized the twelve of these predicted 56 structures and compared

the phases and analysis against the first principles predictions. The phase comparison with single or multiple phases from the experiment confirms that the EFA is correctly predicted the HECs phases. They focused on a systematic study on the phase stability and mechanical properties of HEC synthesized from group IV, V and VI metal carbides. Nine of the twelve compositions are determined to be a single phase at a high temperature over 2400K. Mechanical properties are also examined in terms of hardness and elastic modulus. The high entropy transition metal carbides result significantly enhanced hardness over the weighted average binary constituent carbides.

In this chapter, we further analyze the electrical properties of the nine high entropy carbide compositions. These nine compositions and their phase stability are given in Table 3.1. The knowledge of the electronic structure is performed by Density Functional Theory (DFT), and the electronic transport properties, i.e. electrical conductivity, of high entropy carbides and the corresponding binaries are calculated with the constant relaxation time using the semi-classical approach provided by the Boltzmann transport theory.^{24,25,26,27} The electronic transport data of the binary carbides and the nine HECs is obtained by BoltzTraP²⁷ and DFT.

4.2 Computational Method

The DFT supercells used for the high entropy carbide compositions and binary carbides contained 40 carbon atoms and 40 metal atoms on the two face-centered cubic sublattices of the rocksalt structure, respectively, with the latter containing equal numbers of five different atom types arranged on their sublattice using the special quasi-random structure (SQS) algorithm.²⁸ The calculations were carried out using plane wave PAW pseudopotential methods^{29,30} as implemented in the Vienna Ab initio Simulation Package (VASP).³⁰⁻³² The generalized gradient

approximation as parameterized by Perdew *et al.*³³ was used for the exchange-correlation potential. The energy of the system was minimized with respect to atom positions and lattice constant. A cut-off energy for the plane wave basis was set to 520 eV, and convergence was assumed when the energy difference between two consecutive self-consistent cycles was less than 2 meV with the Γ -centered 22X11X4 points.

The BoltzTraP code solves Boltzmann equation³⁴²⁵ by interpolating the electronic band structure that computed from DFT. The data of the crystal structure and the electronic band structure are needed as inputs to run BoltzTraP. Practically, the electronic energies for each k points calculated by the DFT are used to interpolate the bands based on a Fourier expansion and compute the Fermi integrals for different temperatures and Fermi level.³⁵³⁶³⁷³⁸ The Boltzmann transport equation can be derived by considering how a distribution function changes in time, and solving the Boltzmann transport theory with the knowledge of the band structure will provide an assessment of the electronic transport tensors.²⁶²⁷ The BoltzTraP code has been verified in many different applications such as superconductors³⁹ and thermoelectric materials.⁴⁰⁴¹⁴² The output values from the BoltzTraP code have shown good agreement with the experimental values.⁴³⁴⁴ We examine the electronic properties obtained by the electronic energies, band structure from the DFT calculation and BoltzTraP within the constant relaxation time approximation.

4.3 Results

Summarized in Table 4.1 are the calculated electrical conductivity over the relaxation time for the eight binaries and the nine high entropy carbides in a rocksalt structure as given by the DFT and BoltTraP calculations and the comparison to the experiment reference values of the binaries for the validation. Experimental values for the electrical conductivity are given in the

parenthesis for the binary carbides. Figure 4.1 is the calculated electrical conductivity over the relaxation time as function of the experimental electrical conductivity values. It represents that our calculations and the experimental values are quite linearly related. For consistency, we compare the calculation values with the relaxation time. Summarized in Table 4.2 and plotted in Figure 4.2 are the number of electrons at the Fermi level like +/- 0.1 and 0.2 eV and the electrical conductivity over the relaxation time (σ/τ) of the eight binary carbides and the nine high entropy carbides in a rocksalt structure as given by the DFT and BoltTraP calculations. The range of the energy is selected from the Fermi Dirac function that the electrons most contribute to the transport properties.

Table 4.1 Composition the calculated σ/τ and the experimental electrical conductivity of the binaries.

	Calculated σ/τ
TiC	1.42E+20 (1.00E+06) ^a
VC	2.01E+20 (1.45E+06) ^a
ZrC	2.86E+20 (2.32E+06) ^{b,c}
NbC	2.94E+20 (2.00E+06) ^d
MoC	2.76E+20 (1.75E+06) ^a
HfC	3.01E+20 (3.09E+06) ^e
TaC	3.06E+20 (3.33E+06) ^f
WC	4.93E+20 (5.88E+06) ^a

^a Reference⁴⁵, ^{b,c} Reference^{46,47}, ^d Reference⁴⁸, ^e Reference⁴⁹, ^f Reference⁵⁰

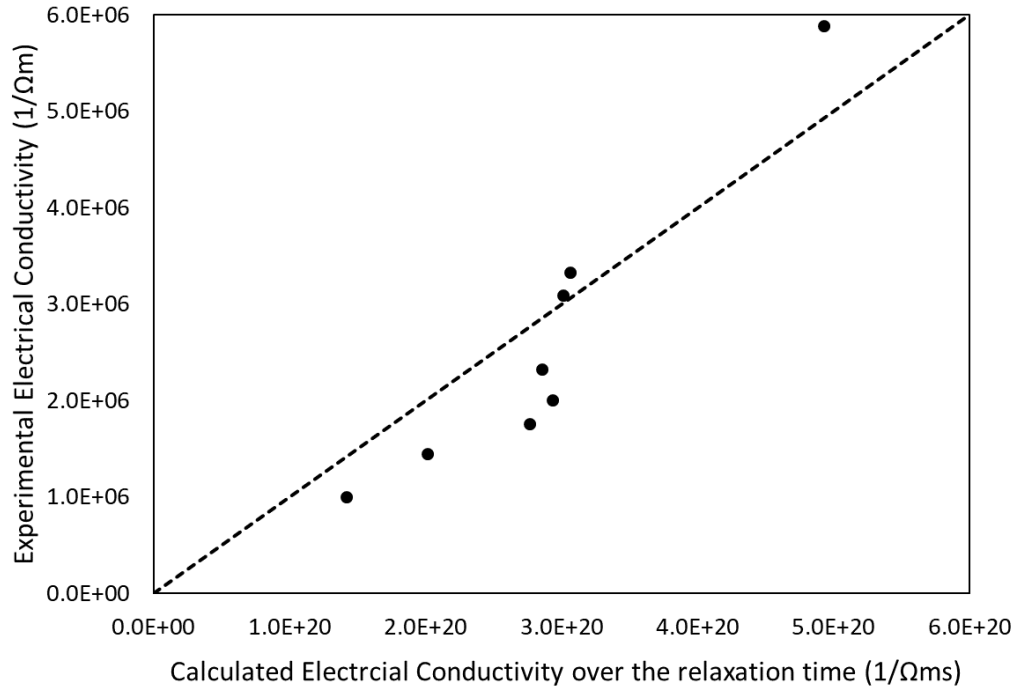


Figure 4.1 The calculated electrical conductivity over the relaxation time for the binaries as function of the experimental electrical conductivity.

The density of states (DOS) of each binary and HEC systems are integrated in the range of +/- 0.1 and 0.2 eV in order to count the number of electrons. The σ/τ is not following the number of electrons. MoC has the largest number of electrons at both +/- 0.1 and 0.2 eV, 9.59 and 19.54, respectively, but the σ/τ is not the highest. WC has the third highest number of electrons, but having the highest σ/τ . Also, HfC has the lowest number of electrons, the σ/τ is the second highest. Our results show the number of electrons and the electrical conductivity are not acting proportionally. Interestingly, all the HECs have lower σ/τ than all eight binaries. TiC has the lowest σ/τ in binaries, and all HECs have lower σ/τ than TiC. Black line in the figure 4.2 indicates that all σ/τ of the HECs are laying below the lowest σ/τ value of TiC. With this finding, we can predict a guideline of the electrical conductivity of HECs based on the knowledge of the corresponding binaries' ones.

Table 4.2 The number of electrons at the Fermi level and the electrical conductivity over the relaxation time of the binary carbides and the HECs calculated from DFT and BoltzTraP.

	The number of electrons at the Fermi level		Calculated σ/τ
	+/- 0.1 eV	+/- 0.2eV	
TiC	2.32	4.74	1.42E+20
VC	9.07	18.31	2.01E+20
ZrC	2.36	4.89	2.86E+20
NbC	5.60	11.82	2.94E+20
MoC	9.57	19.54	2.76E+20
HfC	2.17	4.45	3.01E+20
TaC	4.51	10.11	3.06E+20
WC	7.62	16.36	4.93E+20
HEC3	4.39	9.02	7.18E+19
HEC4	5.99	11.86	3.76E+19
HEC5	6.63	13.22	6.75E+19
HEC6	5.31	10.97	9.71E+19
HEC7	5.07	9.80	6.15E+19
HEC8	6.30	12.05	4.66E+19
HEC9	5.35	10.40	5.79E+19
HEC10	6.47	13.52	3.74E+19
HEC16	7.61	15.17	4.43E+19

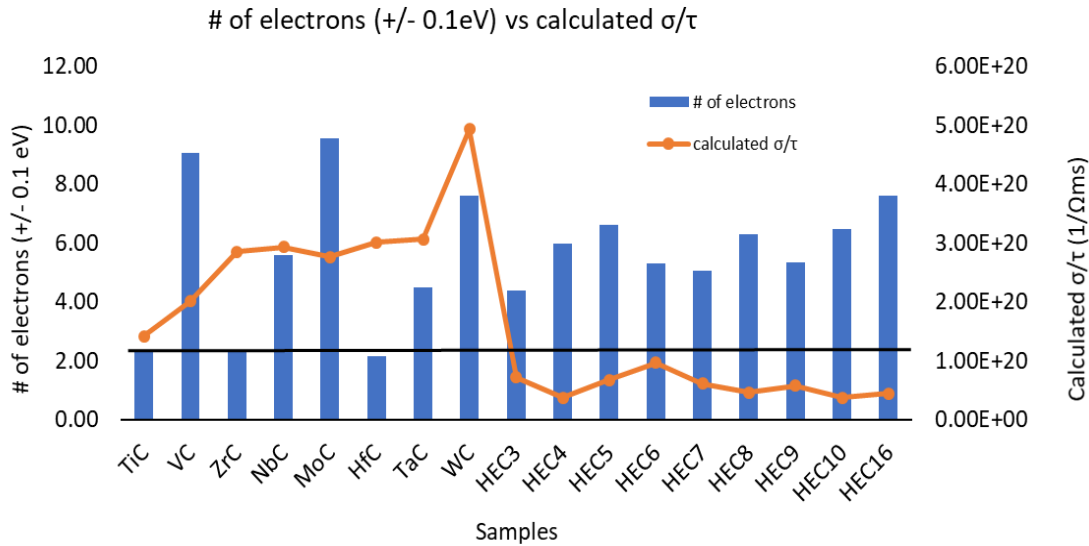
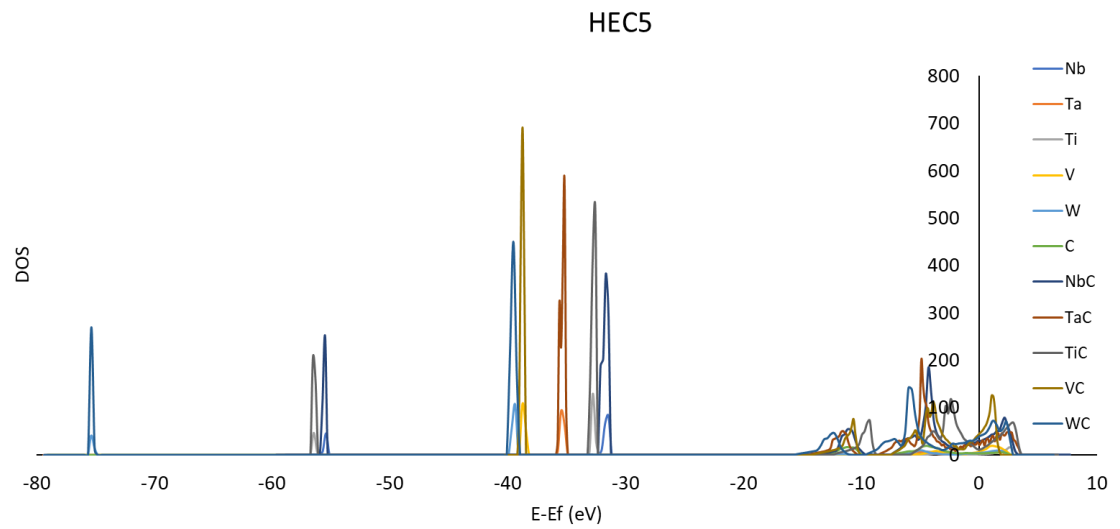
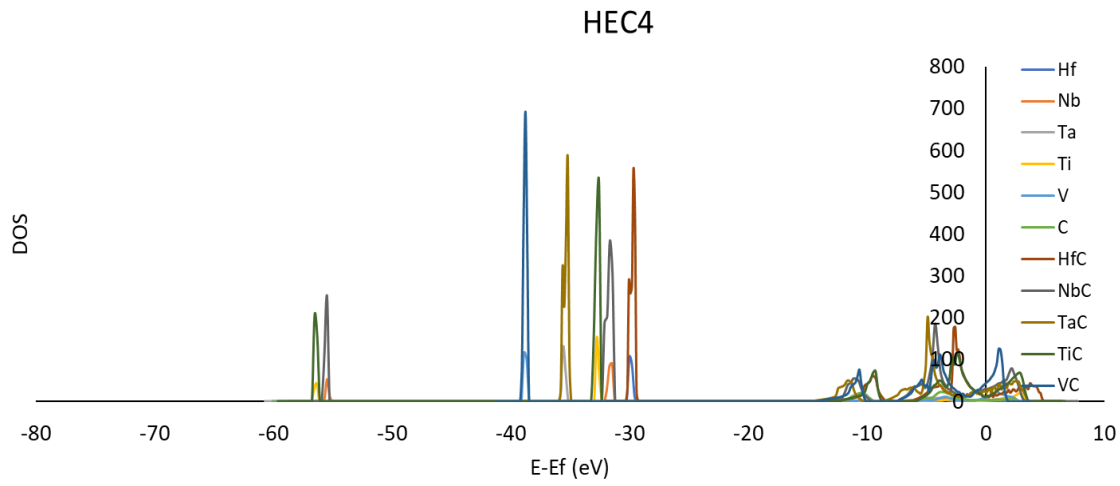
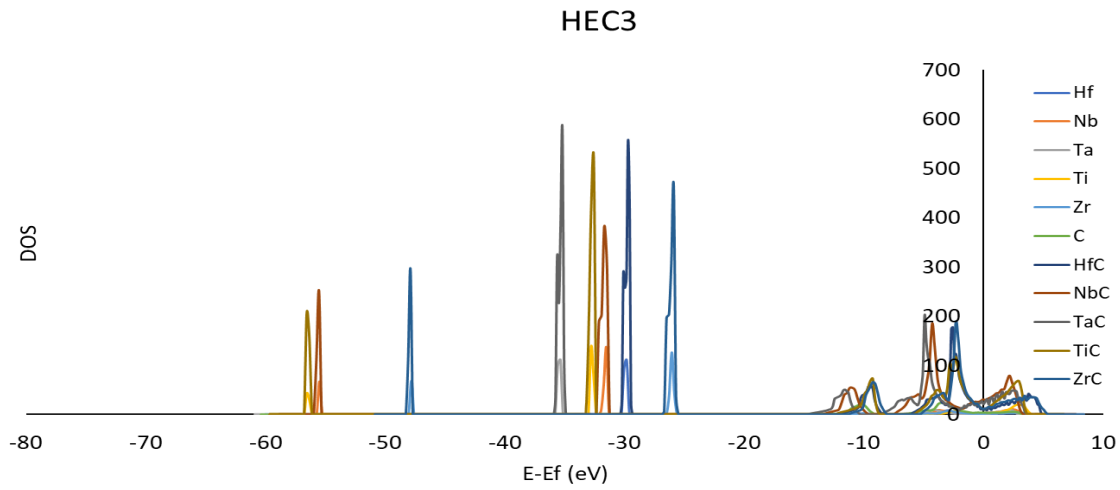
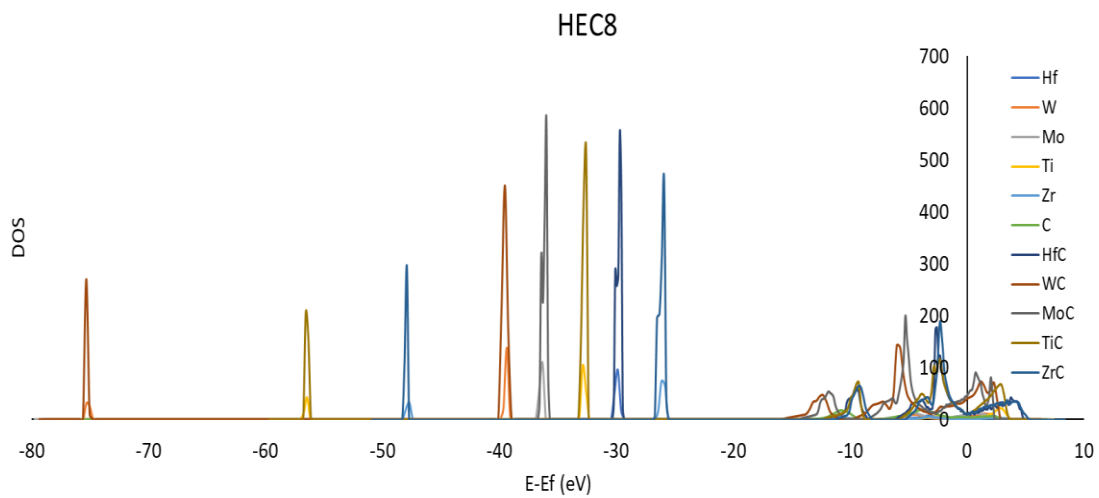
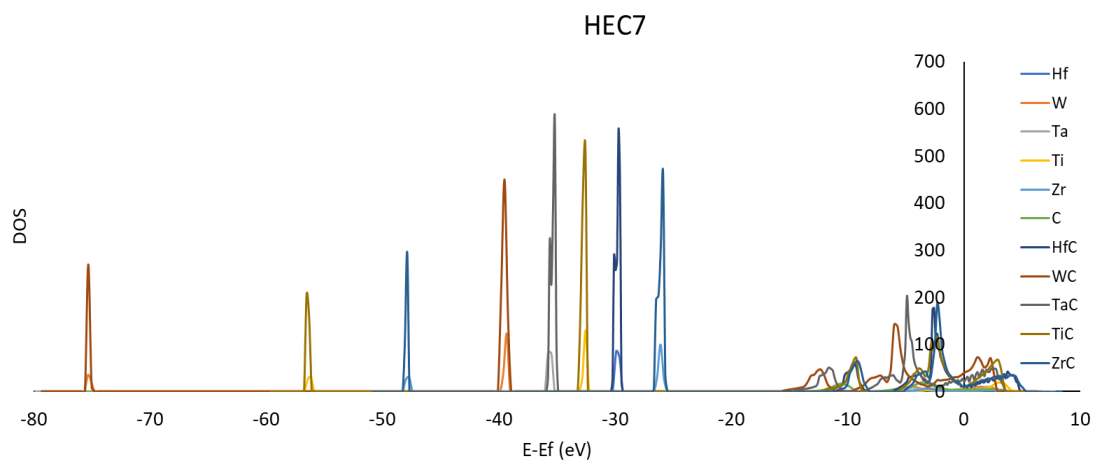
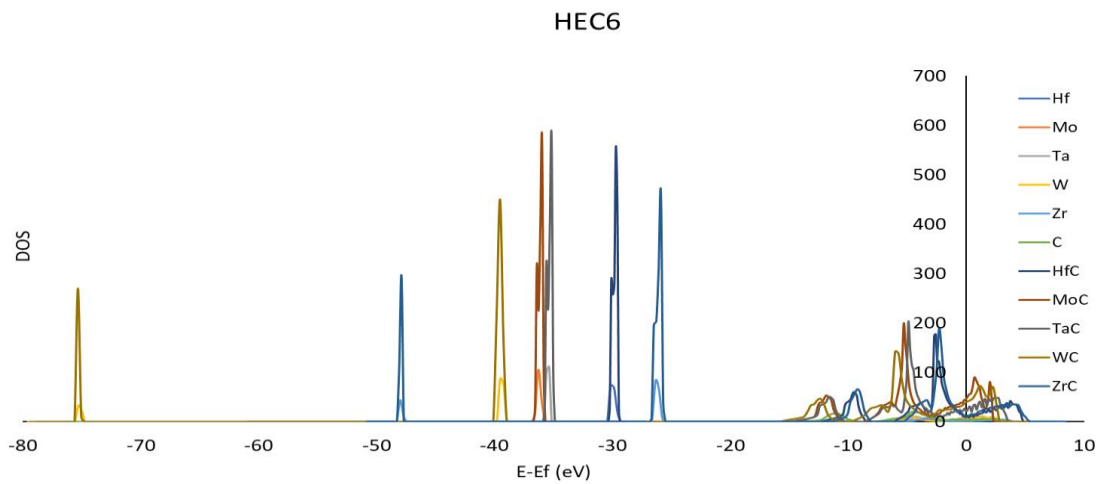


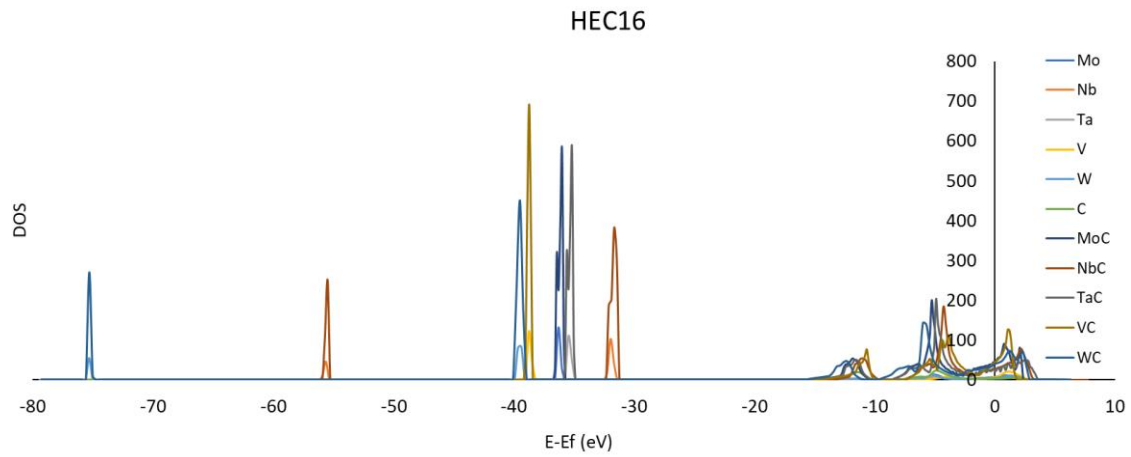
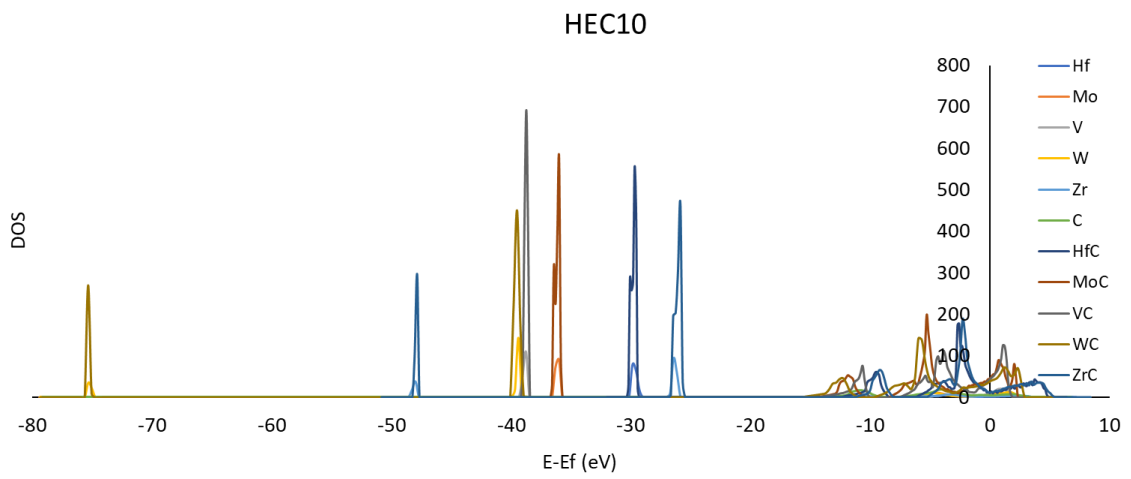
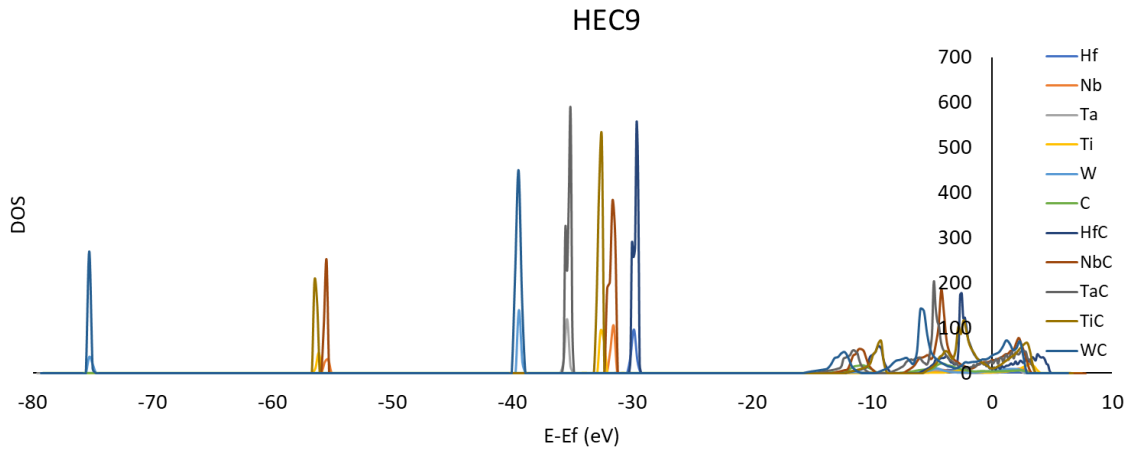
Figure 4.2 The comparison of the number of the electrons at the Fermi level near +/- 0.1 eV and the calculated electrical conductivity over the relaxation time for the binaries and HECs.

The density of states (DOS) is calculated to investigate the electronic structure in HECs and the binaries. Figure 4.3 is summarized the DOS of all HECs and the eight binaries. The DOS of HECs and the corresponding binaries are superimposed and the peaks in the HECs and the binaries are matched. It is shown that the electronic structure in metals in HECs keeps their binary metal characterization within the mixture of five metal compositions.

Figure 4.3 The Density of States (DOS) of HECs and the respective binaries are superimposed.



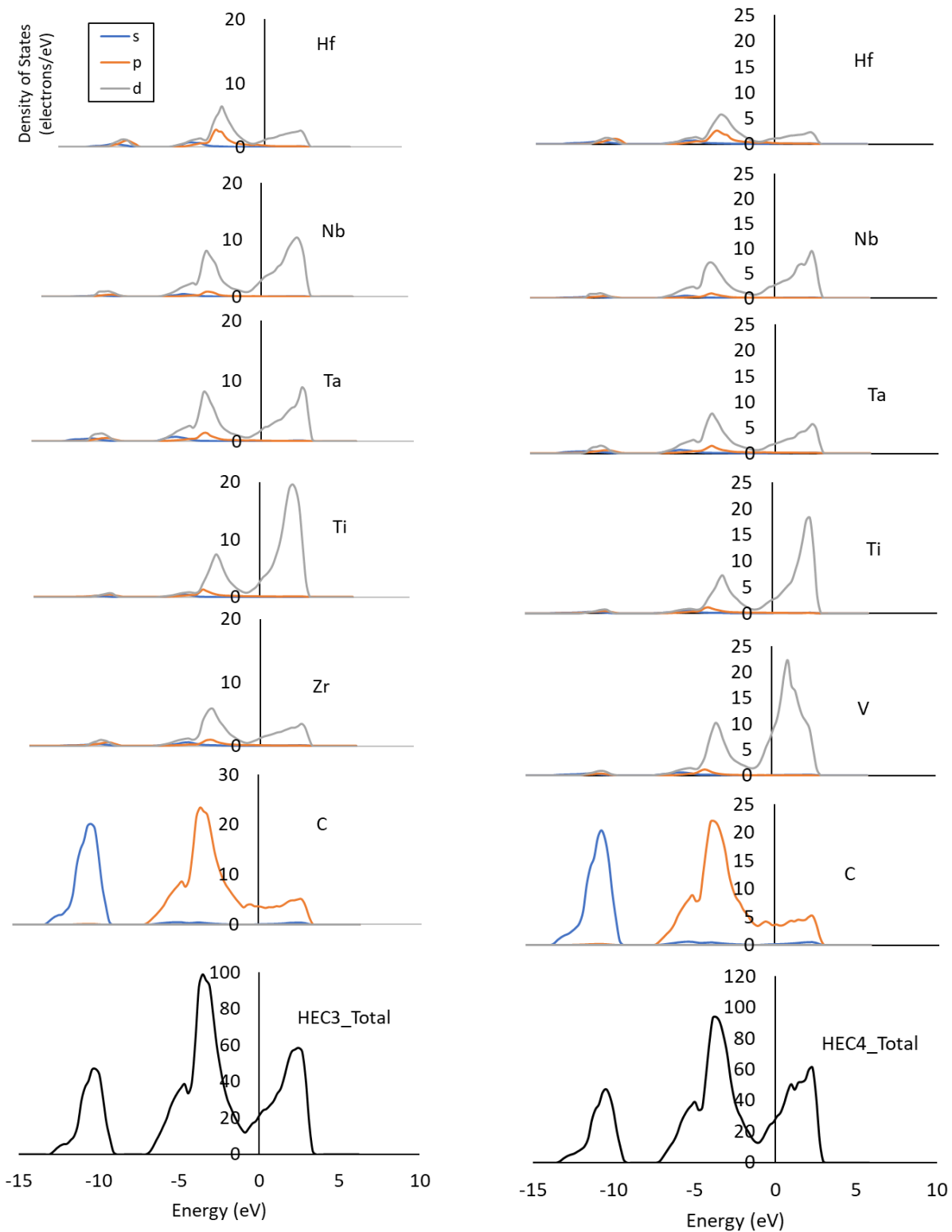


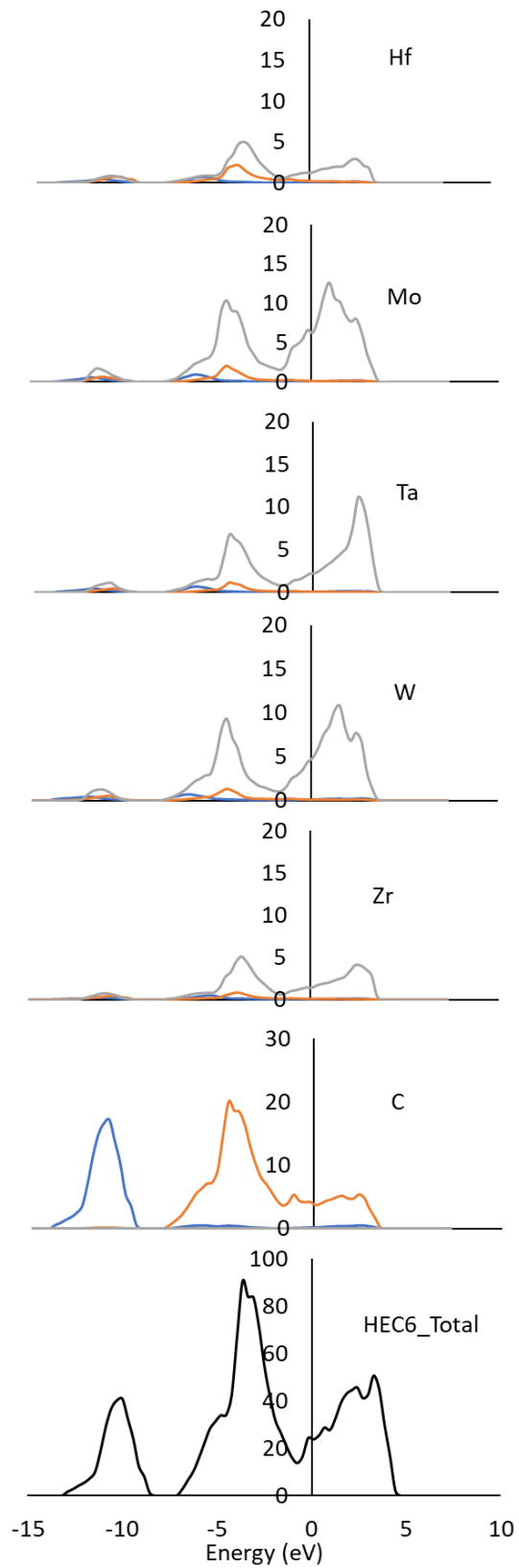
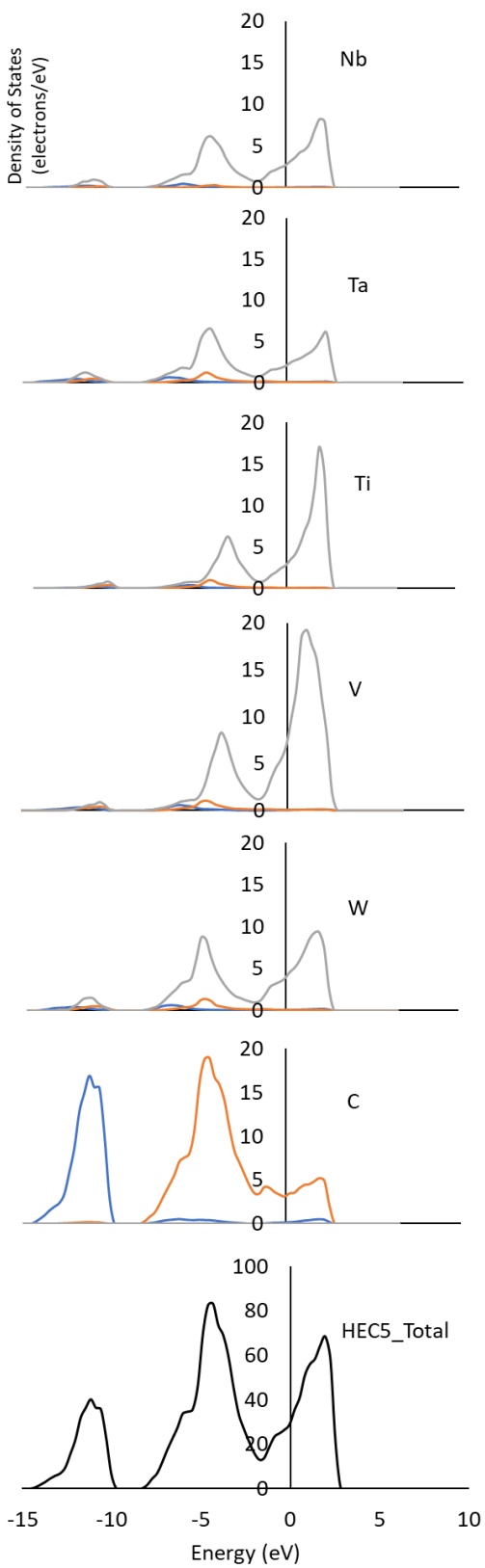


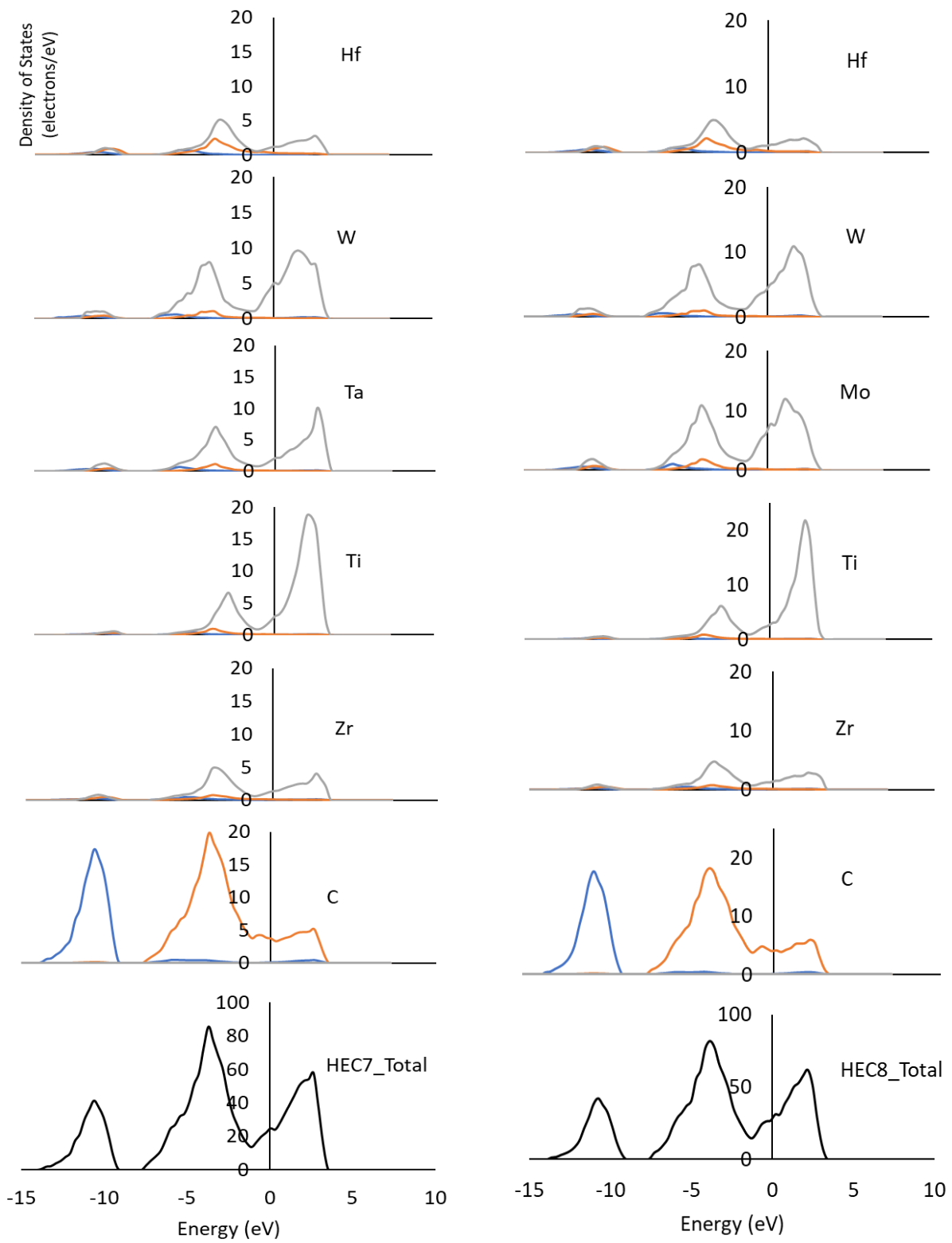
To further understand the details of the electronic structure, we also explored the partial density of states (PDOS) of HECs and binaries near the Fermi level. The PDOS in Fig 4.4 reveals the nature of the orbital hybridization of each element in HECs near the Fermi level at $E=0$. Mainly transition metal d orbitals hybridized with the orbital contribution of Carbon 2p around the Fermi level. It leads to the more metallic character and exhibiting covalent bond characteristics of HECs. The PDOS of all the binary carbides are shown in Fig 4.5 and the total DOS of each carbide is also formed by hybridization of d orbital in transition metals and 2p in carbon. From the Fig 4.4 and 4.5, the HECs and the eight binary carbides have similar electronic properties and the interaction between d orbitals of the metals and p orbitals of carbon determines the DOS. Overall, we observed strong covalent bonds with metallic characteristics in HECs and binaries.

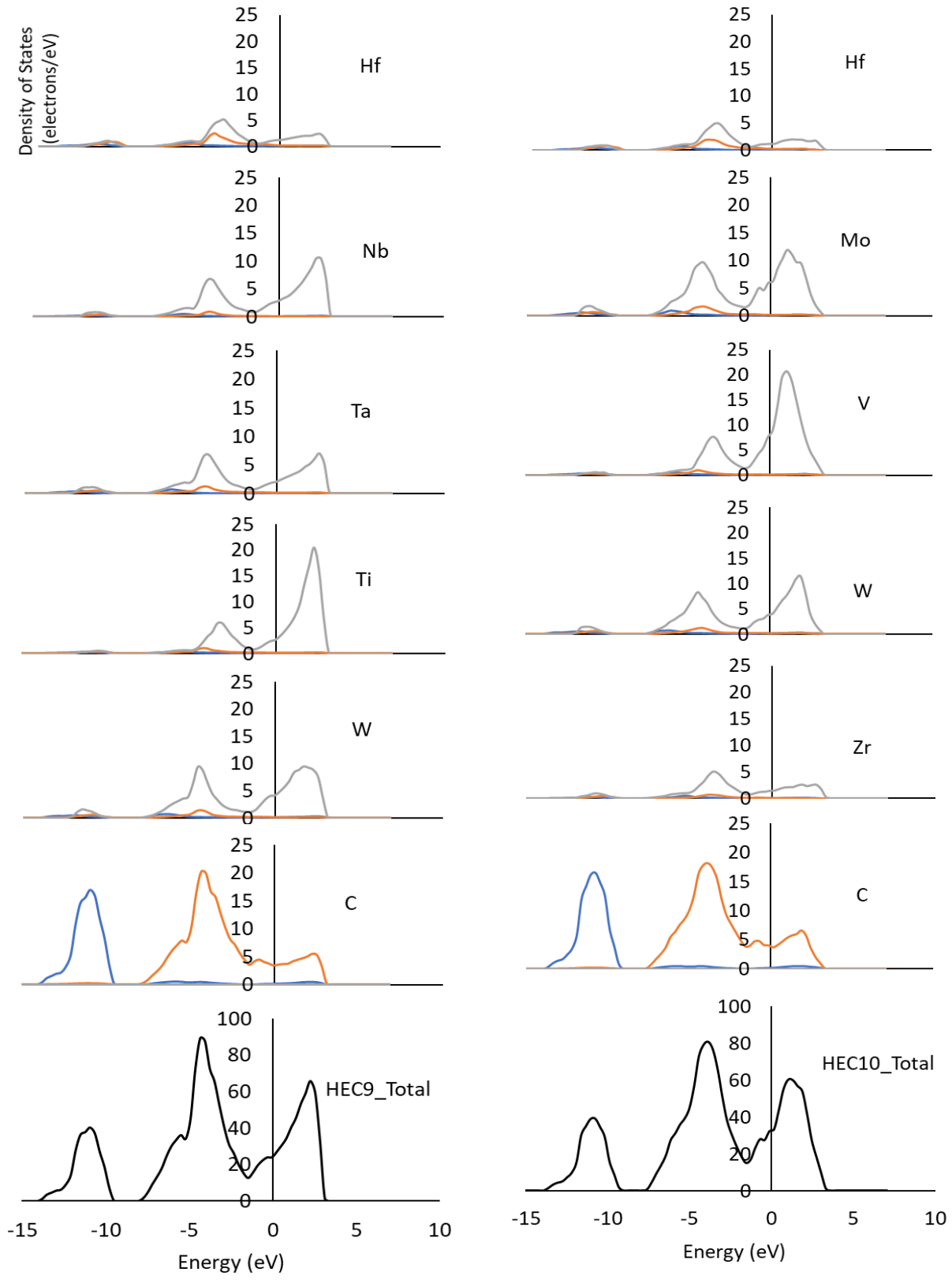
Figure 4.6 is the comparison of the number of the electrons between the average of the binaries and the HECs. The number of electrons is reasonably well approximated from their respective binaries. It applies a possibility that the number of electrons of HECs can be predicted from the binaries. More quantitative study is performed comparing the sum of electrons in binaries to the electrons in HECs in the energy range at -15 eV to 5 eV and summarized in Fig 4.7. Electrons in binaries are divided by 5 because one kind metal with 40 atoms exist in binaries, on the other hand, HECs have 40 metal atoms distributed to the five different metals. Next, we interpolate the energy range and the number of electrons in order to sum the electrons in binaries and compare the total electrons in HECs in the consistent energy range. The electrons in HECs and the sum of binaries are plotted in Fig 4.7 and well overlapped on top of each other. The results from the rule of mixture and the DOS analysis are consistent and we can predict the electrons in HECs from their respective binaries.

Figure 4.4 The Partial Density of States (PDOS) of nine HECs.









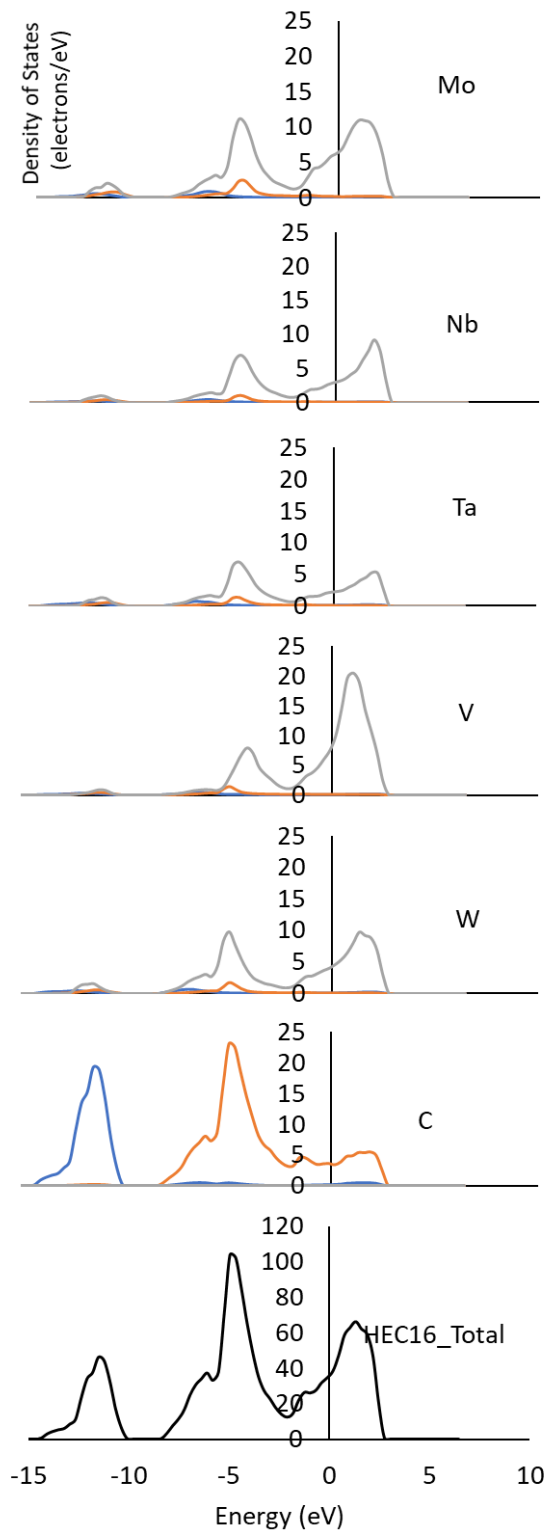
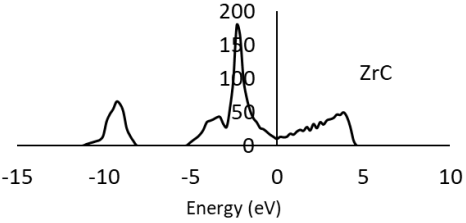
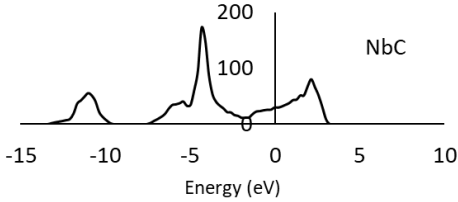
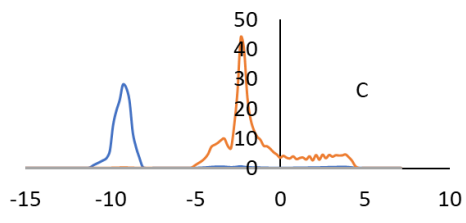
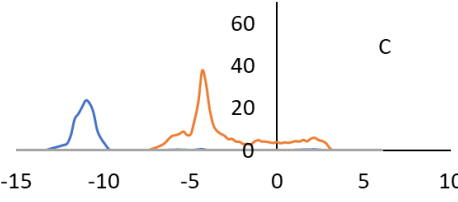
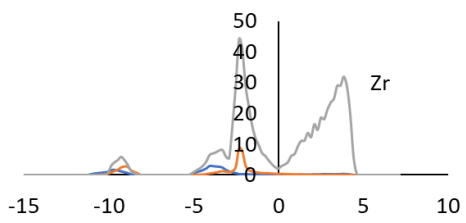
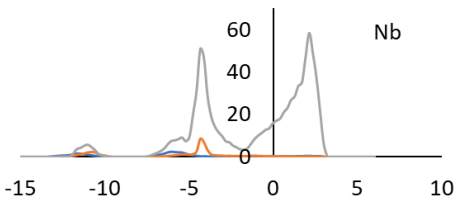
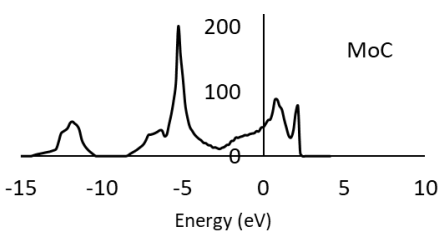
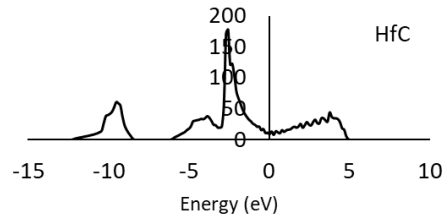
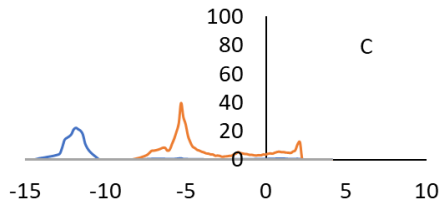
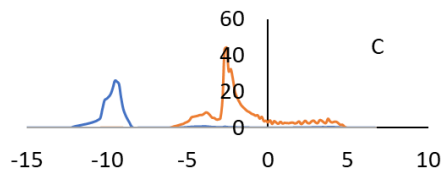
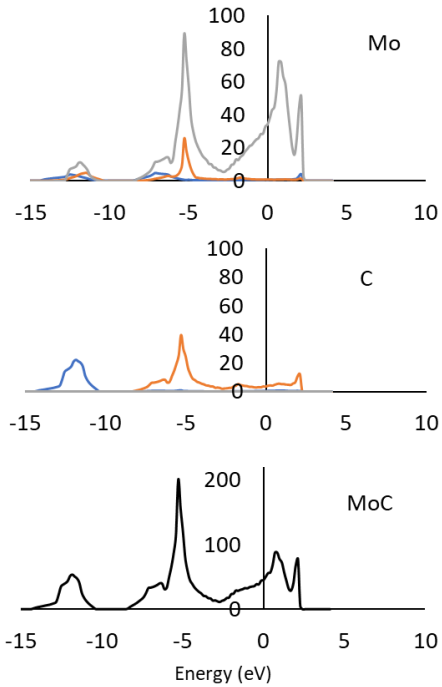
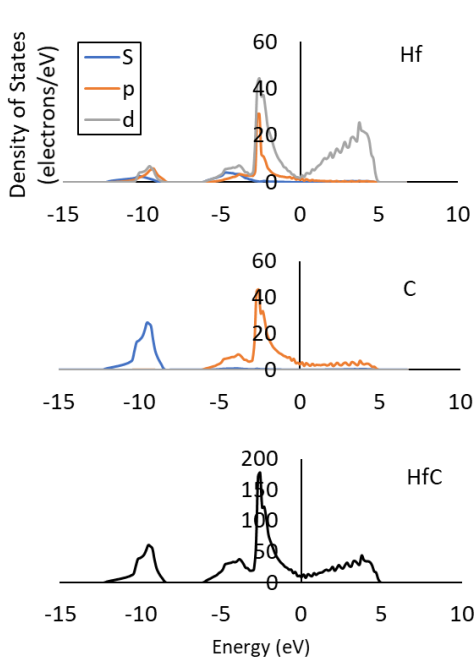
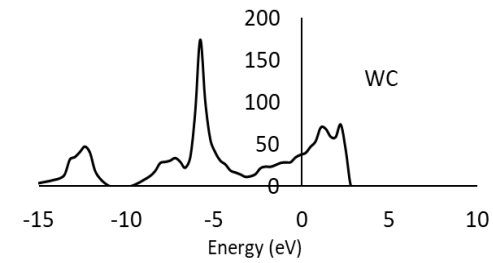
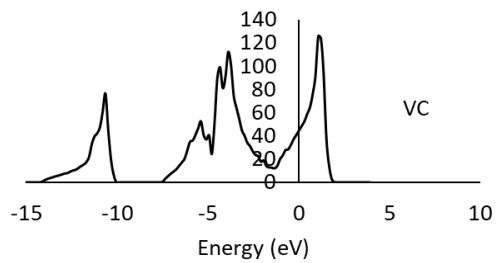
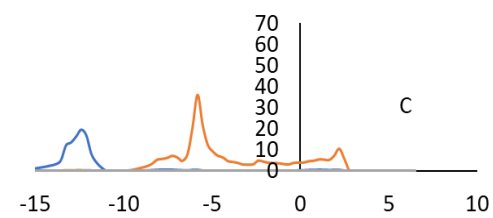
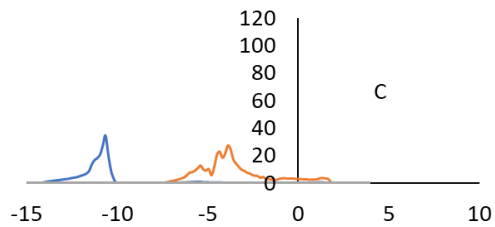
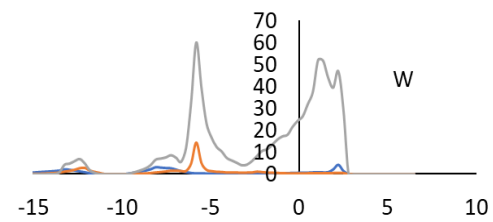
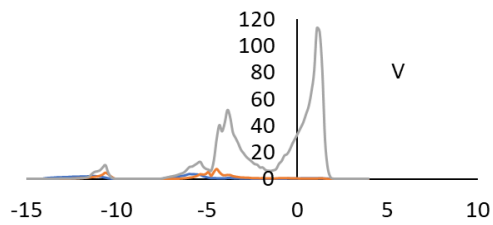
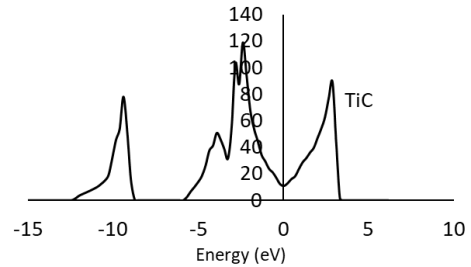
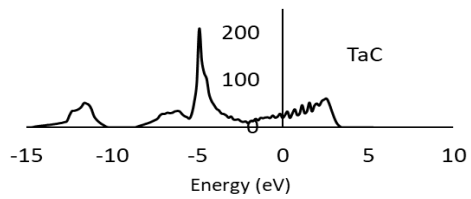
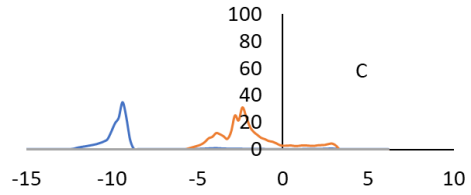
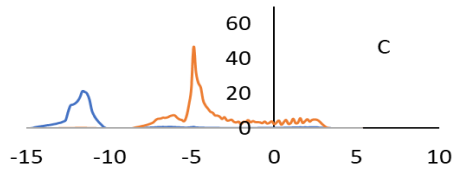
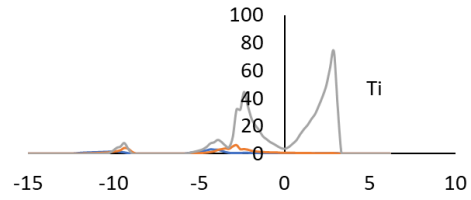
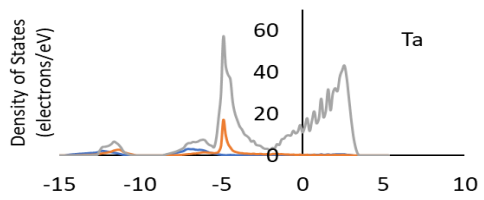


Figure 4.5 PDOS of eight respective binary carbides.





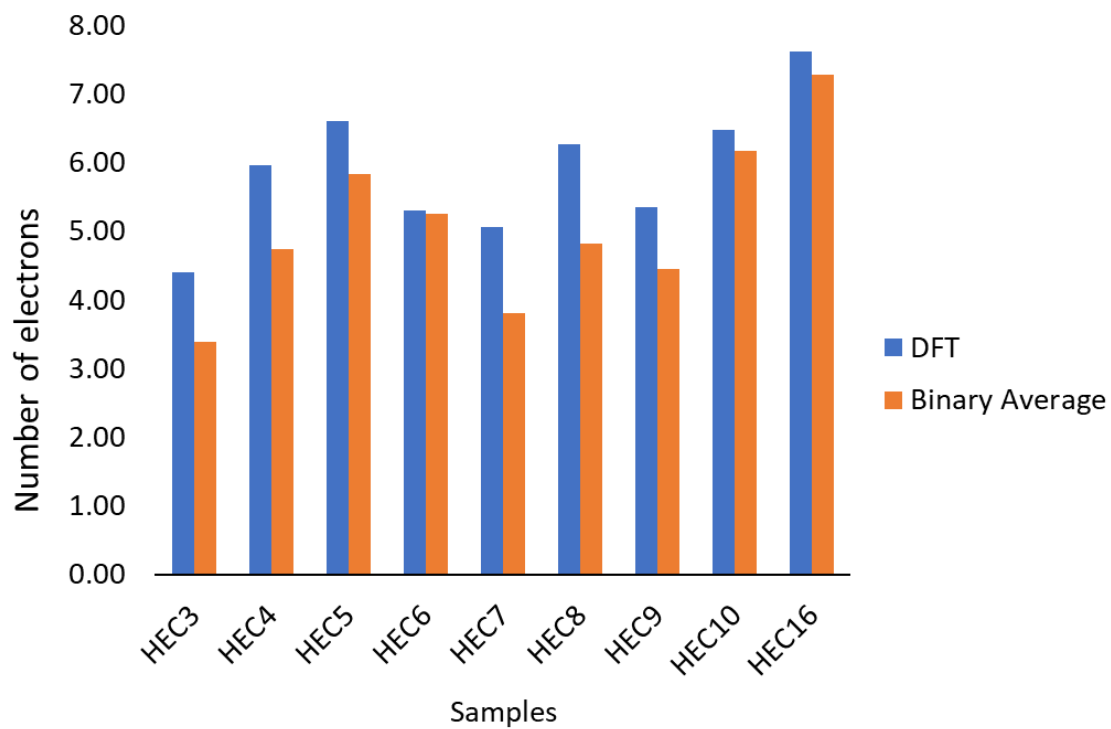


Figure 4.6 Prediction of the number of the electrons of HECs from their respective binaries at the Fermi level near ± 0.1 eV

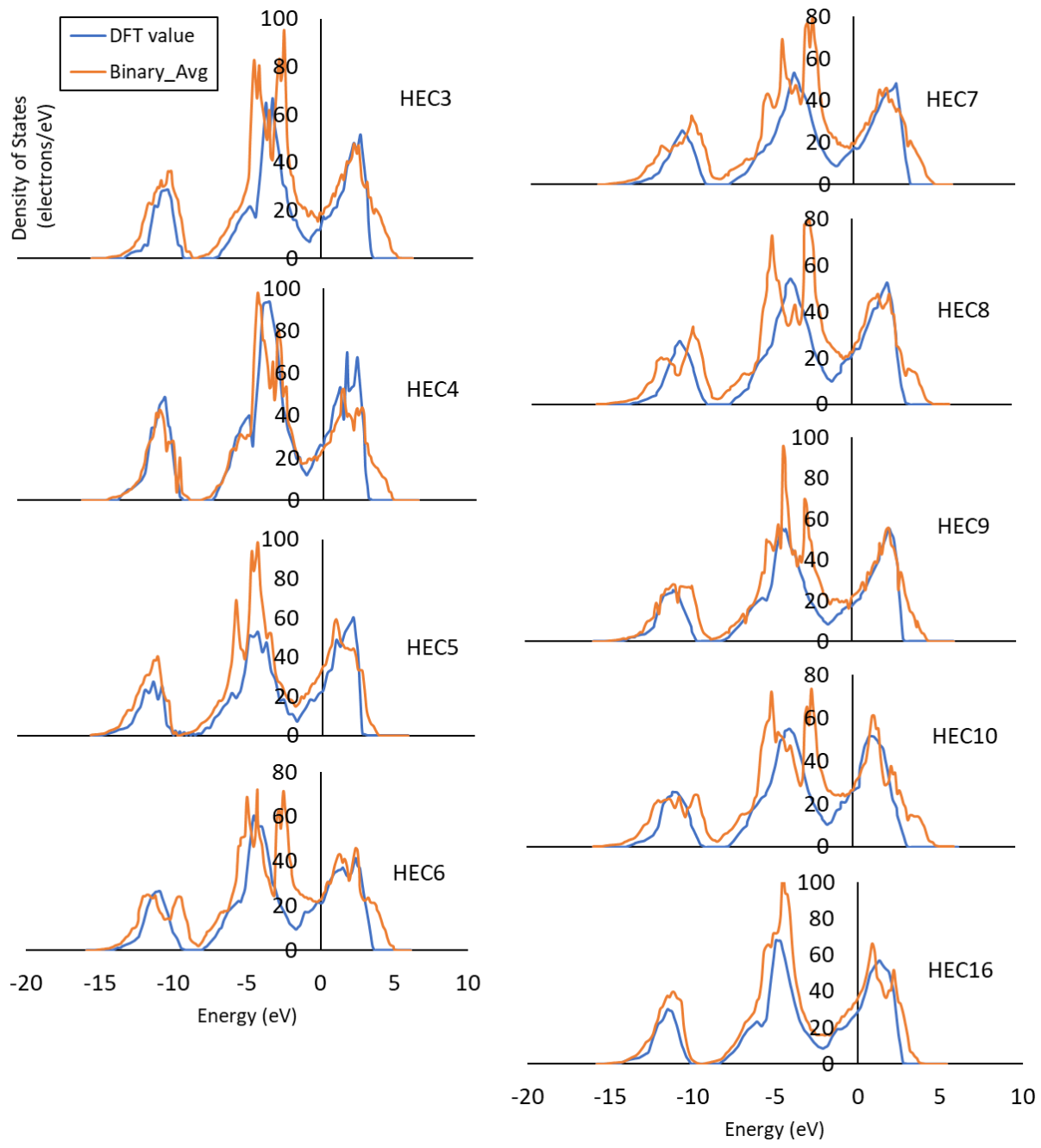


Figure 4.7 Comparison of the number of electrons between HECs and the respective binaries average.

4.4 Conclusion

DFT and BoltzTraP calculations were used to characterize the electronic properties of nine HEC compositions, and the binary carbides that correspond to the composition of each HEC. Electrical conductivity, and the electronic structure were determined. The number of electrons in HECs are well predicted from the averages of their respective binaries. But, the electrical conductivity and the number of electrons is not significantly correlated. In general, the electrical conductivity in all HECs is lower than the lowest in the binary carbide, TiC. This finding can provide a guideline to predict electrical conductivity in HECs with known binary carbides.

From the density of states study, we found that the metal peaks in HECs and the respective binaries are shown mostly in the same energy range. This finding suggests that the electronic structure in HECs remains the same from the binaries with adding more metals in the structure. The PDOS reveals that HECs have strong covalent bonds with metallic characterization from d orbitals in transition metals hybridization with 2p in carbons. Based on this analysis, we can use the number of electrons in binaries to predict the ones in HECs. Understanding its electronic structural characteristics can further broaden our understanding of its properties and lead to future applications.

ACKNOWLEDGEMENTS

The authors acknowledge support through the Office of Naval Research ONR-MURI (grant No. N00014-15-1-2863).

References

1. Ye, Y. F., Wang, Q., Lu, J., Liu, C. T. & Yang, Y. High-entropy alloy: challenges and prospects. *Materials Today* (2016). doi:10.1016/j.mattod.2015.11.026
2. Tsao, T. K. *et al.* The High Temperature Tensile and Creep Behaviors of High Entropy Superalloy. *Sci. Rep.* (2017). doi:10.1038/s41598-017-13026-7
3. Lim, X. Mixed-up metals make for stronger, tougher, stretchier alloys. *Nature* (2016). doi:10.1038/533306a
4. Gali, A. & George, E. P. Tensile properties of high- and medium-entropy alloys. *Intermetallics* (2013). doi:10.1016/j.intermet.2013.03.018
5. Li, Z., Tasan, C. C., Springer, H., Gault, B. & Raabe, D. Interstitial atoms enable joint twinning and transformation induced plasticity in strong and ductile high-entropy alloys. *Sci. Rep.* (2017). doi:10.1038/srep40704
6. Li, Z., Pradeep, K. G., Deng, Y., Raabe, D. & Tasan, C. C. Metastable high-entropy dual-phase alloys overcome the strength-ductility trade-off. *Nature* (2016). doi:10.1038/nature17981
7. Senkov, O. N., Wilks, G. B., Miracle, D. B., Chuang, C. P. & Liaw, P. K. Refractory high-entropy alloys. *Intermetallics* (2010). doi:10.1016/j.intermet.2010.05.014
8. Senkov, O. N., Senkova, S. V., Woodward, C. & Miracle, D. B. Low-density, refractory multi-principal element alloys of the Cr-Nb-Ti-V-Zr system: Microstructure and phase analysis. *Acta Mater.* (2013). doi:10.1016/j.actamat.2012.11.032
9. Bérardan, D., Franger, S., Meena, A. K. & Dragoë, N. Room temperature lithium superionic conductivity in high entropy oxides. *J. Mater. Chem. A* (2016). doi:10.1039/c6ta03249d
10. Rost, C. M. *et al.* Entropy-stabilized oxides. *Nat. Commun.* (2015). doi:10.1038/ncomms9485
11. Rak, Z. *et al.* Charge compensation and electrostatic transferability in three entropy-stabilized oxides: Results from density functional theory calculations. *J. Appl. Phys.* (2016). doi:10.1063/1.4962135
12. Meisenheimer, P. B., Kratočil, T. J. & Heron, J. T. Giant enhancement of exchange coupling in entropy-stabilized oxide heterostructures. *Sci. Rep.* (2017).

doi:10.1038/s41598-017-13810-5

13. Bérardan, D., Franger, S., Dragoe, D., Meena, A. K. & Dragoe, N. Colossal dielectric constant in high entropy oxides. *Phys. Status Solidi - Rapid Res. Lett.* (2016). doi:10.1002/pssr.201600043
14. Gild, J. *et al.* High-Entropy Metal Diborides: A New Class of High-Entropy Materials and a New Type of Ultrahigh Temperature Ceramics. *Sci. Rep.* (2016). doi:10.1038/srep37946
15. Zhou, J. *et al.* High-entropy carbide: A novel class of multicomponent ceramics. *Ceram. Int.* (2018). doi:10.1016/j.ceramint.2018.08.100
16. Castle, E., Csanádi, T., Grasso, S., Dusza, J. & Reece, M. Processing and Properties of High-Entropy Ultra-High Temperature Carbides. *Sci. Rep.* (2018). doi:10.1038/s41598-018-26827-1
17. Dusza, J. *et al.* Microstructure of (Hf-Ta-Zr-Nb)C high-entropy carbide at micro and nano/atomic level. *J. Eur. Ceram. Soc.* (2018). doi:10.1016/j.jeurceramsoc.2018.05.006
18. Rohrer, G. S. *et al.* Challenges in ceramic science: A report from the workshop on emerging research areas in ceramic science. *J. Am. Ceram. Soc.* (2012). doi:10.1111/jace.12033
19. Andrievskii, R. A., Strel'nikova, N. S., Poltoratskii, N. I., Kharkhardin, E. D. & Smirnov, V. S. Melting point in systems ZrC-HfC, TaC-ZrC, TaC-HfC. *Sov. Powder Metall. Met. Ceram.* (1967). doi:10.1007/BF00773385
20. Hong, Q. J. & Van De Walle, A. Prediction of the material with highest known melting point from ab initio molecular dynamics calculations. *Phys. Rev. B - Condens. Matter Mater. Phys.* (2015). doi:10.1103/PhysRevB.92.020104
21. Sarker, P. *et al.* High-entropy high-hardness metal carbides discovered by entropy descriptors. *Nat. Commun.* (2018). doi:10.1038/s41467-018-07160-7
22. Yang, K., Oses, C. & Curtarolo, S. Modeling off-stoichiometry materials with a high-throughput ab-initio approach. *Chem. Mater.* (2016). doi:10.1021/acs.chemmater.6b01449
23. Harrington, T. J. *et al.* Phase stability and mechanical properties of novel high entropy transition metal carbides. *Acta Mater.* (2019). doi:10.1016/j.actamat.2018.12.054
24. J. M. Ziman. *Principles of the Theory of Solids.* (Cambridge University Press, 1972).
25. B.R. Nag. *Electron Transport in Compound Semiconductors.* (Springer Verlag, 1980).
26. Scheidemantel, J., Ambrosch-Draxl, C., Thonhauser, T., Badding, V. & Sofo, O.

- Transport coefficients from first-principles calculations. *Phys. Rev. B - Condens. Matter Mater. Phys.* (2003). doi:10.1103/PhysRevB.68.125210
27. Madsen, G. K. H. & Singh, D. J. BoltzTraP. A code for calculating band-structure dependent quantities. *Comput. Phys. Commun.* (2006). doi:10.1016/j.cpc.2006.03.007
 28. Zunger, A., Wei, S., Ferreira, L. & Bernard, J. Special Quasirandom Structures. *Phys. Rev. Lett.* **65**, 353–356 (1990).
 29. Nosé, S. & Nosé, S. A unified formulation of the constant temperature molecular dynamics methods. *J. Chem. Phys.* **81**, 511 (1984).
 30. Kresse, G. & Furthmüller, J. Efficiency of ab-initio total energy calculations for metals and semiconductors using a plane-wave basis set. *Comput. Mater. Sci.* **6**, 15–50 (1996).
 31. Kresse, G. & Furthmüller, J. Efficient iterative schemes for ab initio total-energy calculations using a plane-wave basis set. *Phys. Rev. B. Condens. Matter* **54**, 11169–11186 (1996).
 32. Kresse, G. & Hafner, J. Ab initio molecular dynamics for liquid metals. *Phys. Rev. B* **47**, 558–561 (1993).
 33. Perdew, J. P., Burke, K. & Ernzerhof, M. Generalized gradient approximation made simple. *Phys. Rev. Lett.* (1996). doi:10.1103/PhysRevLett.77.3865
 34. Ziman, J. M. *Principles of the Theory of Solids*. (Cambridge University Press, 1972).
 35. Paul M. Marcus. *Computational Methods in Band Theory*. (Plenum, 1971).
 36. Koelling, D. D. & Wood, J. H. On the interpolation of eigenvalues and a resultant integration scheme. *J. Comput. Phys.* (1986). doi:10.1016/0021-9991(86)90261-5
 37. Pickett, W. E., Krakauer, H. & Allen, P. B. Smooth Fourier interpolation of periodic functions. *Phys. Rev. B* (1988). doi:10.1103/PhysRevB.38.2721
 38. Ricci, F. *et al.* An electronic transport ab initio database for inorganic materials. *Sci. Data* (2017).
 39. Allen, P. B., Pickett, W. E. & Krakauer, H. Anisotropic normal-state transport properties predicted and analyzed for high-T_c oxide superconductors. *Phys. Rev. B* (1988). doi:10.1103/PhysRevB.37.7482
 40. Zhu, H., Sun, W., Armiento, R., Lazic, P. & Ceder, G. Band structure engineering through orbital interaction for enhanced thermoelectric power factor. *Appl. Phys. Lett.* (2014). doi:10.1063/1.4866861

41. Ong, K. P., Singh, D. J. & Wu, P. Analysis of the thermoelectric properties of n-type ZnO. *Phys. Rev. B - Condens. Matter Mater. Phys.* (2011). doi:10.1103/PhysRevB.83.115110
42. Zhu, H. *et al.* Computational and experimental investigation of TmAgTe₂ and XYZ₂ compounds, a new group of thermoelectric materials identified by first-principles high-throughput screening. *J. Mater. Chem. C* (2015). doi:10.1039/c5tc01440a
43. Madsen, G. H., Schwarz, K., Blaha, P. & Singh, D. Electronic structure and transport in type-I and type-VIII clathrates containing strontium, barium, and europium. *Phys. Rev. B - Condens. Matter Mater. Phys.* (2003). doi:10.1103/PhysRevB.68.125212
44. Bentien, A., Pacheco, V., Paschen, S., Grin, Y. & Steglich, F. Transport properties of composition tuned α - $\text{Eu}_8\text{Ga}_{16-x}\text{Ge}_{30+x}$. *Phys. Rev. B - Condens. Matter Mater. Phys.* (2005). doi:10.1103/PhysRevB.71.165206
45. Lengauer, W. Transition Metal Carbides, Nitrides, and Carbonitrides. in *Handbook of Ceramic Hard Materials* (2008). doi:10.1002/9783527618217.ch7
46. Perry, D. . *Handbook of Inorganic Compounds*. (CRC Press, 2011).
47. Lide, D. R. *CRC Handbook of Chemistry and Physics*. (CRC Press, 2009).
48. Davison K.V., Riley R.E., T. J. M. *Carbide-Graphite Composites Second Progress Report*. (1967).
49. Modine F.A., Foegelle M.D., Finch C.B., A. C. Y. Electrical properties of transition-metal carbides of group IV. *Phys. Rev. B* **40**, (1989).
50. Baucio, M. *ASM Engineered Materials Reference Book*. (ASM International, Materials Park, 1994).

Chapter 5. Conclusion and Future work

In this dissertation, we explored the thermal and electronic properties of the high entropy oxides and carbides using the computational modelling. The molecular dynamics (MD) simulations and the Density Functional Theory (DFT) were applied to calculate the properties of those materials.

In the first part, classical molecular dynamics simulations have been used to characterize the phonon thermal conductivity of J14 with composition $(\text{Mg}_{0.1}\text{Co}_{0.1}\text{Ni}_{0.1}\text{Cu}_{0.1}\text{Zn}_{0.1})\text{O}_{0.5}$, and J14 plus Sc, Sn, Cr or Ge in equi-molar cation proportions. Our results show that the thermal conductivity is reduced by adding 6th metal component. We have manipulated the mass and the atom-centered charges used in the Coulombic contribution to the potential energy. It was shown that the phonon scattering from disorder in atomic charges can explain the prior experiment results lowering the thermal conductivity with addition of a sixth cation to J14. Also, the comparison from the Bridgeman equations suggest that the thermal conductivity is still above the analytic limit for an amorphous system even though the phonon scattering is added from disorder in mass and atomic charges.

The properties of the high entropy carbides are investigated in the second and third part of this dissertation. In the second part, two aspects are explored. First one is to what degree can the properties of HECs be predicted from their respective binaries. Second one is focused on whether there are relationships between the properties of the binary compounds that correspond to a given HEC composition and the values of that composition's EFA. Average of the constitute binary carbides results good approximations of lattice constant, bulk modulus, average the cohesive energies and ζ , and binding energy of corresponding HEC composition. The properties of all 56 possible compositions were calculated from the binary averaging and the correlations were found

between the EFA of a given composition and the standard deviation of the distribution of bulk moduli and ζ of the respective binaries. Also, it was shown that a correlation between the standard deviation of the CVFEs for each HEC and the EFA of that composition exist. Therefore, our result supports the EFA as a central quantity for estimating properties of HECs beyond phase stability.

The electrical properties of HECs are investigated in the third part. The DOS indicates that the electronic structure of HECs remains the same as the binary. The PDOS analysis proves that the HECs are having a strong covalent bond with metallic characterization and keeping the similar characteristics of the binaries as well. The number of electrons of each HEC is well predicted from the electrons in the constituent binaries. Our result showed that even though the number of electrons is not proportionally influencing the electrical conductivity of the binaries and the HECs, it can be useful as a guideline to predict the limit of the electrical conductivity of the HECs from the known binary carbides.

Overall, the molecular dynamics simulations and the density functional theory study enhance our understanding of properties of the high entropy oxides and carbides in the microscopic scale. Our findings support the experimental results and highlight the importance of these high entropy ceramics. There are still numerous opportunities for further study on this topic. Since there are gap existing between experiments and computational simulations in exact system conditions like sizes, timescales and potentials. Using proper potentials to the system is always a challenge for the computational simulations study. In this dissertation, we also have used the approximated potentials for both the high entropy oxides and carbides. Applying potentials that more closely represent the systems is inevitable to provide more detailed information closer to the experimental systems. To fully reproduce an experiment environment and predict the properties, exploring potential close to the experiment elements can be suggested a future study for these high entropy

materials. In this work, we are focused on the phonon thermal conductivity behavior on the high entropy oxides. Other mechanical or electrical properties can be calculated and used to determine the correlations between the experimental results and the calculations for the future applications. In case of the high entropy carbides, we can suggest studying more about the physical origin from the correlations of the properties and the phase stability. We have studied the electronic properties of the high entropy carbides using DFT, but the phonon part of properties would provide improved understanding in depth and unfold the potentials of the high entropy carbides. Since the electrical conductivity is not well predicted from their binaries and is not correlated the number of the electrons, more studies for the electronic structures may be needed by starting with the exploring the band structures of each systems. Defects and grain boundary in the systems can be added to implement more experiment environment and studied to understand the role of defects. Lastly, we can also extend these computational techniques to more high entropy materials, i.e., nitrides, borides, and boron carbides, etc.

Appendix

Appendix A

A Final atom positions and Bader charges of J14 samples

J14

Atom type	x	y	z	Bader charge
Mg	0.00	8.51	4.26	1.70
Mg	0.00	12.77	4.26	1.70
Mg	6.39	4.26	6.38	1.70
Mg	10.64	8.51	6.38	1.70
Mg	2.13	4.26	14.90	1.70
Mg	8.51	12.77	4.26	1.70
Mg	6.39	8.51	6.38	1.70
Mg	2.13	0.00	6.38	1.70
Mg	4.26	4.26	8.51	1.69
Mg	6.39	6.38	8.51	1.69
Mg	8.51	8.51	8.51	1.69
Mg	0.00	12.77	8.51	1.69
Mg	8.51	6.38	10.64	1.69
Mg	0.00	10.64	10.64	1.70
Mg	8.51	4.26	12.77	1.69
Mg	10.64	4.26	14.90	1.70
Mg	2.13	6.38	17.03	1.70
Mg	8.51	0.00	4.26	1.70
Mg	8.51	12.77	8.51	1.70
Mg	10.64	14.90	8.51	1.70
Mg	6.39	4.26	14.90	1.70
Mg	10.64	6.38	17.03	1.70
Mg	10.64	4.26	19.15	1.69
Mg	0.00	6.38	19.15	1.69
Mg	0.00	4.26	0.00	1.69
Mg	4.26	14.90	6.38	1.70
Mg	6.39	0.00	6.38	1.70
Mg	6.39	14.90	8.51	1.69
Mg	8.51	0.00	8.51	1.70
Mg	0.00	2.13	10.64	1.70
Mg	4.26	8.51	12.77	1.70
Mg	8.51	10.64	14.90	1.70
Mg	0.00	14.90	14.90	1.70
Mg	8.51	8.51	17.03	1.70
Mg	0.00	12.77	17.03	1.70
Mg	4.26	12.77	12.77	1.70
Mg	10.64	2.13	12.77	1.69
Mg	4.26	10.64	14.90	1.70

Mg	10.64	14.90	17.03	1.70
Mg	6.39	4.26	2.13	1.70
Mg	10.64	8.51	2.13	1.70
Mg	6.39	2.13	12.77	1.70
Mg	6.39	14.90	17.03	1.70
Mg	0.00	2.13	19.15	1.70
Mg	4.26	6.38	2.13	1.70
Mg	6.39	8.51	2.13	1.70
Mg	6.39	12.77	2.13	1.70
Mg	8.51	14.90	2.13	1.69
Co	2.13	6.38	4.26	1.26
Co	2.13	8.51	6.38	1.27
Co	0.00	4.26	8.51	1.27
Co	2.13	6.38	8.51	1.26
Co	2.13	14.90	4.26	1.25
Co	0.00	10.64	6.38	1.26
Co	2.13	12.77	6.38	1.26
Co	2.13	6.38	12.77	1.25
Co	0.00	0.00	4.26	1.26
Co	0.00	14.90	6.38	1.25
Co	10.64	8.51	10.64	1.25
Co	10.64	6.38	12.77	1.25
Co	0.00	4.26	17.03	1.24
Co	8.51	10.64	10.64	1.26
Co	0.00	10.64	14.90	1.26
Co	0.00	8.51	17.03	1.25
Co	2.13	6.38	0.00	1.27
Co	6.39	12.77	10.64	1.24
Co	10.64	0.00	10.64	1.24
Co	8.51	12.77	12.77	1.27
Co	0.00	0.00	12.77	1.26
Co	6.39	8.51	14.90	1.25
Co	10.64	12.77	14.90	1.25
Co	10.64	10.64	17.03	1.26
Co	10.64	6.38	0.00	1.24
Co	0.00	6.38	2.13	1.26
Co	2.13	8.51	2.13	1.26
Co	4.26	2.13	6.38	1.25
Co	4.26	0.00	8.51	1.25
Co	8.51	0.00	12.77	1.26
Co	8.51	14.90	14.90	1.26
Co	6.39	10.64	17.03	1.26
Co	0.00	0.00	17.03	1.26
Co	4.26	4.26	0.00	1.23
Co	8.51	8.51	0.00	1.25

Co	10.64	10.64	0.00	1.26
Co	0.00	10.64	2.13	1.25
Co	4.26	2.13	10.64	1.24
Co	6.39	12.77	19.15	1.27
Co	2.13	0.00	2.13	1.27
Co	4.26	0.00	17.03	1.27
Co	4.26	14.90	19.15	1.26
Co	8.51	2.13	19.15	1.26
Co	6.39	14.90	0.00	1.25
Co	8.51	0.00	0.00	1.25
Co	10.64	0.00	2.13	1.26
Co	6.39	0.00	2.13	1.26
Co	8.51	2.13	2.13	1.26
Ni	0.00	4.26	4.26	1.19
Ni	2.13	10.64	4.26	1.19
Ni	10.64	10.64	4.26	1.18
Ni	8.51	6.38	6.38	1.18
Ni	8.51	4.26	8.51	1.20
Ni	10.64	4.26	10.64	1.22
Ni	10.64	14.90	4.26	1.18
Ni	4.26	6.38	6.38	1.17
Ni	8.51	10.64	6.38	1.18
Ni	2.13	12.77	10.64	1.24
Ni	0.00	8.51	12.77	1.20
Ni	2.13	8.51	14.90	1.18
Ni	2.13	4.26	19.15	1.18
Ni	10.64	0.00	6.38	1.19
Ni	0.00	2.13	6.38	1.20
Ni	2.13	2.13	8.51	1.18
Ni	2.13	0.00	10.64	1.26
Ni	4.26	4.26	12.77	1.20
Ni	8.51	8.51	12.77	1.21
Ni	0.00	12.77	12.77	1.21
Ni	2.13	14.90	12.77	1.18
Ni	2.13	4.26	2.13	1.19
Ni	6.39	2.13	4.26	1.18
Ni	8.51	2.13	6.38	1.19
Ni	10.64	2.13	8.51	1.20
Ni	4.26	10.64	10.64	1.25
Ni	10.64	14.90	12.77	1.20
Ni	4.26	6.38	14.90	1.17
Ni	6.39	4.26	19.15	1.22
Ni	0.00	10.64	19.15	1.19
Ni	2.13	12.77	19.15	1.20
Ni	4.26	14.90	10.64	1.24

Ni	6.39	0.00	10.64	1.24
Ni	6.39	12.77	14.90	1.18
Ni	0.00	2.13	14.90	1.18
Ni	8.51	12.77	17.03	1.18
Ni	6.39	8.51	19.15	1.21
Ni	2.13	0.00	19.15	1.21
Ni	4.26	0.00	12.77	1.22
Ni	4.26	10.64	19.15	1.20
Ni	10.64	14.90	0.00	1.25
Ni	0.00	0.00	0.00	1.25
Ni	2.13	2.13	0.00	1.24
Ni	10.64	12.77	2.13	1.19
Ni	0.00	14.90	2.13	1.20
Ni	6.39	2.13	17.03	1.18
Ni	6.39	0.00	19.15	1.19
Ni	0.00	2.13	2.13	1.21
Cu	8.51	4.26	4.26	1.10
Cu	10.64	6.38	4.26	1.09
Cu	10.64	4.26	6.38	1.13
Cu	0.00	6.38	6.38	1.09
Cu	6.39	6.38	4.26	1.08
Cu	8.51	8.51	4.26	1.09
Cu	10.64	6.38	8.51	1.08
Cu	0.00	8.51	8.51	1.11
Cu	4.26	8.51	4.26	1.08
Cu	2.13	14.90	8.51	1.15
Cu	6.39	4.26	10.64	1.15
Cu	2.13	10.64	12.77	1.07
Cu	4.26	12.77	4.26	1.10
Cu	4.26	10.64	6.38	1.10
Cu	6.39	12.77	6.38	1.09
Cu	8.51	14.90	6.38	1.07
Cu	6.39	10.64	8.51	1.08
Cu	4.26	6.38	10.64	1.08
Cu	6.39	8.51	10.64	1.02
Cu	10.64	12.77	10.64	1.02
Cu	10.64	10.64	12.77	1.08
Cu	8.51	6.38	14.90	1.10
Cu	10.64	8.51	14.90	1.11
Cu	8.51	4.26	17.03	1.09
Cu	2.13	10.64	17.03	1.10
Cu	2.13	8.51	19.15	1.09
Cu	4.26	12.77	8.51	1.06
Cu	6.39	10.64	12.77	1.09
Cu	2.13	2.13	12.77	1.09

Cu	2.13	0.00	14.90	1.10
Cu	6.39	6.38	17.03	1.10
Cu	2.13	14.90	17.03	1.10
Cu	8.51	6.38	19.15	1.09
Cu	0.00	8.51	0.00	1.03
Cu	2.13	10.64	0.00	1.16
Cu	10.64	4.26	2.13	1.10
Cu	8.51	2.13	10.64	1.05
Cu	2.13	2.13	17.03	1.10
Cu	8.51	10.64	19.15	1.07
Cu	6.39	6.38	0.00	1.03
Cu	2.13	14.90	0.00	1.05
Cu	8.51	0.00	17.03	1.09
Cu	8.51	14.90	19.15	1.09
Cu	10.64	0.00	19.15	1.09
Cu	4.26	8.51	0.00	1.14
Cu	6.39	10.64	0.00	1.16
Cu	8.51	10.64	2.13	1.04
Cu	4.26	10.64	2.13	1.10
Zn	2.13	4.26	6.38	1.19
Zn	2.13	4.26	10.64	1.20
Zn	4.26	4.26	4.26	1.18
Zn	2.13	10.64	8.51	1.18
Zn	0.00	6.38	10.64	1.17
Zn	2.13	8.51	10.64	1.16
Zn	0.00	4.26	12.77	1.18
Zn	6.39	10.64	4.26	1.18
Zn	2.13	2.13	4.26	1.19
Zn	10.64	12.77	6.38	1.17
Zn	10.64	10.64	8.51	1.17
Zn	0.00	6.38	14.90	1.17
Zn	6.39	14.90	4.26	1.17
Zn	10.64	2.13	4.26	1.19
Zn	4.26	8.51	8.51	1.19
Zn	0.00	0.00	8.51	1.18
Zn	0.00	14.90	10.64	1.19
Zn	6.39	6.38	12.77	1.18
Zn	2.13	12.77	14.90	1.18
Zn	4.26	0.00	4.26	1.17
Zn	8.51	14.90	10.64	1.18
Zn	4.26	4.26	17.03	1.18
Zn	10.64	8.51	19.15	1.18
Zn	8.51	4.26	0.00	1.16
Zn	6.39	2.13	8.51	1.18
Zn	6.39	14.90	12.77	1.19

Zn	10.64	0.00	14.90	1.18
Zn	4.26	8.51	17.03	1.19
Zn	4.26	6.38	19.15	1.19
Zn	10.64	12.77	19.15	1.19
Zn	0.00	14.90	19.15	1.18
Zn	0.00	12.77	0.00	1.25
Zn	8.51	6.38	2.13	1.19
Zn	2.13	12.77	2.13	1.19
Zn	4.26	14.90	14.90	1.18
Zn	6.39	0.00	14.90	1.18
Zn	8.51	2.13	14.90	1.17
Zn	4.26	12.77	17.03	1.18
Zn	10.64	2.13	17.03	1.18
Zn	8.51	12.77	0.00	1.20
Zn	4.26	2.13	14.90	1.18
Zn	4.26	12.77	0.00	1.19
Zn	10.64	2.13	0.00	1.15
Zn	4.26	2.13	19.15	1.19
Zn	4.26	0.00	0.00	1.21
Zn	6.39	2.13	0.00	1.16
Zn	4.26	14.90	2.13	1.19
Zn	4.26	2.13	2.13	1.19
O	10.64	2.13	2.13	-1.20
O	0.00	4.26	2.13	-1.27
O	0.00	2.13	4.26	-1.23
O	6.39	2.13	2.13	-1.27
O	8.51	4.26	2.13	-1.26
O	10.64	6.38	2.13	-1.27
O	0.00	8.51	2.13	-1.36
O	8.51	2.13	4.26	-1.28
O	10.64	4.26	4.26	-1.17
O	0.00	6.38	4.26	-1.27
O	10.64	2.13	6.38	-1.21
O	0.00	4.26	6.38	-1.18
O	0.00	2.13	8.51	-1.28
O	2.13	2.13	2.13	-1.23
O	4.26	4.26	2.13	-1.35
O	6.39	6.38	2.13	-1.36
O	8.51	8.51	2.13	-1.29
O	10.64	10.64	2.13	-1.25
O	0.00	12.77	2.13	-1.31
O	4.26	2.13	4.26	-1.23
O	6.39	4.26	4.26	-1.33
O	8.51	6.38	4.26	-1.16
O	10.64	8.51	4.26	-1.40

O	0.00	10.64	4.26	-1.39
O	6.39	2.13	6.38	-1.39
O	8.51	4.26	6.38	-1.27
O	10.64	6.38	6.38	-1.24
O	0.00	8.51	6.38	-1.35
O	8.51	2.13	8.51	-1.24
O	10.64	4.26	8.51	-1.24
O	0.00	6.38	8.51	-1.17
O	10.64	2.13	10.64	-1.34
O	0.00	4.26	10.64	-1.25
O	0.00	2.13	12.77	-1.34
O	2.13	6.38	2.13	-1.32
O	4.26	8.51	2.13	-1.33
O	6.39	10.64	2.13	-1.31
O	8.51	12.77	2.13	-1.44
O	10.64	14.90	2.13	-1.32
O	0.00	0.00	2.13	-1.25
O	2.13	4.26	4.26	-1.23
O	4.26	6.38	4.26	-1.26
O	6.39	8.51	4.26	-1.29
O	8.51	10.64	4.26	-1.26
O	10.64	12.77	4.26	-1.38
O	0.00	14.90	4.26	-1.33
O	2.13	2.13	6.38	-1.31
O	4.26	4.26	6.38	-1.37
O	6.39	6.38	6.38	-1.40
O	8.51	8.51	6.38	-1.41
O	10.64	10.64	6.38	-1.31
O	0.00	12.77	6.38	-1.37
O	4.26	2.13	8.51	-1.29
O	6.39	4.26	8.51	-1.43
O	8.51	6.38	8.51	-1.42
O	10.64	8.51	8.51	-1.36
O	0.00	10.64	8.51	-1.33
O	6.39	2.13	10.64	-1.25
O	8.51	4.26	10.64	-1.30
O	10.64	6.38	10.64	-1.25
O	0.00	8.51	10.64	-1.24
O	8.51	2.13	12.77	-1.42
O	10.64	4.26	12.77	-1.46
O	0.00	6.38	12.77	-1.20
O	10.64	2.13	14.90	-1.35
O	0.00	4.26	14.90	-1.39
O	0.00	2.13	17.03	-1.27
O	2.13	10.64	2.13	-1.22

O	4.26	12.77	2.13	-1.20
O	6.39	14.90	2.13	-1.35
O	8.51	0.00	2.13	-1.39
O	2.13	8.51	4.26	-1.30
O	4.26	10.64	4.26	-1.16
O	6.39	12.77	4.26	-1.32
O	8.51	14.90	4.26	-1.44
O	10.64	0.00	4.26	-1.32
O	2.13	6.38	6.38	-1.25
O	4.26	8.51	6.38	-1.29
O	6.39	10.64	6.38	-1.24
O	8.51	12.77	6.38	-1.29
O	10.64	14.90	6.38	-1.27
O	0.00	0.00	6.38	-1.32
O	2.13	4.26	8.51	-1.28
O	4.26	6.38	8.51	-1.33
O	6.39	8.51	8.51	-1.37
O	8.51	10.64	8.51	-1.31
O	10.64	12.77	8.51	-1.40
O	0.00	14.90	8.51	-1.33
O	2.13	2.13	10.64	-1.24
O	4.26	4.26	10.64	-1.25
O	6.39	6.38	10.64	-1.30
O	8.51	8.51	10.64	-1.35
O	10.64	10.64	10.64	-1.22
O	0.00	12.77	10.64	-1.33
O	4.26	2.13	12.77	-1.25
O	6.39	4.26	12.77	-1.42
O	8.51	6.38	12.77	-1.35
O	10.64	8.51	12.77	-1.19
O	0.00	10.64	12.77	-1.24
O	6.39	2.13	14.90	-1.35
O	8.51	4.26	14.90	-1.41
O	10.64	6.38	14.90	-1.33
O	0.00	8.51	14.90	-1.24
O	8.51	2.13	17.03	-1.20
O	10.64	4.26	17.03	-1.43
O	0.00	6.38	17.03	-1.46
O	10.64	2.13	19.15	-1.33
O	0.00	4.26	19.15	-1.52
O	0.00	2.13	0.00	-1.34
O	2.13	14.90	2.13	-1.18
O	4.26	0.00	2.13	-1.20
O	2.13	12.77	4.26	-1.29
O	4.26	14.90	4.26	-1.30

O	6.39	0.00	4.26	-1.38
O	2.13	10.64	6.38	-1.22
O	4.26	12.77	6.38	-1.20
O	6.39	14.90	6.38	-1.43
O	8.51	0.00	6.38	-1.40
O	2.13	8.51	8.51	-1.17
O	4.26	10.64	8.51	-1.17
O	6.39	12.77	8.51	-1.29
O	8.51	14.90	8.51	-1.50
O	10.64	0.00	8.51	-1.35
O	2.13	6.38	10.64	-1.16
O	4.26	8.51	10.64	-1.23
O	6.39	10.64	10.64	-1.13
O	8.51	12.77	10.64	-1.27
O	10.64	14.90	10.64	-1.24
O	0.00	0.00	10.64	-1.26
O	2.13	4.26	12.77	-1.31
O	4.26	6.38	12.77	-1.24
O	6.39	8.51	12.77	-1.23
O	8.51	10.64	12.77	-1.26
O	10.64	12.77	12.77	-1.18
O	0.00	14.90	12.77	-1.32
O	2.13	2.13	14.90	-1.26
O	4.26	4.26	14.90	-1.38
O	6.39	6.38	14.90	-1.27
O	8.51	8.51	14.90	-1.34
O	10.64	10.64	14.90	-1.31
O	0.00	12.77	14.90	-1.38
O	4.26	2.13	17.03	-1.21
O	6.39	4.26	17.03	-1.29
O	8.51	6.38	17.03	-1.31
O	10.64	8.51	17.03	-1.37
O	0.00	10.64	17.03	-1.30
O	6.39	2.13	19.15	-1.19
O	8.51	4.26	19.15	-1.28
O	10.64	6.38	19.15	-1.42
O	0.00	8.51	19.15	-1.25
O	8.51	2.13	0.00	-1.19
O	10.64	4.26	0.00	-1.32
O	0.00	6.38	0.00	-1.35
O	2.13	0.00	4.26	-1.31
O	2.13	14.90	6.38	-1.38
O	4.26	0.00	6.38	-1.47
O	2.13	12.77	8.51	-1.30
O	4.26	14.90	8.51	-1.35

O	6.39	0.00	8.51	-1.46
O	2.13	10.64	10.64	-1.23
O	4.26	12.77	10.64	-1.26
O	6.39	14.90	10.64	-1.26
O	8.51	0.00	10.64	-1.25
O	2.13	8.51	12.77	-1.28
O	4.26	10.64	12.77	-1.42
O	6.39	12.77	12.77	-1.27
O	8.51	14.90	12.77	-1.25
O	10.64	0.00	12.77	-1.28
O	2.13	6.38	14.90	-1.37
O	4.26	8.51	14.90	-1.36
O	6.39	10.64	14.90	-1.38
O	8.51	12.77	14.90	-1.33
O	10.64	14.90	14.90	-1.39
O	0.00	0.00	14.90	-1.31
O	2.13	4.26	17.03	-1.34
O	4.26	6.38	17.03	-1.28
O	6.39	8.51	17.03	-1.32
O	8.51	10.64	17.03	-1.37
O	10.64	12.77	17.03	-1.40
O	0.00	14.90	17.03	-1.43
O	2.13	2.13	19.15	-1.30
O	4.26	4.26	19.15	-1.20
O	6.39	6.38	19.15	-1.11
O	8.51	8.51	19.15	-1.26
O	10.64	10.64	19.15	-1.21
O	0.00	12.77	19.15	-1.30
O	4.26	2.13	0.00	-1.17
O	6.39	4.26	0.00	-1.25
O	8.51	6.38	0.00	-1.15
O	10.64	8.51	0.00	-1.26
O	0.00	10.64	0.00	-1.17
O	2.13	0.00	8.51	-1.30
O	2.13	14.90	10.64	-1.16
O	4.26	0.00	10.64	-1.21
O	2.13	12.77	12.77	-1.31
O	4.26	14.90	12.77	-1.29
O	6.39	0.00	12.77	-1.30
O	2.13	10.64	14.90	-1.29
O	4.26	12.77	14.90	-1.35
O	6.39	14.90	14.90	-1.29
O	8.51	0.00	14.90	-1.21
O	2.13	8.51	17.03	-1.25
O	4.26	10.64	17.03	-1.28

O	6.39	12.77	17.03	-1.31
O	8.51	14.90	17.03	-1.37
O	10.64	0.00	17.03	-1.25
O	2.13	6.38	19.15	-1.36
O	4.26	8.51	19.15	-1.19
O	6.39	10.64	19.15	-1.22
O	8.51	12.77	19.15	-1.15
O	10.64	14.90	19.15	-1.28
O	0.00	0.00	19.15	-1.30
O	2.13	4.26	0.00	-1.27
O	4.26	6.38	0.00	-1.24
O	6.39	8.51	0.00	-1.23
O	8.51	10.64	0.00	-1.14
O	10.64	12.77	0.00	-1.17
O	0.00	14.90	0.00	-1.15
O	2.13	0.00	12.77	-1.21
O	2.13	14.90	14.90	-1.27
O	4.26	0.00	14.90	-1.22
O	2.13	12.77	17.03	-1.26
O	4.26	14.90	17.03	-1.29
O	6.39	0.00	17.03	-1.28
O	2.13	10.64	19.15	-1.18
O	4.26	12.77	19.15	-1.24
O	6.39	14.90	19.15	-1.31
O	8.51	0.00	19.15	-1.15
O	2.13	8.51	0.00	-1.12
O	4.26	10.64	0.00	-1.10
O	6.39	12.77	0.00	-1.27
O	8.51	14.90	0.00	-1.26
O	10.64	0.00	0.00	-1.16
O	2.13	0.00	17.03	-1.19
O	2.13	14.90	19.15	-1.14
O	4.26	0.00	19.15	-1.24
O	2.13	12.77	0.00	-1.12
O	4.26	14.90	0.00	-1.17
O	6.39	0.00	0.00	-1.19
O	2.13	0.00	0.00	-1.17

J14+Sc

Atom type	x	y	z	Bader charge
Mg	2.17	15.18	4.35	1.70
Mg	0.00	10.84	6.53	1.70
Mg	0.00	0.00	4.35	1.70
Mg	6.51	6.50	8.71	1.69
Mg	10.84	10.84	8.71	1.69

Mg	0.00	13.01	8.71	1.69
Mg	8.68	6.50	10.89	1.70
Mg	2.17	10.84	13.06	1.69
Mg	8.68	0.00	4.35	1.69
Mg	6.51	13.01	6.53	1.69
Mg	8.68	15.18	6.53	1.70
Mg	4.34	6.50	10.89	1.69
Mg	8.68	8.67	13.06	1.68
Mg	6.51	4.34	15.24	1.70
Mg	8.68	6.50	15.24	1.70
Mg	10.84	4.34	19.59	1.69
Mg	10.84	2.17	8.71	1.69
Mg	6.51	13.01	10.89	1.69
Mg	10.84	0.00	10.89	1.69
Mg	6.51	10.84	13.06	1.68
Mg	0.00	0.00	13.06	1.70
Mg	6.51	8.67	15.24	1.69
Mg	10.84	13.01	15.24	1.69
Mg	4.34	4.34	17.42	1.68
Mg	8.68	6.50	19.59	1.69
Mg	10.84	8.67	19.59	1.70
Mg	0.00	10.84	19.59	1.69
Mg	2.17	13.01	19.59	1.68
Mg	4.34	10.84	15.24	1.69
Mg	6.51	13.01	15.24	1.68
Mg	10.84	0.00	15.24	1.70
Mg	10.84	15.18	17.42	1.70
Mg	6.51	8.67	19.59	1.69
Mg	10.84	13.01	2.18	1.69
Mg	0.00	15.18	2.18	1.69
Mg	4.34	13.01	0.00	1.70
Mg	4.34	2.17	19.59	1.69
Mg	6.51	2.17	0.00	1.69
Mg	4.34	15.18	2.18	1.69
Mg	6.51	0.00	2.18	1.70
Sc	10.84	6.50	4.35	2.07
Sc	2.17	8.67	6.53	2.06
Sc	4.34	4.34	4.35	2.06
Sc	2.17	4.34	15.24	2.05
Sc	8.68	10.84	6.53	2.08
Sc	2.17	0.00	6.53	2.04
Sc	4.34	4.34	8.71	2.03
Sc	6.51	4.34	10.89	2.04
Sc	2.17	6.50	17.42	2.04
Sc	4.34	10.84	6.53	2.07

Sc	0.00	0.00	8.71	2.04
Sc	10.84	13.01	10.89	2.06
Sc	10.84	8.67	15.24	2.01
Sc	0.00	10.84	15.24	1.98
Sc	2.17	10.84	17.42	1.98
Sc	0.00	4.34	0.00	2.03
Sc	2.17	4.34	2.18	2.04
Sc	4.34	15.18	6.53	2.05
Sc	6.51	0.00	6.53	2.05
Sc	8.68	2.17	6.53	2.05
Sc	4.34	10.84	10.89	2.02
Sc	8.68	10.84	15.24	2.01
Sc	2.17	0.00	15.24	2.03
Sc	10.84	10.84	17.42	1.95
Sc	0.00	13.01	17.42	1.97
Sc	8.68	4.34	0.00	2.03
Sc	6.51	0.00	10.89	2.04
Sc	4.34	13.01	13.06	1.86
Sc	6.51	15.18	13.06	1.98
Sc	4.34	8.67	17.42	2.03
Sc	2.17	15.18	0.00	1.98
Sc	8.68	6.50	2.18	2.03
Sc	4.34	15.18	15.24	1.93
Sc	4.34	13.01	17.42	2.02
Sc	10.84	15.18	0.00	1.99
Sc	0.00	0.00	0.00	1.99
Sc	4.34	2.17	15.24	2.03
Sc	6.51	2.17	17.42	2.05
Sc	8.68	15.18	2.18	2.03
Sc	4.34	0.00	0.00	2.02
Co	0.00	4.34	4.35	1.24
Co	2.17	4.34	6.53	1.22
Co	8.68	4.34	4.35	1.24
Co	0.00	8.67	4.35	1.22
Co	0.00	4.34	8.71	1.25
Co	2.17	6.50	8.71	1.22
Co	8.68	8.67	4.35	1.22
Co	8.68	6.50	6.53	1.26
Co	0.00	6.50	10.89	1.30
Co	2.17	8.67	10.89	1.25
Co	2.17	15.18	8.71	1.23
Co	2.17	8.67	15.24	0.84
Co	10.84	15.18	8.71	1.23
Co	2.17	2.17	8.71	1.21
Co	6.51	8.67	10.89	1.24

Co	0.00	13.01	13.06	1.22
Co	0.00	6.50	19.59	1.22
Co	8.68	0.00	8.71	1.18
Co	10.84	15.18	13.06	1.23
Co	8.68	8.67	17.42	1.11
Co	10.84	6.50	0.00	1.23
Co	0.00	8.67	0.00	1.28
Co	8.68	0.00	13.06	1.23
Co	10.84	2.17	13.06	1.25
Co	8.68	15.18	15.24	1.23
Co	0.00	2.17	15.24	1.24
Co	0.00	15.18	19.59	1.15
Co	0.00	13.01	0.00	1.22
Co	10.84	8.67	2.18	1.22
Co	2.17	13.01	2.18	1.23
Co	4.34	0.00	13.06	1.19
Co	10.84	2.17	17.42	1.27
Co	10.84	0.00	19.59	1.22
Co	0.00	2.17	19.59	1.22
Co	4.34	8.67	0.00	1.28
Co	8.68	13.01	0.00	1.26
Co	2.17	2.17	0.00	1.21
Co	8.68	10.84	2.18	1.27
Co	6.51	0.00	19.59	1.21
Co	10.84	0.00	2.18	1.19
Ni	2.17	10.84	4.35	1.15
Ni	6.51	6.50	4.35	1.16
Ni	2.17	13.01	6.53	1.17
Ni	0.00	8.67	8.71	1.19
Ni	2.17	10.84	8.71	1.19
Ni	8.68	13.01	4.35	1.07
Ni	10.84	15.18	4.35	1.17
Ni	2.17	2.17	4.35	1.11
Ni	10.84	13.01	6.53	1.15
Ni	8.68	8.67	8.71	1.19
Ni	10.84	8.67	10.89	1.24
Ni	8.68	4.34	13.06	1.13
Ni	0.00	6.50	15.24	1.19
Ni	2.17	4.34	19.59	1.16
Ni	6.51	15.18	4.35	1.06
Ni	10.84	2.17	4.35	1.15
Ni	10.84	0.00	6.53	1.15
Ni	4.34	8.67	8.71	1.06
Ni	6.51	10.84	8.71	1.06
Ni	8.68	13.01	8.71	1.10

Ni	2.17	13.01	15.24	0.75
Ni	0.00	8.67	17.42	0.75
Ni	2.17	6.50	0.00	1.23
Ni	4.34	13.01	8.71	0.76
Ni	8.68	15.18	10.89	1.02
Ni	0.00	2.17	10.89	1.23
Ni	2.17	15.18	17.42	0.86
Ni	8.68	2.17	10.89	1.24
Ni	6.51	10.84	17.42	1.07
Ni	8.68	13.01	17.42	1.07
Ni	0.00	0.00	17.42	1.13
Ni	6.51	4.34	2.18	1.16
Ni	0.00	10.84	2.18	1.24
Ni	4.34	2.17	10.89	1.25
Ni	8.68	2.17	15.24	1.20
Ni	4.34	15.18	19.59	1.15
Ni	8.68	0.00	0.00	1.22
Ni	4.34	10.84	2.18	1.22
Ni	6.51	13.01	2.18	1.16
Ni	0.00	2.17	2.18	1.06
Cu	2.17	4.34	10.89	0.86
Cu	0.00	13.01	4.35	0.83
Cu	10.84	8.67	6.53	0.79
Cu	8.68	4.34	8.71	0.76
Cu	10.84	4.34	10.89	0.92
Cu	0.00	4.34	13.06	0.93
Cu	2.17	6.50	13.06	0.91
Cu	4.34	8.67	4.35	0.78
Cu	0.00	10.84	10.89	0.80
Cu	0.00	8.67	13.06	0.82
Cu	0.00	4.34	17.42	0.84
Cu	0.00	2.17	6.53	0.78
Cu	0.00	15.18	10.89	0.76
Cu	2.17	0.00	10.89	0.78
Cu	4.34	4.34	13.06	0.77
Cu	10.84	10.84	13.06	0.71
Cu	8.68	4.34	17.42	0.93
Cu	4.34	0.00	4.35	0.72
Cu	6.51	2.17	4.35	0.80
Cu	2.17	2.17	13.06	0.80
Cu	6.51	4.34	19.59	0.83
Cu	2.17	10.84	0.00	0.87
Cu	10.84	4.34	2.18	0.72
Cu	0.00	6.50	2.18	0.74
Cu	6.51	2.17	8.71	0.66

Cu	4.34	6.50	19.59	0.84
Cu	2.17	0.00	19.59	0.71
Cu	4.34	4.34	0.00	0.79
Cu	10.84	10.84	0.00	0.82
Cu	6.51	2.17	13.06	0.75
Cu	6.51	0.00	15.24	0.77
Cu	8.68	0.00	17.42	0.89
Cu	4.34	10.84	19.59	0.74
Cu	6.51	13.01	19.59	0.80
Cu	6.51	10.84	0.00	0.94
Cu	4.34	6.50	2.18	0.90
Cu	8.68	2.17	19.59	0.83
Cu	6.51	15.18	0.00	0.76
Cu	8.68	2.17	2.18	0.89
Cu	4.34	2.17	2.18	0.80
Zn	2.17	6.50	4.35	1.16
Zn	10.84	4.34	6.53	1.14
Zn	0.00	6.50	6.53	1.14
Zn	10.84	10.84	4.35	1.17
Zn	6.51	4.34	6.53	1.16
Zn	10.84	6.50	8.71	1.19
Zn	6.51	10.84	4.35	1.14
Zn	4.34	6.50	6.53	1.14
Zn	6.51	8.67	6.53	1.15
Zn	0.00	15.18	6.53	1.13
Zn	2.17	13.01	10.89	1.11
Zn	10.84	6.50	13.06	1.15
Zn	10.84	4.34	15.24	1.18
Zn	4.34	13.01	4.35	1.11
Zn	8.68	10.84	10.89	1.11
Zn	6.51	6.50	13.06	1.13
Zn	2.17	15.18	13.06	1.13
Zn	10.84	6.50	17.42	1.17
Zn	2.17	8.67	19.59	1.15
Zn	6.51	15.18	8.71	1.11
Zn	4.34	8.67	13.06	1.13
Zn	8.68	13.01	13.06	1.12
Zn	4.34	6.50	15.24	1.14
Zn	0.00	15.18	15.24	1.14
Zn	6.51	6.50	17.42	1.16
Zn	2.17	8.67	2.18	1.20
Zn	4.34	2.17	6.53	1.13
Zn	4.34	0.00	8.71	1.12
Zn	4.34	15.18	10.89	1.09
Zn	2.17	2.17	17.42	1.13

Zn	8.68	10.84	19.59	1.16
Zn	10.84	13.01	19.59	1.12
Zn	6.51	6.50	0.00	1.13
Zn	8.68	8.67	0.00	1.14
Zn	6.51	15.18	17.42	1.16
Zn	8.68	15.18	19.59	1.17
Zn	6.51	8.67	2.18	1.18
Zn	2.17	0.00	2.18	1.13
Zn	4.34	0.00	17.42	1.14
Zn	10.84	2.17	0.00	1.17
O	10.84	2.17	2.18	-1.17
O	0.00	4.34	2.18	-1.30
O	0.00	2.17	4.35	-1.30
O	6.51	2.17	2.18	-1.31
O	8.68	4.34	2.18	-1.30
O	10.84	6.50	2.18	-1.34
O	0.00	8.67	2.18	-1.22
O	8.68	2.17	4.35	-1.35
O	10.84	4.34	4.35	-1.24
O	0.00	6.50	4.35	-1.24
O	10.84	2.17	6.53	-1.33
O	0.00	4.34	6.53	-1.23
O	0.00	2.17	8.71	-1.37
O	2.17	2.17	2.18	-1.26
O	4.34	4.34	2.18	-1.28
O	6.51	6.50	2.18	-1.23
O	8.68	8.67	2.18	-1.26
O	10.84	10.84	2.18	-1.26
O	0.00	13.01	2.18	-1.39
O	4.34	2.17	4.35	-1.21
O	6.51	4.34	4.35	-1.29
O	8.68	6.50	4.35	-1.34
O	10.84	8.67	4.35	-1.31
O	0.00	10.84	4.35	-1.30
O	6.51	2.17	6.53	-1.28
O	8.68	4.34	6.53	-1.24
O	10.84	6.50	6.53	-1.27
O	0.00	8.67	6.53	-1.36
O	8.68	2.17	8.71	-1.36
O	10.84	4.34	8.71	-1.23
O	0.00	6.50	8.71	-1.22
O	10.84	2.17	10.89	-1.39
O	0.00	4.34	10.89	-1.14
O	0.00	2.17	13.06	-1.30
O	2.17	6.50	2.18	-1.26

O	4.34	8.67	2.18	-1.20
O	6.51	10.84	2.18	-1.18
O	8.68	13.01	2.18	-1.37
O	10.84	15.18	2.18	-1.45
O	0.00	0.00	2.18	-1.40
O	2.17	4.34	4.35	-1.32
O	4.34	6.50	4.35	-1.28
O	6.51	8.67	4.35	-1.22
O	8.68	10.84	4.35	-1.28
O	10.84	13.01	4.35	-1.26
O	0.00	15.18	4.35	-1.47
O	2.17	2.17	6.53	-1.29
O	4.34	4.34	6.53	-1.30
O	6.51	6.50	6.53	-1.28
O	8.68	8.67	6.53	-1.29
O	10.84	10.84	6.53	-1.40
O	0.00	13.01	6.53	-1.38
O	4.34	2.17	8.71	-1.28
O	6.51	4.34	8.71	-1.38
O	8.68	6.50	8.71	-1.35
O	10.84	8.67	8.71	-1.32
O	0.00	10.84	8.71	-1.43
O	6.51	2.17	10.89	-1.29
O	8.68	4.34	10.89	-1.28
O	10.84	6.50	10.89	-1.25
O	0.00	8.67	10.89	-1.19
O	8.68	2.17	13.06	-1.23
O	10.84	4.34	13.06	-1.15
O	0.00	6.50	13.06	-1.15
O	10.84	2.17	15.24	-1.33
O	0.00	4.34	15.24	-1.23
O	0.00	2.17	17.42	-1.24
O	2.17	10.84	2.18	-1.18
O	4.34	13.01	2.18	-1.37
O	6.51	15.18	2.18	-1.37
O	8.68	0.00	2.18	-1.44
O	2.17	8.67	4.35	-1.27
O	4.34	10.84	4.35	-1.27
O	6.51	13.01	4.35	-1.30
O	8.68	15.18	4.35	-1.41
O	10.84	0.00	4.35	-1.40
O	2.17	6.50	6.53	-1.29
O	4.34	8.67	6.53	-1.31
O	6.51	10.84	6.53	-1.41
O	8.68	13.01	6.53	-1.45

O	10.84	15.18	6.53	-1.31
O	0.00	0.00	6.53	-1.38
O	2.17	4.34	8.71	-1.26
O	4.34	6.50	8.71	-1.41
O	6.51	8.67	8.71	-1.31
O	8.68	10.84	8.71	-1.32
O	10.84	13.01	8.71	-1.41
O	0.00	15.18	8.71	-1.32
O	2.17	2.17	10.89	-1.18
O	4.34	4.34	10.89	-1.36
O	6.51	6.50	10.89	-1.48
O	8.68	8.67	10.89	-1.37
O	10.84	10.84	10.89	-1.31
O	0.00	13.01	10.89	-1.31
O	4.34	2.17	13.06	-1.26
O	6.51	4.34	13.06	-1.30
O	8.68	6.50	13.06	-1.43
O	10.84	8.67	13.06	-1.36
O	0.00	10.84	13.06	-1.31
O	6.51	2.17	15.24	-1.37
O	8.68	4.34	15.24	-1.38
O	10.84	6.50	15.24	-1.36
O	0.00	8.67	15.24	-1.30
O	8.68	2.17	17.42	-1.22
O	10.84	4.34	17.42	-1.24
O	0.00	6.50	17.42	-1.29
O	10.84	2.17	19.59	-1.32
O	0.00	4.34	19.59	-1.34
O	0.00	2.17	0.00	-1.30
O	2.17	15.18	2.18	-1.48
O	4.34	0.00	2.18	-1.40
O	2.17	13.01	4.35	-1.30
O	4.34	15.18	4.35	-1.42
O	6.51	0.00	4.35	-1.41
O	2.17	10.84	6.53	-1.40
O	4.34	13.01	6.53	-1.37
O	6.51	15.18	6.53	-1.48
O	8.68	0.00	6.53	-1.48
O	2.17	8.67	8.71	-1.30
O	4.34	10.84	8.71	-1.28
O	6.51	13.01	8.71	-1.38
O	8.68	15.18	8.71	-1.33
O	10.84	0.00	8.71	-1.40
O	2.17	6.50	10.89	-1.28
O	4.34	8.67	10.89	-1.31

O	6.51	10.84	10.89	-1.41
O	8.68	13.01	10.89	-1.31
O	10.84	15.18	10.89	-1.30
O	0.00	0.00	10.89	-1.39
O	2.17	4.34	13.06	-1.16
O	4.34	6.50	13.06	-1.24
O	6.51	8.67	13.06	-1.46
O	8.68	10.84	13.06	-1.40
O	10.84	13.01	13.06	-1.34
O	0.00	15.18	13.06	-1.26
O	2.17	2.17	15.24	-1.34
O	4.34	4.34	15.24	-1.44
O	6.51	6.50	15.24	-1.45
O	8.68	8.67	15.24	-1.55
O	10.84	10.84	15.24	-1.47
O	0.00	13.01	15.24	-1.43
O	4.34	2.17	17.42	-1.44
O	6.51	4.34	17.42	-1.39
O	8.68	6.50	17.42	-1.35
O	10.84	8.67	17.42	-1.37
O	0.00	10.84	17.42	-1.50
O	6.51	2.17	19.59	-1.41
O	8.68	4.34	19.59	-1.40
O	10.84	6.50	19.59	-1.46
O	0.00	8.67	19.59	-1.39
O	8.68	2.17	0.00	-1.27
O	10.84	4.34	0.00	-1.39
O	0.00	6.50	0.00	-1.26
O	2.17	0.00	4.35	-1.44
O	2.17	15.18	6.53	-1.41
O	4.34	0.00	6.53	-1.35
O	2.17	13.01	8.71	-1.28
O	4.34	15.18	8.71	-1.25
O	6.51	0.00	8.71	-1.28
O	2.17	10.84	10.89	-1.35
O	4.34	13.01	10.89	-1.38
O	6.51	15.18	10.89	-1.36
O	8.68	0.00	10.89	-1.33
O	2.17	8.67	13.06	-1.29
O	4.34	10.84	13.06	-1.53
O	6.51	13.01	13.06	-1.54
O	8.68	15.18	13.06	-1.31
O	10.84	0.00	13.06	-1.46
O	2.17	6.50	15.24	-1.29
O	4.34	8.67	15.24	-1.46

O	6.51	10.84	15.24	-1.58
O	8.68	13.01	15.24	-1.46
O	10.84	15.18	15.24	-1.46
O	0.00	0.00	15.24	-1.41
O	2.17	4.34	17.42	-1.41
O	4.34	6.50	17.42	-1.35
O	6.51	8.67	17.42	-1.41
O	8.68	10.84	17.42	-1.35
O	10.84	13.01	17.42	-1.49
O	0.00	15.18	17.42	-1.37
O	2.17	2.17	19.59	-1.30
O	4.34	4.34	19.59	-1.32
O	6.51	6.50	19.59	-1.34
O	8.68	8.67	19.59	-1.43
O	10.84	10.84	19.59	-1.38
O	0.00	13.01	19.59	-1.42
O	4.34	2.17	0.00	-1.40
O	6.51	4.34	0.00	-1.31
O	8.68	6.50	0.00	-1.36
O	10.84	8.67	0.00	-1.29
O	0.00	10.84	0.00	-1.28
O	2.17	0.00	8.71	-1.30
O	2.17	15.18	10.89	-1.16
O	4.34	0.00	10.89	-1.23
O	2.17	13.01	13.06	-1.33
O	4.34	15.18	13.06	-1.36
O	6.51	0.00	13.06	-1.32
O	2.17	10.84	15.24	-1.49
O	4.34	13.01	15.24	-1.53
O	6.51	15.18	15.24	-1.41
O	8.68	0.00	15.24	-1.31
O	2.17	8.67	17.42	-1.39
O	4.34	10.84	17.42	-1.42
O	6.51	13.01	17.42	-1.32
O	8.68	15.18	17.42	-1.29
O	10.84	0.00	17.42	-1.38
O	2.17	6.50	19.59	-1.29
O	4.34	8.67	19.59	-1.33
O	6.51	10.84	19.59	-1.21
O	8.68	13.01	19.59	-1.19
O	10.84	15.18	19.59	-1.33
O	0.00	0.00	19.59	-1.26
O	2.17	4.34	0.00	-1.32
O	4.34	6.50	0.00	-1.13
O	6.51	8.67	0.00	-1.24

O	8.68	10.84	0.00	-1.15
O	10.84	13.01	0.00	-1.34
O	0.00	15.18	0.00	-1.45
O	2.17	0.00	13.06	-1.31
O	2.17	15.18	15.24	-1.35
O	4.34	0.00	15.24	-1.40
O	2.17	13.01	17.42	-1.47
O	4.34	15.18	17.42	-1.32
O	6.51	0.00	17.42	-1.27
O	2.17	10.84	19.59	-1.40
O	4.34	13.01	19.59	-1.40
O	6.51	15.18	19.59	-1.16
O	8.68	0.00	19.59	-1.22
O	2.17	8.67	0.00	-1.16
O	4.34	10.84	0.00	-1.23
O	6.51	13.01	0.00	-1.22
O	8.68	15.18	0.00	-1.30
O	10.84	0.00	0.00	-1.31
O	2.17	0.00	17.42	-1.22
O	2.17	15.18	19.59	-1.34
O	4.34	0.00	19.59	-1.32
O	2.17	13.01	0.00	-1.41
O	4.34	15.18	0.00	-1.46
O	6.51	0.00	0.00	-1.42
O	2.17	0.00	0.00	-1.35

J14+Sn

Atom				Bader
type	x	y	z	charge
Mg	2.24	15.65	4.42	1.70
Mg	0.00	11.18	6.64	1.70
Mg	0.00	0.00	4.42	1.70
Mg	6.72	6.71	8.85	1.70
Mg	11.19	11.18	8.85	1.70
Mg	0.00	13.41	8.85	1.70
Mg	8.95	6.71	11.06	1.70
Mg	2.24	11.18	13.27	1.70
Mg	8.95	0.00	4.42	1.70
Mg	6.72	13.41	6.64	1.70
Mg	8.95	15.65	6.64	1.70
Mg	4.48	6.71	11.06	1.70
Mg	8.95	8.94	13.27	1.69
Mg	6.72	4.47	15.48	1.70
Mg	8.95	6.71	15.48	1.70
Mg	11.19	4.47	19.91	1.70
Mg	11.19	2.24	8.85	1.70

Mg	6.72	13.41	11.06	1.70
Mg	11.19	0.00	11.06	1.70
Mg	6.72	11.18	13.27	1.69
Mg	0.00	0.00	13.27	1.70
Mg	6.72	8.94	15.48	1.70
Mg	11.19	13.41	15.48	1.70
Mg	4.48	4.47	17.70	1.69
Mg	8.95	6.71	19.91	1.70
Mg	11.19	8.94	19.91	1.70
Mg	0.00	11.18	19.91	1.70
Mg	2.24	13.41	19.91	1.69
Mg	4.48	11.18	15.48	1.69
Mg	6.72	13.41	15.48	1.69
Mg	11.19	0.00	15.48	1.71
Mg	11.19	15.65	17.70	1.70
Mg	6.72	8.94	19.91	1.70
Mg	11.19	13.41	2.21	1.70
Mg	0.00	15.65	2.21	1.70
Mg	4.48	13.41	0.00	1.70
Mg	4.48	2.24	19.91	1.69
Mg	6.72	2.24	0.00	1.70
Mg	4.48	15.65	2.21	1.70
Mg	6.72	0.00	2.21	1.70
Sn	11.19	6.71	4.42	1.94
Sn	2.24	8.94	6.64	1.92
Sn	4.48	4.47	4.42	1.94
Sn	2.24	4.47	15.48	1.93
Sn	8.95	11.18	6.64	1.93
Sn	2.24	0.00	6.64	1.86
Sn	4.48	4.47	8.85	1.87
Sn	6.72	4.47	11.06	2.02
Sn	2.24	6.71	17.70	1.89
Sn	4.48	11.18	6.64	1.88
Sn	0.00	0.00	8.85	1.93
Sn	11.19	13.41	11.06	2.03
Sn	11.19	8.94	15.48	1.85
Sn	0.00	11.18	15.48	1.82
Sn	2.24	11.18	17.70	1.76
Sn	0.00	4.47	0.00	1.98
Sn	2.24	4.47	2.21	1.93
Sn	4.48	15.65	6.64	1.81
Sn	6.72	0.00	6.64	1.83
Sn	8.95	2.24	6.64	1.95
Sn	4.48	11.18	11.06	1.92
Sn	8.95	11.18	15.48	1.71

Sn	2.24	0.00	15.48	1.92
Sn	11.19	11.18	17.70	1.73
Sn	0.00	13.41	17.70	1.74
Sn	8.95	4.47	0.00	2.00
Sn	6.72	0.00	11.06	1.98
Sn	4.48	13.41	13.27	1.72
Sn	6.72	15.65	13.27	1.79
Sn	4.48	8.94	17.70	1.87
Sn	2.24	15.65	0.00	1.86
Sn	8.95	6.71	2.21	1.92
Sn	4.48	15.65	15.48	1.77
Sn	4.48	13.41	17.70	1.83
Sn	11.19	15.65	0.00	1.85
Sn	0.00	0.00	0.00	1.87
Sn	4.48	2.24	15.48	1.86
Sn	6.72	2.24	17.70	1.99
Sn	8.95	15.65	2.21	1.89
Sn	4.48	0.00	0.00	1.99
Co	0.00	4.47	4.42	1.23
Co	2.24	4.47	6.64	1.17
Co	8.95	4.47	4.42	1.22
Co	0.00	8.94	4.42	1.21
Co	0.00	4.47	8.85	1.25
Co	2.24	6.71	8.85	1.21
Co	8.95	8.94	4.42	1.20
Co	8.95	6.71	6.64	1.22
Co	0.00	6.71	11.06	1.28
Co	2.24	8.94	11.06	1.24
Co	2.24	15.65	8.85	1.23
Co	2.24	8.94	15.48	0.78
Co	11.19	15.65	8.85	1.21
Co	2.24	2.24	8.85	1.21
Co	6.72	8.94	11.06	1.25
Co	0.00	13.41	13.27	1.21
Co	0.00	6.71	19.91	1.22
Co	8.95	0.00	8.85	1.15
Co	11.19	15.65	13.27	1.21
Co	8.95	8.94	17.70	1.15
Co	11.19	6.71	0.00	1.17
Co	0.00	8.94	0.00	1.28
Co	8.95	0.00	13.27	1.21
Co	11.19	2.24	13.27	1.24
Co	8.95	15.65	15.48	1.19
Co	0.00	2.24	15.48	1.21
Co	0.00	15.65	19.91	1.19

Co	0.00	13.41	0.00	1.19
Co	11.19	8.94	2.21	1.22
Co	2.24	13.41	2.21	1.24
Co	4.48	0.00	13.27	0.78
Co	11.19	2.24	17.70	1.27
Co	11.19	0.00	19.91	1.22
Co	0.00	2.24	19.91	1.22
Co	4.48	8.94	0.00	1.25
Co	8.95	13.41	0.00	1.27
Co	2.24	2.24	0.00	1.24
Co	8.95	11.18	2.21	1.25
Co	6.72	0.00	19.91	1.20
Co	11.19	0.00	2.21	1.19
Ni	2.24	11.18	4.42	1.17
Ni	6.72	6.71	4.42	1.10
Ni	2.24	13.41	6.64	1.09
Ni	0.00	8.94	8.85	1.22
Ni	2.24	11.18	8.85	1.11
Ni	8.95	13.41	4.42	1.06
Ni	11.19	15.65	4.42	1.14
Ni	2.24	2.24	4.42	1.09
Ni	11.19	13.41	6.64	1.15
Ni	8.95	8.94	8.85	1.21
Ni	11.19	8.94	11.06	1.22
Ni	8.95	4.47	13.27	1.18
Ni	0.00	6.71	15.48	1.18
Ni	2.24	4.47	19.91	1.09
Ni	6.72	15.65	4.42	1.08
Ni	11.19	2.24	4.42	1.16
Ni	11.19	0.00	6.64	1.05
Ni	4.48	8.94	8.85	1.02
Ni	6.72	11.18	8.85	1.00
Ni	8.95	13.41	8.85	1.06
Ni	2.24	13.41	15.48	0.69
Ni	0.00	8.94	17.70	0.92
Ni	2.24	6.71	0.00	1.22
Ni	4.48	13.41	8.85	1.00
Ni	8.95	15.65	11.06	1.07
Ni	0.00	2.24	11.06	1.23
Ni	2.24	15.65	17.70	0.93
Ni	8.95	2.24	11.06	1.23
Ni	6.72	11.18	17.70	1.01
Ni	8.95	13.41	17.70	1.07
Ni	0.00	0.00	17.70	1.11
Ni	6.72	4.47	2.21	1.14

Ni	0.00	11.18	2.21	1.25
Ni	4.48	2.24	11.06	1.23
Ni	8.95	2.24	15.48	1.17
Ni	4.48	15.65	19.91	1.13
Ni	8.95	0.00	0.00	1.16
Ni	4.48	11.18	2.21	1.24
Ni	6.72	13.41	2.21	1.21
Ni	0.00	2.24	2.21	1.08
Cu	2.24	4.47	11.06	0.83
Cu	0.00	13.41	4.42	0.82
Cu	11.19	8.94	6.64	0.77
Cu	8.95	4.47	8.85	0.73
Cu	11.19	4.47	11.06	0.91
Cu	0.00	4.47	13.27	0.91
Cu	2.24	6.71	13.27	0.86
Cu	4.48	8.94	4.42	0.79
Cu	0.00	11.18	11.06	0.77
Cu	0.00	8.94	13.27	0.81
Cu	0.00	4.47	17.70	0.78
Cu	0.00	2.24	6.64	0.77
Cu	0.00	15.65	11.06	0.72
Cu	2.24	0.00	11.06	0.79
Cu	4.48	4.47	13.27	0.73
Cu	11.19	11.18	13.27	0.69
Cu	8.95	4.47	17.70	0.84
Cu	4.48	0.00	4.42	0.76
Cu	6.72	2.24	4.42	0.78
Cu	2.24	2.24	13.27	0.79
Cu	6.72	4.47	19.91	0.74
Cu	2.24	11.18	0.00	0.83
Cu	11.19	4.47	2.21	0.70
Cu	0.00	6.71	2.21	0.71
Cu	6.72	2.24	8.85	0.67
Cu	4.48	6.71	19.91	0.82
Cu	2.24	0.00	19.91	0.70
Cu	4.48	4.47	0.00	0.79
Cu	11.19	11.18	0.00	0.79
Cu	6.72	2.24	13.27	0.74
Cu	6.72	0.00	15.48	0.77
Cu	8.95	0.00	17.70	0.85
Cu	4.48	11.18	19.91	0.72
Cu	6.72	13.41	19.91	0.82
Cu	6.72	11.18	0.00	0.91
Cu	4.48	6.71	2.21	0.85
Cu	8.95	2.24	19.91	0.74

Cu	6.72	15.65	0.00	0.72
Cu	8.95	2.24	2.21	0.76
Cu	4.48	2.24	2.21	0.72
Zn	2.24	6.71	4.42	1.14
Zn	11.19	4.47	6.64	1.13
Zn	0.00	6.71	6.64	1.13
Zn	11.19	11.18	4.42	1.15
Zn	6.72	4.47	6.64	1.13
Zn	11.19	6.71	8.85	1.17
Zn	6.72	11.18	4.42	1.14
Zn	4.48	6.71	6.64	1.12
Zn	6.72	8.94	6.64	1.14
Zn	0.00	15.65	6.64	1.11
Zn	2.24	13.41	11.06	1.12
Zn	11.19	6.71	13.27	1.14
Zn	11.19	4.47	15.48	1.16
Zn	4.48	13.41	4.42	1.10
Zn	8.95	11.18	11.06	1.08
Zn	6.72	6.71	13.27	1.12
Zn	2.24	15.65	13.27	1.13
Zn	11.19	6.71	17.70	1.14
Zn	2.24	8.94	19.91	1.15
Zn	6.72	15.65	8.85	1.10
Zn	4.48	8.94	13.27	1.11
Zn	8.95	13.41	13.27	1.11
Zn	4.48	6.71	15.48	1.12
Zn	0.00	15.65	15.48	1.11
Zn	6.72	6.71	17.70	1.14
Zn	2.24	8.94	2.21	1.19
Zn	4.48	2.24	6.64	1.11
Zn	4.48	0.00	8.85	1.12
Zn	4.48	15.65	11.06	1.06
Zn	2.24	2.24	17.70	1.11
Zn	8.95	11.18	19.91	1.14
Zn	11.19	13.41	19.91	1.13
Zn	6.72	6.71	0.00	1.13
Zn	8.95	8.94	0.00	1.12
Zn	6.72	15.65	17.70	1.14
Zn	8.95	15.65	19.91	1.15
Zn	6.72	8.94	2.21	1.17
Zn	2.24	0.00	2.21	1.12
Zn	4.48	0.00	17.70	1.11
Zn	11.19	2.24	0.00	1.13
O	11.19	2.24	2.21	-1.18
O	0.00	4.47	2.21	-1.26

O	0.00	2.24	4.42	-1.30
O	6.72	2.24	2.21	-1.33
O	8.95	4.47	2.21	-1.26
O	11.19	6.71	2.21	-1.22
O	0.00	8.94	2.21	-1.22
O	8.95	2.24	4.42	-1.24
O	11.19	4.47	4.42	-1.20
O	0.00	6.71	4.42	-1.21
O	11.19	2.24	6.64	-1.28
O	0.00	4.47	6.64	-1.22
O	0.00	2.24	8.85	-1.32
O	2.24	2.24	2.21	-1.24
O	4.48	4.47	2.21	-1.17
O	6.72	6.71	2.21	-1.18
O	8.95	8.94	2.21	-1.22
O	11.19	11.18	2.21	-1.27
O	0.00	13.41	2.21	-1.39
O	4.48	2.24	4.42	-1.15
O	6.72	4.47	4.42	-1.25
O	8.95	6.71	4.42	-1.30
O	11.19	8.94	4.42	-1.27
O	0.00	11.18	4.42	-1.31
O	6.72	2.24	6.64	-1.23
O	8.95	4.47	6.64	-1.20
O	11.19	6.71	6.64	-1.22
O	0.00	8.94	6.64	-1.31
O	8.95	2.24	8.85	-1.29
O	11.19	4.47	8.85	-1.22
O	0.00	6.71	8.85	-1.21
O	11.19	2.24	11.06	-1.40
O	0.00	4.47	11.06	-1.13
O	0.00	2.24	13.27	-1.29
O	2.24	6.71	2.21	-1.22
O	4.48	8.94	2.21	-1.18
O	6.72	11.18	2.21	-1.17
O	8.95	13.41	2.21	-1.34
O	11.19	15.65	2.21	-1.44
O	0.00	0.00	2.21	-1.41
O	2.24	4.47	4.42	-1.29
O	4.48	6.71	4.42	-1.21
O	6.72	8.94	4.42	-1.21
O	8.95	11.18	4.42	-1.25
O	11.19	13.41	4.42	-1.25
O	0.00	15.65	4.42	-1.48
O	2.24	2.24	6.64	-1.26

O	4.48	4.47	6.64	-1.26
O	6.72	6.71	6.64	-1.28
O	8.95	8.94	6.64	-1.25
O	11.19	11.18	6.64	-1.36
O	0.00	13.41	6.64	-1.40
O	4.48	2.24	8.85	-1.25
O	6.72	4.47	8.85	-1.34
O	8.95	6.71	8.85	-1.35
O	11.19	8.94	8.85	-1.32
O	0.00	11.18	8.85	-1.41
O	6.72	2.24	11.06	-1.24
O	8.95	4.47	11.06	-1.26
O	11.19	6.71	11.06	-1.24
O	0.00	8.94	11.06	-1.22
O	8.95	2.24	13.27	-1.23
O	11.19	4.47	13.27	-1.15
O	0.00	6.71	13.27	-1.15
O	11.19	2.24	15.48	-1.32
O	0.00	4.47	15.48	-1.19
O	0.00	2.24	17.70	-1.23
O	2.24	11.18	2.21	-1.19
O	4.48	13.41	2.21	-1.38
O	6.72	15.65	2.21	-1.34
O	8.95	0.00	2.21	-1.39
O	2.24	8.94	4.42	-1.22
O	4.48	11.18	4.42	-1.24
O	6.72	13.41	4.42	-1.29
O	8.95	15.65	4.42	-1.42
O	11.19	0.00	4.42	-1.40
O	2.24	6.71	6.64	-1.25
O	4.48	8.94	6.64	-1.27
O	6.72	11.18	6.64	-1.35
O	8.95	13.41	6.64	-1.42
O	11.19	15.65	6.64	-1.31
O	0.00	0.00	6.64	-1.33
O	2.24	4.47	8.85	-1.23
O	4.48	6.71	8.85	-1.38
O	6.72	8.94	8.85	-1.32
O	8.95	11.18	8.85	-1.25
O	11.19	13.41	8.85	-1.39
O	0.00	15.65	8.85	-1.27
O	2.24	2.24	11.06	-1.18
O	4.48	4.47	11.06	-1.24
O	6.72	6.71	11.06	-1.44
O	8.95	8.94	11.06	-1.39

O	11.19	11.18	11.06	-1.26
O	0.00	13.41	11.06	-1.27
O	4.48	2.24	13.27	-1.19
O	6.72	4.47	13.27	-1.30
O	8.95	6.71	13.27	-1.43
O	11.19	8.94	13.27	-1.29
O	0.00	11.18	13.27	-1.23
O	6.72	2.24	15.48	-1.26
O	8.95	4.47	15.48	-1.37
O	11.19	6.71	15.48	-1.33
O	0.00	8.94	15.48	-1.23
O	8.95	2.24	17.70	-1.16
O	11.19	4.47	17.70	-1.25
O	0.00	6.71	17.70	-1.25
O	11.19	2.24	19.91	-1.28
O	0.00	4.47	19.91	-1.32
O	0.00	2.24	0.00	-1.26
O	2.24	15.65	2.21	-1.48
O	4.48	0.00	2.21	-1.38
O	2.24	13.41	4.42	-1.29
O	4.48	15.65	4.42	-1.40
O	6.72	0.00	4.42	-1.36
O	2.24	11.18	6.64	-1.34
O	4.48	13.41	6.64	-1.36
O	6.72	15.65	6.64	-1.44
O	8.95	0.00	6.64	-1.43
O	2.24	8.94	8.85	-1.25
O	4.48	11.18	8.85	-1.25
O	6.72	13.41	8.85	-1.37
O	8.95	15.65	8.85	-1.32
O	11.19	0.00	8.85	-1.38
O	2.24	6.71	11.06	-1.26
O	4.48	8.94	11.06	-1.29
O	6.72	11.18	11.06	-1.38
O	8.95	13.41	11.06	-1.28
O	11.19	15.65	11.06	-1.26
O	0.00	0.00	11.06	-1.31
O	2.24	4.47	13.27	-1.08
O	4.48	6.71	13.27	-1.24
O	6.72	8.94	13.27	-1.47
O	8.95	11.18	13.27	-1.35
O	11.19	13.41	13.27	-1.33
O	0.00	15.65	13.27	-1.25
O	2.24	2.24	15.48	-1.27
O	4.48	4.47	15.48	-1.38

O	6.72	6.71	15.48	-1.45
O	8.95	8.94	15.48	-1.50
O	11.19	11.18	15.48	-1.34
O	0.00	13.41	15.48	-1.36
O	4.48	2.24	17.70	-1.39
O	6.72	4.47	17.70	-1.34
O	8.95	6.71	17.70	-1.35
O	11.19	8.94	17.70	-1.33
O	0.00	11.18	17.70	-1.40
O	6.72	2.24	19.91	-1.34
O	8.95	4.47	19.91	-1.36
O	11.19	6.71	19.91	-1.47
O	0.00	8.94	19.91	-1.39
O	8.95	2.24	0.00	-1.24
O	11.19	4.47	0.00	-1.32
O	0.00	6.71	0.00	-1.23
O	2.24	0.00	4.42	-1.39
O	2.24	15.65	6.64	-1.36
O	4.48	0.00	6.64	-1.32
O	2.24	13.41	8.85	-1.29
O	4.48	15.65	8.85	-1.20
O	6.72	0.00	8.85	-1.26
O	2.24	11.18	11.06	-1.31
O	4.48	13.41	11.06	-1.30
O	6.72	15.65	11.06	-1.29
O	8.95	0.00	11.06	-1.29
O	2.24	8.94	13.27	-1.29
O	4.48	11.18	13.27	-1.52
O	6.72	13.41	13.27	-1.51
O	8.95	15.65	13.27	-1.29
O	11.19	0.00	13.27	-1.47
O	2.24	6.71	15.48	-1.21
O	4.48	8.94	15.48	-1.41
O	6.72	11.18	15.48	-1.57
O	8.95	13.41	15.48	-1.43
O	11.19	15.65	15.48	-1.46
O	0.00	0.00	15.48	-1.37
O	2.24	4.47	17.70	-1.34
O	4.48	6.71	17.70	-1.29
O	6.72	8.94	17.70	-1.38
O	8.95	11.18	17.70	-1.30
O	11.19	13.41	17.70	-1.43
O	0.00	15.65	17.70	-1.35
O	2.24	2.24	19.91	-1.30
O	4.48	4.47	19.91	-1.32

O	6.72	6.71	19.91	-1.35
O	8.95	8.94	19.91	-1.43
O	11.19	11.18	19.91	-1.32
O	0.00	13.41	19.91	-1.37
O	4.48	2.24	0.00	-1.34
O	6.72	4.47	0.00	-1.25
O	8.95	6.71	0.00	-1.28
O	11.19	8.94	0.00	-1.28
O	0.00	11.18	0.00	-1.29
O	2.24	0.00	8.85	-1.22
O	2.24	15.65	11.06	-1.15
O	4.48	0.00	11.06	-1.18
O	2.24	13.41	13.27	-1.30
O	4.48	15.65	13.27	-1.28
O	6.72	0.00	13.27	-1.25
O	2.24	11.18	15.48	-1.43
O	4.48	13.41	15.48	-1.45
O	6.72	15.65	15.48	-1.37
O	8.95	0.00	15.48	-1.30
O	2.24	8.94	17.70	-1.32
O	4.48	11.18	17.70	-1.35
O	6.72	13.41	17.70	-1.28
O	8.95	15.65	17.70	-1.28
O	11.19	0.00	17.70	-1.39
O	2.24	6.71	19.91	-1.23
O	4.48	8.94	19.91	-1.25
O	6.72	11.18	19.91	-1.21
O	8.95	13.41	19.91	-1.19
O	11.19	15.65	19.91	-1.34
O	0.00	0.00	19.91	-1.26
O	2.24	4.47	0.00	-1.19
O	4.48	6.71	0.00	-1.13
O	6.72	8.94	0.00	-1.23
O	8.95	11.18	0.00	-1.14
O	11.19	13.41	0.00	-1.30
O	0.00	15.65	0.00	-1.37
O	2.24	0.00	13.27	-1.21
O	2.24	15.65	15.48	-1.28
O	4.48	0.00	15.48	-1.29
O	2.24	13.41	17.70	-1.38
O	4.48	15.65	17.70	-1.28
O	6.72	0.00	17.70	-1.22
O	2.24	11.18	19.91	-1.33
O	4.48	13.41	19.91	-1.34
O	6.72	15.65	19.91	-1.16

O	8.95	0.00	19.91	-1.21
O	2.24	8.94	0.00	-1.15
O	4.48	11.18	0.00	-1.23
O	6.72	13.41	0.00	-1.25
O	8.95	15.65	0.00	-1.21
O	11.19	0.00	0.00	-1.26
O	2.24	0.00	17.70	-1.16
O	2.24	15.65	19.91	-1.34
O	4.48	0.00	19.91	-1.31
O	2.24	13.41	0.00	-1.37
O	4.48	15.65	0.00	-1.38
O	6.72	0.00	0.00	-1.37
O	2.24	0.00	0.00	-1.27

J14+Ge

Atom type	x	y	z	Bader charge
Mg	2.18	15.24	4.40	1.70
Mg	0.00	10.88	6.60	1.70
Mg	0.00	0.00	4.40	1.70
Mg	6.55	6.53	8.80	1.70
Mg	10.91	10.88	8.80	1.70
Mg	0.00	13.06	8.80	1.70
Mg	8.73	6.53	11.00	1.70
Mg	2.18	10.88	13.20	1.69
Mg	8.73	0.00	4.40	1.70
Mg	6.55	13.06	6.60	1.70
Mg	8.73	15.24	6.60	1.69
Mg	4.36	6.53	11.00	1.70
Mg	8.73	8.71	13.20	1.69
Mg	6.55	4.35	15.40	1.70
Mg	8.73	6.53	15.40	1.70
Mg	10.91	4.35	19.81	1.70
Mg	10.91	2.18	8.80	1.70
Mg	6.55	13.06	11.00	1.69
Mg	10.91	0.00	11.00	1.69
Mg	6.55	10.88	13.20	1.69
Mg	0.00	0.00	13.20	1.70
Mg	6.55	8.71	15.40	1.69
Mg	10.91	13.06	15.40	1.70
Mg	4.36	4.35	17.61	1.69
Mg	8.73	6.53	19.81	1.69
Mg	10.91	8.71	19.81	1.70
Mg	0.00	10.88	19.81	1.69
Mg	2.18	13.06	19.81	1.69
Mg	4.36	10.88	15.40	1.69

Mg	6.55	13.06	15.40	1.70
Mg	10.91	0.00	15.40	1.70
Mg	10.91	15.24	17.61	1.70
Mg	6.55	8.71	19.81	1.70
Mg	10.91	13.06	2.20	1.70
Mg	0.00	15.24	2.20	1.69
Mg	4.36	13.06	0.00	1.70
Mg	4.36	2.18	19.81	1.69
Mg	6.55	2.18	0.00	1.70
Mg	4.36	15.24	2.20	1.69
Mg	6.55	0.00	2.20	1.70
Ge	10.91	6.53	4.40	1.63
Ge	2.18	8.71	6.60	1.59
Ge	4.36	4.35	4.40	1.66
Ge	2.18	4.35	15.40	1.64
Ge	8.73	10.88	6.60	1.58
Ge	2.18	0.00	6.60	1.59
Ge	4.36	4.35	8.80	1.55
Ge	6.55	4.35	11.00	1.59
Ge	2.18	6.53	17.61	1.59
Ge	4.36	10.88	6.60	1.60
Ge	0.00	0.00	8.80	1.61
Ge	10.91	13.06	11.00	1.57
Ge	10.91	8.71	15.40	1.55
Ge	0.00	10.88	15.40	1.54
Ge	2.18	10.88	17.61	1.52
Ge	0.00	4.35	0.00	1.58
Ge	2.18	4.35	2.20	1.62
Ge	4.36	15.24	6.60	1.53
Ge	6.55	0.00	6.60	1.59
Ge	8.73	2.18	6.60	1.63
Ge	4.36	10.88	11.00	1.49
Ge	8.73	10.88	15.40	1.49
Ge	2.18	0.00	15.40	1.61
Ge	10.91	10.88	17.61	1.53
Ge	0.00	13.06	17.61	1.48
Ge	8.73	4.35	0.00	1.58
Ge	6.55	0.00	11.00	1.58
Ge	4.36	13.06	13.20	1.42
Ge	6.55	15.24	13.20	1.45
Ge	4.36	8.71	17.61	1.55
Ge	2.18	15.24	0.00	1.48
Ge	8.73	6.53	2.20	1.62
Ge	4.36	15.24	15.40	1.51
Ge	4.36	13.06	17.61	1.55

Ge	10.91	15.24	0.00	1.49
Ge	0.00	0.00	0.00	1.52
Ge	4.36	2.18	15.40	1.57
Ge	6.55	2.18	17.61	1.67
Ge	8.73	15.24	2.20	1.53
Ge	4.36	0.00	0.00	1.58
Co	0.00	4.35	4.40	1.26
Co	2.18	4.35	6.60	1.23
Co	8.73	4.35	4.40	1.25
Co	0.00	8.71	4.40	1.25
Co	0.00	4.35	8.80	1.25
Co	2.18	6.53	8.80	1.24
Co	8.73	8.71	4.40	1.15
Co	8.73	6.53	6.60	1.25
Co	0.00	6.53	11.00	1.29
Co	2.18	8.71	11.00	1.26
Co	2.18	15.24	8.80	1.25
Co	2.18	8.71	15.40	1.23
Co	10.91	15.24	8.80	1.24
Co	2.18	2.18	8.80	1.24
Co	6.55	8.71	11.00	1.25
Co	0.00	13.06	13.20	1.16
Co	0.00	6.53	19.81	1.23
Co	8.73	0.00	8.80	1.22
Co	10.91	15.24	13.20	1.23
Co	8.73	8.71	17.61	1.21
Co	10.91	6.53	0.00	1.23
Co	0.00	8.71	0.00	1.28
Co	8.73	0.00	13.20	1.25
Co	10.91	2.18	13.20	1.17
Co	8.73	15.24	15.40	1.23
Co	0.00	2.18	15.40	1.24
Co	0.00	15.24	19.81	1.24
Co	0.00	13.06	0.00	1.22
Co	10.91	8.71	2.20	1.24
Co	2.18	13.06	2.20	1.24
Co	4.36	0.00	13.20	1.24
Co	10.91	2.18	17.61	1.26
Co	10.91	0.00	19.81	1.25
Co	0.00	2.18	19.81	1.26
Co	4.36	8.71	0.00	1.26
Co	8.73	13.06	0.00	1.22
Co	2.18	2.18	0.00	1.26
Co	8.73	10.88	2.20	1.25
Co	6.55	0.00	19.81	1.23

Co	10.91	0.00	2.20	1.23
Ni	2.18	10.88	4.40	1.19
Ni	6.55	6.53	4.40	1.15
Ni	2.18	13.06	6.60	1.15
Ni	0.00	8.71	8.80	1.22
Ni	2.18	10.88	8.80	1.24
Ni	8.73	13.06	4.40	1.16
Ni	10.91	15.24	4.40	1.17
Ni	2.18	2.18	4.40	1.11
Ni	10.91	13.06	6.60	1.17
Ni	8.73	8.71	8.80	1.15
Ni	10.91	8.71	11.00	1.22
Ni	8.73	4.35	13.20	1.18
Ni	0.00	6.53	15.40	1.19
Ni	2.18	4.35	19.81	1.15
Ni	6.55	15.24	4.40	1.15
Ni	10.91	2.18	4.40	1.10
Ni	10.91	0.00	6.60	1.14
Ni	4.36	8.71	8.80	1.17
Ni	6.55	10.88	8.80	1.23
Ni	8.73	13.06	8.80	1.22
Ni	2.18	13.06	15.40	1.15
Ni	0.00	8.71	17.61	1.03
Ni	2.18	6.53	0.00	1.24
Ni	4.36	13.06	8.80	1.16
Ni	8.73	15.24	11.00	1.19
Ni	0.00	2.18	11.00	1.24
Ni	2.18	15.24	17.61	1.13
Ni	8.73	2.18	11.00	1.24
Ni	6.55	10.88	17.61	1.13
Ni	8.73	13.06	17.61	1.15
Ni	0.00	0.00	17.61	1.15
Ni	6.55	4.35	2.20	1.20
Ni	0.00	10.88	2.20	1.25
Ni	4.36	2.18	11.00	1.24
Ni	8.73	2.18	15.40	1.13
Ni	4.36	15.24	19.81	1.20
Ni	8.73	0.00	0.00	1.19
Ni	4.36	10.88	2.20	1.23
Ni	6.55	13.06	2.20	1.16
Ni	0.00	2.18	2.20	1.14
Cu	2.18	4.35	11.00	0.91
Cu	0.00	13.06	4.40	0.94
Cu	10.91	8.71	6.60	0.89
Cu	8.73	4.35	8.80	0.85

Cu	10.91	4.35	11.00	0.96
Cu	0.00	4.35	13.20	0.95
Cu	2.18	6.53	13.20	0.91
Cu	4.36	8.71	4.40	0.87
Cu	0.00	10.88	11.00	0.88
Cu	0.00	8.71	13.20	0.91
Cu	0.00	4.35	17.61	0.87
Cu	0.00	2.18	6.60	0.86
Cu	0.00	15.24	11.00	0.83
Cu	2.18	0.00	11.00	0.84
Cu	4.36	4.35	13.20	0.85
Cu	10.91	10.88	13.20	0.81
Cu	8.73	4.35	17.61	0.92
Cu	4.36	0.00	4.40	0.84
Cu	6.55	2.18	4.40	0.87
Cu	2.18	2.18	13.20	0.88
Cu	6.55	4.35	19.81	0.92
Cu	2.18	10.88	0.00	0.89
Cu	10.91	4.35	2.20	0.82
Cu	0.00	6.53	2.20	0.84
Cu	6.55	2.18	8.80	0.79
Cu	4.36	6.53	19.81	0.91
Cu	2.18	0.00	19.81	0.76
Cu	4.36	4.35	0.00	0.87
Cu	10.91	10.88	0.00	0.86
Cu	6.55	2.18	13.20	0.83
Cu	6.55	0.00	15.40	0.85
Cu	8.73	0.00	17.61	0.95
Cu	4.36	10.88	19.81	0.84
Cu	6.55	13.06	19.81	0.97
Cu	6.55	10.88	0.00	0.94
Cu	4.36	6.53	2.20	0.90
Cu	8.73	2.18	19.81	0.94
Cu	6.55	15.24	0.00	0.81
Cu	8.73	2.18	2.20	0.85
Cu	4.36	2.18	2.20	0.86
Zn	2.18	6.53	4.40	1.17
Zn	10.91	4.35	6.60	1.16
Zn	0.00	6.53	6.60	1.16
Zn	10.91	10.88	4.40	1.17
Zn	6.55	4.35	6.60	1.17
Zn	10.91	6.53	8.80	1.18
Zn	6.55	10.88	4.40	1.17
Zn	4.36	6.53	6.60	1.16
Zn	6.55	8.71	6.60	1.17

Zn	0.00	15.24	6.60	1.14
Zn	2.18	13.06	11.00	1.14
Zn	10.91	6.53	13.20	1.16
Zn	10.91	4.35	15.40	1.17
Zn	4.36	13.06	4.40	1.15
Zn	8.73	10.88	11.00	1.11
Zn	6.55	6.53	13.20	1.14
Zn	2.18	15.24	13.20	1.16
Zn	10.91	6.53	17.61	1.16
Zn	2.18	8.71	19.81	1.18
Zn	6.55	15.24	8.80	1.14
Zn	4.36	8.71	13.20	1.13
Zn	8.73	13.06	13.20	1.15
Zn	4.36	6.53	15.40	1.15
Zn	0.00	15.24	15.40	1.13
Zn	6.55	6.53	17.61	1.15
Zn	2.18	8.71	2.20	1.19
Zn	4.36	2.18	6.60	1.16
Zn	4.36	0.00	8.80	1.16
Zn	4.36	15.24	11.00	1.11
Zn	2.18	2.18	17.61	1.16
Zn	8.73	10.88	19.81	1.17
Zn	10.91	13.06	19.81	1.17
Zn	6.55	6.53	0.00	1.15
Zn	8.73	8.71	0.00	1.14
Zn	6.55	15.24	17.61	1.16
Zn	8.73	15.24	19.81	1.17
Zn	6.55	8.71	2.20	1.19
Zn	2.18	0.00	2.20	1.15
Zn	4.36	0.00	17.61	1.16
Zn	10.91	2.18	0.00	1.16
O	10.91	2.18	2.20	-1.18
O	0.00	4.35	2.20	-1.18
O	0.00	2.18	4.40	-1.28
O	6.55	2.18	2.20	-1.29
O	8.73	4.35	2.20	-1.19
O	10.91	6.53	2.20	-1.21
O	0.00	8.71	2.20	-1.22
O	8.73	2.18	4.40	-1.23
O	10.91	4.35	4.40	-1.19
O	0.00	6.53	4.40	-1.20
O	10.91	2.18	6.60	-1.25
O	0.00	4.35	6.60	-1.23
O	0.00	2.18	8.80	-1.32
O	2.18	2.18	2.20	-1.22

O	4.36	4.35	2.20	-1.16
O	6.55	6.53	2.20	-1.16
O	8.73	8.71	2.20	-1.21
O	10.91	10.88	2.20	-1.26
O	0.00	13.06	2.20	-1.39
O	4.36	2.18	4.40	-1.14
O	6.55	4.35	4.40	-1.23
O	8.73	6.53	4.40	-1.27
O	10.91	8.71	4.40	-1.25
O	0.00	10.88	4.40	-1.29
O	6.55	2.18	6.60	-1.19
O	8.73	4.35	6.60	-1.20
O	10.91	6.53	6.60	-1.23
O	0.00	8.71	6.60	-1.29
O	8.73	2.18	8.80	-1.31
O	10.91	4.35	8.80	-1.23
O	0.00	6.53	8.80	-1.22
O	10.91	2.18	11.00	-1.37
O	0.00	4.35	11.00	-1.12
O	0.00	2.18	13.20	-1.29
O	2.18	6.53	2.20	-1.20
O	4.36	8.71	2.20	-1.19
O	6.55	10.88	2.20	-1.17
O	8.73	13.06	2.20	-1.31
O	10.91	15.24	2.20	-1.38
O	0.00	0.00	2.20	-1.35
O	2.18	4.35	4.40	-1.26
O	4.36	6.53	4.40	-1.16
O	6.55	8.71	4.40	-1.20
O	8.73	10.88	4.40	-1.24
O	10.91	13.06	4.40	-1.27
O	0.00	15.24	4.40	-1.45
O	2.18	2.18	6.60	-1.24
O	4.36	4.35	6.60	-1.20
O	6.55	6.53	6.60	-1.27
O	8.73	8.71	6.60	-1.24
O	10.91	10.88	6.60	-1.35
O	0.00	13.06	6.60	-1.39
O	4.36	2.18	8.80	-1.24
O	6.55	4.35	8.80	-1.26
O	8.73	6.53	8.80	-1.34
O	10.91	8.71	8.80	-1.29
O	0.00	10.88	8.80	-1.43
O	6.55	2.18	11.00	-1.18
O	8.73	4.35	11.00	-1.24

O	10.91	6.53	11.00	-1.24
O	0.00	8.71	11.00	-1.21
O	8.73	2.18	13.20	-1.21
O	10.91	4.35	13.20	-1.14
O	0.00	6.53	13.20	-1.15
O	10.91	2.18	15.40	-1.30
O	0.00	4.35	15.40	-1.17
O	0.00	2.18	17.61	-1.23
O	2.18	10.88	2.20	-1.19
O	4.36	13.06	2.20	-1.34
O	6.55	15.24	2.20	-1.33
O	8.73	0.00	2.20	-1.38
O	2.18	8.71	4.40	-1.23
O	4.36	10.88	4.40	-1.23
O	6.55	13.06	4.40	-1.29
O	8.73	15.24	4.40	-1.36
O	10.91	0.00	4.40	-1.39
O	2.18	6.53	6.60	-1.25
O	4.36	8.71	6.60	-1.25
O	6.55	10.88	6.60	-1.30
O	8.73	13.06	6.60	-1.41
O	10.91	15.24	6.60	-1.31
O	0.00	0.00	6.60	-1.29
O	2.18	4.35	8.80	-1.21
O	4.36	6.53	8.80	-1.37
O	6.55	8.71	8.80	-1.29
O	8.73	10.88	8.80	-1.29
O	10.91	13.06	8.80	-1.37
O	0.00	15.24	8.80	-1.27
O	2.18	2.18	11.00	-1.15
O	4.36	4.35	11.00	-1.23
O	6.55	6.53	11.00	-1.43
O	8.73	8.71	11.00	-1.37
O	10.91	10.88	11.00	-1.24
O	0.00	13.06	11.00	-1.24
O	4.36	2.18	13.20	-1.21
O	6.55	4.35	13.20	-1.23
O	8.73	6.53	13.20	-1.42
O	10.91	8.71	13.20	-1.31
O	0.00	10.88	13.20	-1.24
O	6.55	2.18	15.40	-1.24
O	8.73	4.35	15.40	-1.36
O	10.91	6.53	15.40	-1.33
O	0.00	8.71	15.40	-1.22
O	8.73	2.18	17.61	-1.17

O	10.91	4.35	17.61	-1.25
O	0.00	6.53	17.61	-1.23
O	10.91	2.18	19.81	-1.28
O	0.00	4.35	19.81	-1.27
O	0.00	2.18	0.00	-1.23
O	2.18	15.24	2.20	-1.44
O	4.36	0.00	2.20	-1.31
O	2.18	13.06	4.40	-1.29
O	4.36	15.24	4.40	-1.39
O	6.55	0.00	4.40	-1.35
O	2.18	10.88	6.60	-1.32
O	4.36	13.06	6.60	-1.33
O	6.55	15.24	6.60	-1.42
O	8.73	0.00	6.60	-1.40
O	2.18	8.71	8.80	-1.26
O	4.36	10.88	8.80	-1.22
O	6.55	13.06	8.80	-1.37
O	8.73	15.24	8.80	-1.31
O	10.91	0.00	8.80	-1.36
O	2.18	6.53	11.00	-1.26
O	4.36	8.71	11.00	-1.30
O	6.55	10.88	11.00	-1.40
O	8.73	13.06	11.00	-1.29
O	10.91	15.24	11.00	-1.27
O	0.00	0.00	11.00	-1.33
O	2.18	4.35	13.20	-1.09
O	4.36	6.53	13.20	-1.24
O	6.55	8.71	13.20	-1.45
O	8.73	10.88	13.20	-1.36
O	10.91	13.06	13.20	-1.27
O	0.00	15.24	13.20	-1.25
O	2.18	2.18	15.40	-1.22
O	4.36	4.35	15.40	-1.36
O	6.55	6.53	15.40	-1.45
O	8.73	8.71	15.40	-1.48
O	10.91	10.88	15.40	-1.30
O	0.00	13.06	15.40	-1.36
O	4.36	2.18	17.61	-1.37
O	6.55	4.35	17.61	-1.34
O	8.73	6.53	17.61	-1.34
O	10.91	8.71	17.61	-1.32
O	0.00	10.88	17.61	-1.35
O	6.55	2.18	19.81	-1.34
O	8.73	4.35	19.81	-1.31
O	10.91	6.53	19.81	-1.46

O	0.00	8.71	19.81	-1.38
O	8.73	2.18	0.00	-1.24
O	10.91	4.35	0.00	-1.27
O	0.00	6.53	0.00	-1.21
O	2.18	0.00	4.40	-1.38
O	2.18	15.24	6.60	-1.33
O	4.36	0.00	6.60	-1.26
O	2.18	13.06	8.80	-1.29
O	4.36	15.24	8.80	-1.21
O	6.55	0.00	8.80	-1.20
O	2.18	10.88	11.00	-1.31
O	4.36	13.06	11.00	-1.30
O	6.55	15.24	11.00	-1.29
O	8.73	0.00	11.00	-1.27
O	2.18	8.71	13.20	-1.28
O	4.36	10.88	13.20	-1.46
O	6.55	13.06	13.20	-1.47
O	8.73	15.24	13.20	-1.27
O	10.91	0.00	13.20	-1.45
O	2.18	6.53	15.40	-1.21
O	4.36	8.71	15.40	-1.41
O	6.55	10.88	15.40	-1.54
O	8.73	13.06	15.40	-1.42
O	10.91	15.24	15.40	-1.46
O	0.00	0.00	15.40	-1.36
O	2.18	4.35	17.61	-1.33
O	4.36	6.53	17.61	-1.28
O	6.55	8.71	17.61	-1.36
O	8.73	10.88	17.61	-1.27
O	10.91	13.06	17.61	-1.41
O	0.00	15.24	17.61	-1.34
O	2.18	2.18	19.81	-1.30
O	4.36	4.35	19.81	-1.30
O	6.55	6.53	19.81	-1.34
O	8.73	8.71	19.81	-1.43
O	10.91	10.88	19.81	-1.32
O	0.00	13.06	19.81	-1.39
O	4.36	2.18	0.00	-1.33
O	6.55	4.35	0.00	-1.26
O	8.73	6.53	0.00	-1.29
O	10.91	8.71	0.00	-1.27
O	0.00	10.88	0.00	-1.27
O	2.18	0.00	8.80	-1.21
O	2.18	15.24	11.00	-1.15
O	4.36	0.00	11.00	-1.17

O	2.18	13.06	13.20	-1.27
O	4.36	15.24	13.20	-1.27
O	6.55	0.00	13.20	-1.20
O	2.18	10.88	15.40	-1.41
O	4.36	13.06	15.40	-1.40
O	6.55	15.24	15.40	-1.30
O	8.73	0.00	15.40	-1.29
O	2.18	8.71	17.61	-1.28
O	4.36	10.88	17.61	-1.29
O	6.55	13.06	17.61	-1.28
O	8.73	15.24	17.61	-1.29
O	10.91	0.00	17.61	-1.39
O	2.18	6.53	19.81	-1.24
O	4.36	8.71	19.81	-1.25
O	6.55	10.88	19.81	-1.20
O	8.73	13.06	19.81	-1.19
O	10.91	15.24	19.81	-1.28
O	0.00	0.00	19.81	-1.22
O	2.18	4.35	0.00	-1.20
O	4.36	6.53	0.00	-1.16
O	6.55	8.71	0.00	-1.23
O	8.73	10.88	0.00	-1.14
O	10.91	13.06	0.00	-1.27
O	0.00	15.24	0.00	-1.32
O	2.18	0.00	13.20	-1.24
O	2.18	15.24	15.40	-1.26
O	4.36	0.00	15.40	-1.27
O	2.18	13.06	17.61	-1.33
O	4.36	15.24	17.61	-1.27
O	6.55	0.00	17.61	-1.22
O	2.18	10.88	19.81	-1.33
O	4.36	13.06	19.81	-1.34
O	6.55	15.24	19.81	-1.16
O	8.73	0.00	19.81	-1.22
O	2.18	8.71	0.00	-1.16
O	4.36	10.88	0.00	-1.24
O	6.55	13.06	0.00	-1.22
O	8.73	15.24	0.00	-1.20
O	10.91	0.00	0.00	-1.23
O	2.18	0.00	17.61	-1.17
O	2.18	15.24	19.81	-1.29
O	4.36	0.00	19.81	-1.25
O	2.18	13.06	0.00	-1.36
O	4.36	15.24	0.00	-1.37
O	6.55	0.00	0.00	-1.33

O	2.18	0.00	0.00	-1.22
J14+Cr				
Atom				Bader
type	x	y	z	charge
Mg	2.13	14.97	4.29	1.70
Mg	0.00	10.69	6.43	1.70
Mg	0.00	0.00	4.29	1.70
Mg	6.38	6.41	8.58	1.69
Mg	10.63	10.69	8.58	1.69
Mg	0.00	12.83	8.58	1.70
Mg	8.51	6.41	10.72	1.70
Mg	2.13	10.69	12.87	1.69
Mg	8.51	0.00	4.29	1.70
Mg	6.38	12.83	6.43	1.70
Mg	8.51	14.97	6.43	1.70
Mg	4.25	6.41	10.72	1.70
Mg	8.51	8.55	12.87	1.69
Mg	6.38	4.28	15.01	1.70
Mg	8.51	6.41	15.01	1.70
Mg	10.63	4.28	19.30	1.70
Mg	10.63	2.14	8.58	1.70
Mg	6.38	12.83	10.72	1.69
Mg	10.63	0.00	10.72	1.69
Mg	6.38	10.69	12.87	1.69
Mg	0.00	0.00	12.87	1.70
Mg	6.38	8.55	15.01	1.70
Mg	10.63	12.83	15.01	1.70
Mg	4.25	4.28	17.16	1.69
Mg	8.51	6.41	19.30	1.69
Mg	10.63	8.55	19.30	1.70
Mg	0.00	10.69	19.30	1.69
Mg	2.13	12.83	19.30	1.69
Mg	4.25	10.69	15.01	1.69
Mg	6.38	12.83	15.01	1.69
Mg	10.63	0.00	15.01	1.70
Mg	10.63	14.97	17.16	1.70
Mg	6.38	8.55	19.30	1.70
Mg	10.63	12.83	2.14	1.70
Mg	0.00	14.97	2.14	1.69
Mg	4.25	12.83	0.00	1.70
Mg	4.25	2.14	19.30	1.69
Mg	6.38	2.14	0.00	1.70
Mg	4.25	14.97	2.14	1.69
Mg	6.38	0.00	2.14	1.70
Cr	10.63	6.41	4.29	1.59

Cr	2.13	8.55	6.43	1.56
Cr	4.25	4.28	4.29	1.55
Cr	2.13	4.28	15.01	1.55
Cr	8.51	10.69	6.43	1.54
Cr	2.13	0.00	6.43	1.52
Cr	4.25	4.28	8.58	1.53
Cr	6.38	4.28	10.72	1.62
Cr	2.13	6.41	17.16	1.53
Cr	4.25	10.69	6.43	1.50
Cr	0.00	0.00	8.58	1.58
Cr	10.63	12.83	10.72	1.63
Cr	10.63	8.55	15.01	1.54
Cr	0.00	10.69	15.01	1.47
Cr	2.13	10.69	17.16	1.45
Cr	0.00	4.28	0.00	1.59
Cr	2.13	4.28	2.14	1.57
Cr	4.25	14.97	6.43	1.50
Cr	6.38	0.00	6.43	1.52
Cr	8.51	2.14	6.43	1.55
Cr	4.25	10.69	10.72	1.42
Cr	8.51	10.69	15.01	1.48
Cr	2.13	0.00	15.01	1.51
Cr	10.63	10.69	17.16	1.46
Cr	0.00	12.83	17.16	1.46
Cr	8.51	4.28	0.00	1.61
Cr	6.38	0.00	10.72	1.46
Cr	4.25	12.83	12.87	1.39
Cr	6.38	14.97	12.87	1.49
Cr	4.25	8.55	17.16	1.52
Cr	2.13	14.97	0.00	1.56
Cr	8.51	6.41	2.14	1.55
Cr	4.25	14.97	15.01	1.48
Cr	4.25	12.83	17.16	1.48
Cr	10.63	14.97	0.00	1.55
Cr	0.00	0.00	0.00	1.56
Cr	4.25	2.14	15.01	1.53
Cr	6.38	2.14	17.16	1.57
Cr	8.51	14.97	2.14	1.54
Cr	4.25	0.00	0.00	1.53
Co	0.00	4.28	4.29	1.27
Co	2.13	4.28	6.43	1.26
Co	8.51	4.28	4.29	1.26
Co	0.00	8.55	4.29	1.25
Co	0.00	4.28	8.58	1.27
Co	2.13	6.41	8.58	1.25

Co	8.51	8.55	4.29	1.25
Co	8.51	6.41	6.43	1.27
Co	0.00	6.41	10.72	1.26
Co	2.13	8.55	10.72	1.24
Co	2.13	14.97	8.58	1.26
Co	2.13	8.55	15.01	1.24
Co	10.63	14.97	8.58	1.25
Co	2.13	2.14	8.58	1.25
Co	6.38	8.55	10.72	1.27
Co	0.00	12.83	12.87	1.27
Co	0.00	6.41	19.30	1.24
Co	8.51	0.00	8.58	1.23
Co	10.63	14.97	12.87	1.24
Co	8.51	8.55	17.16	1.23
Co	10.63	6.41	0.00	1.22
Co	0.00	8.55	0.00	1.26
Co	8.51	0.00	12.87	1.25
Co	10.63	2.14	12.87	1.25
Co	8.51	14.97	15.01	1.26
Co	0.00	2.14	15.01	1.26
Co	0.00	14.97	19.30	1.24
Co	0.00	12.83	0.00	1.21
Co	10.63	8.55	2.14	1.25
Co	2.13	12.83	2.14	1.25
Co	4.25	0.00	12.87	1.25
Co	10.63	2.14	17.16	1.28
Co	10.63	0.00	19.30	1.25
Co	0.00	2.14	19.30	1.26
Co	4.25	8.55	0.00	1.26
Co	8.51	12.83	0.00	1.25
Co	2.13	2.14	0.00	1.28
Co	8.51	10.69	2.14	1.27
Co	6.38	0.00	19.30	1.24
Co	10.63	0.00	2.14	1.24
Ni	2.13	10.69	4.29	1.18
Ni	6.38	6.41	4.29	1.18
Ni	2.13	12.83	6.43	1.19
Ni	0.00	8.55	8.58	1.18
Ni	2.13	10.69	8.58	1.21
Ni	8.51	12.83	4.29	1.14
Ni	10.63	14.97	4.29	1.18
Ni	2.13	2.14	4.29	1.17
Ni	10.63	12.83	6.43	1.17
Ni	8.51	8.55	8.58	1.19
Ni	10.63	8.55	10.72	1.24

Ni	8.51	4.28	12.87	1.14
Ni	0.00	6.41	15.01	1.20
Ni	2.13	4.28	19.30	1.17
Ni	6.38	14.97	4.29	1.13
Ni	10.63	2.14	4.29	1.18
Ni	10.63	0.00	6.43	1.17
Ni	4.25	8.55	8.58	1.15
Ni	6.38	10.69	8.58	1.19
Ni	8.51	12.83	8.58	1.17
Ni	2.13	12.83	15.01	1.12
Ni	0.00	8.55	17.16	1.12
Ni	2.13	6.41	0.00	1.24
Ni	4.25	12.83	8.58	1.17
Ni	8.51	14.97	10.72	1.18
Ni	0.00	2.14	10.72	1.24
Ni	2.13	14.97	17.16	1.18
Ni	8.51	2.14	10.72	1.25
Ni	6.38	10.69	17.16	1.15
Ni	8.51	12.83	17.16	1.16
Ni	0.00	0.00	17.16	1.15
Ni	6.38	4.28	2.14	1.18
Ni	0.00	10.69	2.14	1.22
Ni	4.25	2.14	10.72	1.27
Ni	8.51	2.14	15.01	1.20
Ni	4.25	14.97	19.30	1.19
Ni	8.51	0.00	0.00	1.23
Ni	4.25	10.69	2.14	1.21
Ni	6.38	12.83	2.14	1.18
Ni	0.00	2.14	2.14	1.13
Cu	2.13	4.28	10.72	0.89
Cu	0.00	12.83	4.29	0.91
Cu	10.63	8.55	6.43	0.86
Cu	8.51	4.28	8.58	0.82
Cu	10.63	4.28	10.72	0.94
Cu	0.00	4.28	12.87	0.96
Cu	2.13	6.41	12.87	0.91
Cu	4.25	8.55	4.29	0.87
Cu	0.00	10.69	10.72	0.85
Cu	0.00	8.55	12.87	0.89
Cu	0.00	4.28	17.16	0.90
Cu	0.00	2.14	6.43	0.86
Cu	0.00	14.97	10.72	0.79
Cu	2.13	0.00	10.72	0.84
Cu	4.25	4.28	12.87	0.85
Cu	10.63	10.69	12.87	0.77

Cu	8.51	4.28	17.16	0.95
Cu	4.25	0.00	4.29	0.85
Cu	6.38	2.14	4.29	0.92
Cu	2.13	2.14	12.87	0.89
Cu	6.38	4.28	19.30	0.94
Cu	2.13	10.69	0.00	0.85
Cu	10.63	4.28	2.14	0.79
Cu	0.00	6.41	2.14	0.85
Cu	6.38	2.14	8.58	0.83
Cu	4.25	6.41	19.30	0.91
Cu	2.13	0.00	19.30	0.77
Cu	4.25	4.28	0.00	0.88
Cu	10.63	10.69	0.00	0.83
Cu	6.38	2.14	12.87	0.84
Cu	6.38	0.00	15.01	0.87
Cu	8.51	0.00	17.16	0.92
Cu	4.25	10.69	19.30	0.85
Cu	6.38	12.83	19.30	0.94
Cu	6.38	10.69	0.00	0.98
Cu	4.25	6.41	2.14	0.92
Cu	8.51	2.14	19.30	0.93
Cu	6.38	14.97	0.00	0.85
Cu	8.51	2.14	2.14	0.85
Cu	4.25	2.14	2.14	0.89
Zn	2.13	6.41	4.29	1.19
Zn	10.63	4.28	6.43	1.17
Zn	0.00	6.41	6.43	1.17
Zn	10.63	10.69	4.29	1.18
Zn	6.38	4.28	6.43	1.19
Zn	10.63	6.41	8.58	1.20
Zn	6.38	10.69	4.29	1.18
Zn	4.25	6.41	6.43	1.17
Zn	6.38	8.55	6.43	1.17
Zn	0.00	14.97	6.43	1.16
Zn	2.13	12.83	10.72	1.14
Zn	10.63	6.41	12.87	1.17
Zn	10.63	4.28	15.01	1.19
Zn	4.25	12.83	4.29	1.15
Zn	8.51	10.69	10.72	1.13
Zn	6.38	6.41	12.87	1.15
Zn	2.13	14.97	12.87	1.18
Zn	10.63	6.41	17.16	1.18
Zn	2.13	8.55	19.30	1.18
Zn	6.38	14.97	8.58	1.16
Zn	4.25	8.55	12.87	1.16

Zn	8.51	12.83	12.87	1.17
Zn	4.25	6.41	15.01	1.17
Zn	0.00	14.97	15.01	1.16
Zn	6.38	6.41	17.16	1.18
Zn	2.13	8.55	2.14	1.21
Zn	4.25	2.14	6.43	1.17
Zn	4.25	0.00	8.58	1.18
Zn	4.25	14.97	10.72	1.12
Zn	2.13	2.14	17.16	1.17
Zn	8.51	10.69	19.30	1.18
Zn	10.63	12.83	19.30	1.17
Zn	6.38	6.41	0.00	1.15
Zn	8.51	8.55	0.00	1.15
Zn	6.38	14.97	17.16	1.19
Zn	8.51	14.97	19.30	1.19
Zn	6.38	8.55	2.14	1.19
Zn	2.13	0.00	2.14	1.17
Zn	4.25	0.00	17.16	1.18
Zn	10.63	2.14	0.00	1.17
O	10.63	2.14	2.14	-1.17
O	0.00	4.28	2.14	-1.23
O	0.00	2.14	4.29	-1.30
O	6.38	2.14	2.14	-1.29
O	8.51	4.28	2.14	-1.23
O	10.63	6.41	2.14	-1.19
O	0.00	8.55	2.14	-1.21
O	8.51	2.14	4.29	-1.24
O	10.63	4.28	4.29	-1.18
O	0.00	6.41	4.29	-1.19
O	10.63	2.14	6.43	-1.26
O	0.00	4.28	6.43	-1.24
O	0.00	2.14	8.58	-1.31
O	2.13	2.14	2.14	-1.22
O	4.25	4.28	2.14	-1.15
O	6.38	6.41	2.14	-1.17
O	8.51	8.55	2.14	-1.21
O	10.63	10.69	2.14	-1.25
O	0.00	12.83	2.14	-1.37
O	4.25	2.14	4.29	-1.16
O	6.38	4.28	4.29	-1.23
O	8.51	6.41	4.29	-1.27
O	10.63	8.55	4.29	-1.25
O	0.00	10.69	4.29	-1.30
O	6.38	2.14	6.43	-1.17
O	8.51	4.28	6.43	-1.18

O	10.63	6.41	6.43	-1.22
O	0.00	8.55	6.43	-1.29
O	8.51	2.14	8.58	-1.30
O	10.63	4.28	8.58	-1.23
O	0.00	6.41	8.58	-1.20
O	10.63	2.14	10.72	-1.36
O	0.00	4.28	10.72	-1.13
O	0.00	2.14	12.87	-1.30
O	2.13	6.41	2.14	-1.19
O	4.25	8.55	2.14	-1.20
O	6.38	10.69	2.14	-1.17
O	8.51	12.83	2.14	-1.29
O	10.63	14.97	2.14	-1.40
O	0.00	0.00	2.14	-1.40
O	2.13	4.28	4.29	-1.26
O	4.25	6.41	4.29	-1.17
O	6.38	8.55	4.29	-1.22
O	8.51	10.69	4.29	-1.24
O	10.63	12.83	4.29	-1.26
O	0.00	14.97	4.29	-1.44
O	2.13	2.14	6.43	-1.24
O	4.25	4.28	6.43	-1.26
O	6.38	6.41	6.43	-1.28
O	8.51	8.55	6.43	-1.24
O	10.63	10.69	6.43	-1.35
O	0.00	12.83	6.43	-1.37
O	4.25	2.14	8.58	-1.23
O	6.38	4.28	8.58	-1.30
O	8.51	6.41	8.58	-1.35
O	10.63	8.55	8.58	-1.30
O	0.00	10.69	8.58	-1.42
O	6.38	2.14	10.72	-1.19
O	8.51	4.28	10.72	-1.22
O	10.63	6.41	10.72	-1.25
O	0.00	8.55	10.72	-1.17
O	8.51	2.14	12.87	-1.23
O	10.63	4.28	12.87	-1.14
O	0.00	6.41	12.87	-1.13
O	10.63	2.14	15.01	-1.32
O	0.00	4.28	15.01	-1.17
O	0.00	2.14	17.16	-1.24
O	2.13	10.69	2.14	-1.17
O	4.25	12.83	2.14	-1.36
O	6.38	14.97	2.14	-1.31
O	8.51	0.00	2.14	-1.38

O	2.13	8.55	4.29	-1.22
O	4.25	10.69	4.29	-1.23
O	6.38	12.83	4.29	-1.29
O	8.51	14.97	4.29	-1.38
O	10.63	0.00	4.29	-1.39
O	2.13	6.41	6.43	-1.24
O	4.25	8.55	6.43	-1.25
O	6.38	10.69	6.43	-1.33
O	8.51	12.83	6.43	-1.40
O	10.63	14.97	6.43	-1.31
O	0.00	0.00	6.43	-1.31
O	2.13	4.28	8.58	-1.21
O	4.25	6.41	8.58	-1.36
O	6.38	8.55	8.58	-1.29
O	8.51	10.69	8.58	-1.27
O	10.63	12.83	8.58	-1.39
O	0.00	14.97	8.58	-1.26
O	2.13	2.14	10.72	-1.16
O	4.25	4.28	10.72	-1.22
O	6.38	6.41	10.72	-1.43
O	8.51	8.55	10.72	-1.36
O	10.63	10.69	10.72	-1.25
O	0.00	12.83	10.72	-1.25
O	4.25	2.14	12.87	-1.20
O	6.38	4.28	12.87	-1.28
O	8.51	6.41	12.87	-1.42
O	10.63	8.55	12.87	-1.29
O	0.00	10.69	12.87	-1.25
O	6.38	2.14	15.01	-1.24
O	8.51	4.28	15.01	-1.38
O	10.63	6.41	15.01	-1.31
O	0.00	8.55	15.01	-1.19
O	8.51	2.14	17.16	-1.19
O	10.63	4.28	17.16	-1.24
O	0.00	6.41	17.16	-1.23
O	10.63	2.14	19.30	-1.28
O	0.00	4.28	19.30	-1.33
O	0.00	2.14	0.00	-1.22
O	2.13	14.97	2.14	-1.48
O	4.25	0.00	2.14	-1.32
O	2.13	12.83	4.29	-1.29
O	4.25	14.97	4.29	-1.37
O	6.38	0.00	4.29	-1.36
O	2.13	10.69	6.43	-1.32
O	4.25	12.83	6.43	-1.35

O	6.38	14.97	6.43	-1.40
O	8.51	0.00	6.43	-1.40
O	2.13	8.55	8.58	-1.21
O	4.25	10.69	8.58	-1.22
O	6.38	12.83	8.58	-1.35
O	8.51	14.97	8.58	-1.32
O	10.63	0.00	8.58	-1.35
O	2.13	6.41	10.72	-1.27
O	4.25	8.55	10.72	-1.27
O	6.38	10.69	10.72	-1.37
O	8.51	12.83	10.72	-1.26
O	10.63	14.97	10.72	-1.26
O	0.00	0.00	10.72	-1.32
O	2.13	4.28	12.87	-1.08
O	4.25	6.41	12.87	-1.24
O	6.38	8.55	12.87	-1.46
O	8.51	10.69	12.87	-1.34
O	10.63	12.83	12.87	-1.32
O	0.00	14.97	12.87	-1.25
O	2.13	2.14	15.01	-1.21
O	4.25	4.28	15.01	-1.34
O	6.38	6.41	15.01	-1.45
O	8.51	8.55	15.01	-1.45
O	10.63	10.69	15.01	-1.31
O	0.00	12.83	15.01	-1.35
O	4.25	2.14	17.16	-1.36
O	6.38	4.28	17.16	-1.33
O	8.51	6.41	17.16	-1.35
O	10.63	8.55	17.16	-1.32
O	0.00	10.69	17.16	-1.35
O	6.38	2.14	19.30	-1.34
O	8.51	4.28	19.30	-1.37
O	10.63	6.41	19.30	-1.43
O	0.00	8.55	19.30	-1.35
O	8.51	2.14	0.00	-1.22
O	10.63	4.28	0.00	-1.29
O	0.00	6.41	0.00	-1.21
O	2.13	0.00	4.29	-1.39
O	2.13	14.97	6.43	-1.32
O	4.25	0.00	6.43	-1.27
O	2.13	12.83	8.58	-1.27
O	4.25	14.97	8.58	-1.20
O	6.38	0.00	8.58	-1.21
O	2.13	10.69	10.72	-1.28
O	4.25	12.83	10.72	-1.30

O	6.38	14.97	10.72	-1.28
O	8.51	0.00	10.72	-1.28
O	2.13	8.55	12.87	-1.27
O	4.25	10.69	12.87	-1.45
O	6.38	12.83	12.87	-1.46
O	8.51	14.97	12.87	-1.26
O	10.63	0.00	12.87	-1.46
O	2.13	6.41	15.01	-1.20
O	4.25	8.55	15.01	-1.41
O	6.38	10.69	15.01	-1.55
O	8.51	12.83	15.01	-1.41
O	10.63	14.97	15.01	-1.46
O	0.00	0.00	15.01	-1.37
O	2.13	4.28	17.16	-1.33
O	4.25	6.41	17.16	-1.26
O	6.38	8.55	17.16	-1.36
O	8.51	10.69	17.16	-1.27
O	10.63	12.83	17.16	-1.40
O	0.00	14.97	17.16	-1.33
O	2.13	2.14	19.30	-1.30
O	4.25	4.28	19.30	-1.29
O	6.38	6.41	19.30	-1.33
O	8.51	8.55	19.30	-1.42
O	10.63	10.69	19.30	-1.33
O	0.00	12.83	19.30	-1.35
O	4.25	2.14	0.00	-1.34
O	6.38	4.28	0.00	-1.23
O	8.51	6.41	0.00	-1.27
O	10.63	8.55	0.00	-1.28
O	0.00	10.69	0.00	-1.27
O	2.13	0.00	8.58	-1.19
O	2.13	14.97	10.72	-1.15
O	4.25	0.00	10.72	-1.17
O	2.13	12.83	12.87	-1.27
O	4.25	14.97	12.87	-1.24
O	6.38	0.00	12.87	-1.18
O	2.13	10.69	15.01	-1.41
O	4.25	12.83	15.01	-1.40
O	6.38	14.97	15.01	-1.34
O	8.51	0.00	15.01	-1.31
O	2.13	8.55	17.16	-1.28
O	4.25	10.69	17.16	-1.30
O	6.38	12.83	17.16	-1.27
O	8.51	14.97	17.16	-1.30
O	10.63	0.00	17.16	-1.37

O	2.13	6.41	19.30	-1.23
O	4.25	8.55	19.30	-1.23
O	6.38	10.69	19.30	-1.21
O	8.51	12.83	19.30	-1.18
O	10.63	14.97	19.30	-1.32
O	0.00	0.00	19.30	-1.26
O	2.13	4.28	0.00	-1.18
O	4.25	6.41	0.00	-1.14
O	6.38	8.55	0.00	-1.24
O	8.51	10.69	0.00	-1.15
O	10.63	12.83	0.00	-1.27
O	0.00	14.97	0.00	-1.32
O	2.13	0.00	12.87	-1.25
O	2.13	14.97	15.01	-1.26
O	4.25	0.00	15.01	-1.27
O	2.13	12.83	17.16	-1.33
O	4.25	14.97	17.16	-1.25
O	6.38	0.00	17.16	-1.22
O	2.13	10.69	19.30	-1.33
O	4.25	12.83	19.30	-1.35
O	6.38	14.97	19.30	-1.15
O	8.51	0.00	19.30	-1.22
O	2.13	8.55	0.00	-1.17
O	4.25	10.69	0.00	-1.21
O	6.38	12.83	0.00	-1.22
O	8.51	14.97	0.00	-1.18
O	10.63	0.00	0.00	-1.22
O	2.13	0.00	17.16	-1.17
O	2.13	14.97	19.30	-1.33
O	4.25	0.00	19.30	-1.31
O	2.13	12.83	0.00	-1.35
O	4.25	14.97	0.00	-1.34
O	6.38	0.00	0.00	-1.34
O	2.13	0.00	0.00	-1.22